ARSENATE PRECIPITATION FROM

POLYELECTROLYTE-ARSENATE COMPLEX

SOLUTIONS

Winya Dungkaew

A Thesis Submitted in Partial Fulfillment of the Requirements for the

Degree of Doctor of Philosophy in Chemistry

Suranaree University of Technology

Academic Year 2010

การตกตะกอนอาร์ซีเนตจากสารละลายเชิงซ้อนพอลิอิเล็กโทรไลต์-อาร์ซีเนต

นายวิญญา ดุงแก้ว

วิทยานิพนธ์นี้เป็นส่วนหนึ่งของการศึกษาตามหลักสูตรปริญญาวิทยาศาสตรดุษฎีบัณฑิต
สาขาวิชาเคมี
มหาวิทยาลัยเทคโนโลยีสุรนารี
ปีการศึกษา 2553

ARSENATE PRECIPITATION FROM

POLYELECTROLYTE-ARSENATE COMPLEX SOLUTIONS

Suranaree University of Technology has approved this thesis submitted in partial fulfillment of the requirements for the Degree of Doctor of Philosophy.

Thesis Examining Committee

_____

(Assoc. Prof. Dr. Malee Tangsathitkulchai)

Chairperson

_____

(Assoc. Prof. Dr. Kenneth J. Haller)

Member (Thesis Advisor)

_____

(Assoc. Prof. Dr. Adrian E. Flood)

Member

_____

(Asst. Prof. Dr. Sirirat Tubsungnoen Rattanachan)

Member

_____

(Dr. Sukhwan Soontravanich)

Member

_____   _____

(Prof. Dr. Sukit Limpijumnong)   (Assoc. Prof. Dr. Prapun Manyum)

Vice Rector for Academic Affairs   Dean of Institute of Science

วิญญา ดุงแก้ว : การตกตะกอนอาร์ซีเนตจากสารละลายเชิงซ้อนพอลิอิเล็กโทรไลต์-อาร์ซีเนต (ARSENATE PRECIPITATION FROM POLYELECTROLYTE-ARSENATE COMPLEX SOLUTIONS) อาจารย์ที่ปรึกษา : รองศาสตราจารย์ ดร.เค็นเนท เจ. แฮลเลอร์, 117 หน้า.

งานวิจัยนี้ศึกษาการตกตะกอนของสารอาร์ซีเนตจากสารละลายเชิงซ้อนพอลิอิเล็กโทรไลต์-อาร์ซีเนตซึ่งเป็นส่วนหนึ่งของงานการนำพอลิอิเล็กโทรไลต์หรือควอท (QUAT) กลับจากกระแสของน้ำเสียจากกระบวนการพีอียูเอฟ (PEUF) งานนี้เริ่มต้นจากการตกตะกอนของสารแบเรียม-อาร์ซีเนต พบว่าเฟสเดี่ยวสามแบบของสารแบเรียม-อาร์ซีเนต ประกอบด้วย แบเรียมไฮโครเจนอาร์ซีเนตโมโนไฮเดรต ($BaHAsO_4 \cdot H_2O$) โซเดียมแบเรียมอาร์ซีเนตโนนาไฮเดรต ($NaBaAsO_4 \cdot 9H_2O$) และแบเรียมคลอไรด์อาร์ซีเนต ($Ba_5Cl(AsO_4)_3$) และสารผสมเกิดขึ้นที่ค่าพีเอชอัตราส่วนโมลของแบเรียมต่ออาร์ซีเนตและความเข้มข้นของอิออนร่วมที่ต่างกัน ผลจากการที่มีอิออนร่วม และมีค่าพีเอชและอัตราส่วนโมลของแบเรียมต่ออาร์ซีเนตที่เหมาะสมในระบบส่งผลให้มีการเหนี่ยวนำให้เกิดสารประกอบที่มีอิออนร่วมเหล่านั้นเป็นองค์ประกอบและยับยั้งการเกิดของสารแบเรียมอาร์ซีเนต ($Ba_3(AsO_4)_2$) โดยสารกึ่งเสถียรของโซเดียมแบเรียมอาร์ซีเนตโนนาไฮเดรตและแบเรียมคลอไรด์อาร์ซีเนตมักที่จะเกิดแทนที่สภาวะเหล่านั้น เมื่อควอทร่วมอยู่ในระบบการตกตะกอนส่งผลต่อรูปผลึกและขนาดของแบเรียมไฮโครเจนอาร์ซีเนตโมโนไฮเดรตและแบเรียมคลอไรด์อาร์ซีเนตในทางที่ยาวขึ้น การศึกษาการสลายของแบเรียมไฮโครเจนอาร์ซีเนตโมโนไฮเดรต โซเดียมแบเรียมอาร์ซีเนตโนนาไฮเดรต และแบเรียมคลอไรด์อาร์ซีเนตพบค่าคงที่ของการละลาย ($-\log K_{sp}$) ของแบเรียมไฮโครเจนอาร์ซีเนตโมโนไฮเดรตเท่ากับ 5.60(5) ซึ่งใกล้เคียงกับงานวิจัยอื่นที่ได้รายงานไว้ และเท่ากับ 10.77(30) และ 35.30(37) สำหรับโซเดียมแบเรียมอาร์ซีเนตโนนาไฮเดรตและแบเรียมคลอไรด์อาร์ซีเนตตามลำดับ ทั้งสองค่าเป็นค่าใหม่ที่รายงานสำหรับสารกึ่งเสถียรทั้งสอง การละลายแบบไม่เป็นไปตามอัตราส่วนโมลเริ่มต้น (Incongruent dissolution) ได้เกิดขึ้นในระบบของโซเดียมแบเรียมอาร์ซีเนตโนนาไฮเดรตและแบเรียมคลอไรด์อาร์ซีเนตซึ่งเกิดจากการเกิดของสารแบเรียมอาร์ซีเนตในระบบ การเกิดดังกล่าวยืนยันได้ด้วยค่าดรรชนีความอิ่มตัวที่คำนวณได้ ข้อสังเกตนี้ชี้ว่าการตกตะกอนของสารแบเรียมอาร์ซีเนตสามารถที่จะเกิดได้แต่เนื่องจากมีโซเดียมและคลอไรด์ในระบบ สมดุลจึงผลักให้เกิดโซเดียมแบเรียมอาร์ซีเนตโนนาไฮเดรตและแบเรียมคลอไรด์อาร์ซีเนตแทน จากการศึกษาการตกตะกอนและการละลายของสารพบว่าการตกตะกอนของสารแบเรียมอาร์ซีเนตไม่เหมาะสมสำหรับการตกตะกอนอาร์ซีเนตจากกระแสของน้ำเสียจากกระบวนการพีอียูเอฟ

การขจัดอาร์ซีเนตประสบผลสำเร็จโดยการตกตะกอนร่วมกับสารแคลเซียมฟอสเฟต
ไฮดรอกซีอะพาไทท์ซึ่งมีค่าการละลายที่ต่ำ พบว่าประสิทธิภาพในการขจัดอาร์ซีเนตสูงถึงร้อยละ
99 จากสารละลายอาร์เซนิคเข้มข้น 25 ส่วนในล้านส่วน (ppm) ทั้งในระบบที่มีและไม่มีควอทอยู่
ประสิทธิภาพในการขจัดอาร์เซนิคสูงขึ้นเมื่ออัตราส่วนโมลของแคลเซียมต่อฟอสฟอรัสและ
อาร์เซนิค (Ca/(P+As)) และฟอสฟอรัสต่ออาร์เซนิค (P/As) เพิ่มขึ้น โดยพบประสิทธิภาพสูงสุดที่
อัตราส่วนโมลของแคลเซียมต่อฟอสฟอรัสและอาร์เซนิคเท่ากับ 3 และฟอสฟอรัสต่ออาร์เซนิค
เท่ากับ 5 ค่าพีเอชของสารละลายเริ่มต้นไม่ส่งผลต่อการขจัดอาร์เซนิคดังกล่าวอย่างมีนัยสำคัญ การ
ตกผลึกแบบต่อเนื่องของกระบวนการดังกล่าวได้ถูกทำขึ้นเพื่อเชื่อมต่อกับระบบพีอียูเอฟเพื่อ
จุดประสงค์ในการนำกลับของพอลิอิเล็กโทรไลต์ พบว่าสารประกอบที่เกิดขึ้นเหมือนกับ
สารประกอบที่เกิดขึ้นในการตกตะกอนแบบไม่ต่อเนื่องซึ่งรายงานไปก่อนหน้านี้ โดยสามารถ
ยืนยันได้จากเทคนิค XRD และ TEM/EDX ซึ่งพบอาร์เซนิคเป็นองค์ประกอบของสารดังกล่าว ทำ
ให้คาดได้ว่าจะได้รับการขจัดอาร์เซนิคในประสิทธิภาพที่สูงเช่นกัน จากวิธีการที่ศึกษาในงานวิจัย
นี้อาร์เซนิคสามารถที่จะถูกขจัดจากสารละลายเชิงซ้อนพอลิอิเล็กโทรไลต์-อาร์ซีเนต ทำให้ควอท
เป็นอิสระและสามารถที่จะนำกลับไปใช้ซ้ำได้

สาขาวิชาเคมี   ลายมือชื่อนักศึกษา_____

ปีการศึกษา 2553   ลายมือชื่ออาจารย์ที่ปรึกษา_____

WINYA DUNGKAEW : ARSENATE PRECIPITATION FROM

POLYELECTROLYTE-ARSENATE COMPLEX SOLUTIONS.

THESIS ADVISOR : ASSOC. PROF. KENNETH J. HALLER, Ph.D.

117 PP.

ARSENIC REMOVAL/BARIUM-ARSENATE PRECIPITATION/INCONGRUENT

DISSOLUTION/CALCIUM-ARSENATE-PHOSPHATE APATITE/PEUF

This research studied arsenate precipitation from aqueous solutions of polyelectrolyte-arsenate complex as a part of QUAT polyelectrolyte recovery from PEUF process retentate stream. Barium-arsenate is the first precipitation system studied in this work. Three single phases of $BaHAsO_4 \cdot H_2O$, $NaBaAsO_4 \cdot 9H_2O$, and $Ba_5Cl(AsO_4)_3$ and their mixtures were formed as the dominant solid phases in different regions of pH, Ba/As molar ratio, and common/diverse ion concentration. The availability of sodium and chloride ions at suitable pH and Ba/As molar ratio in the system induces formation of $NaBaAsO_4 \cdot 9H_2O$ and $Ba_5Cl(AsO_4)_3$ thereby inhibiting formation of $Ba_3(AsO_4)_2$ in such conditions. When QUAT is present during the precipitation, the $BaHAsO_4 \cdot H_2O$ and $Ba_5Cl(AsO_4)_3$ crystals were observed to change morphology by elongating and to increase the size of the crystals formed. Dissolution studies of $BaHAsO_4 \cdot H_2O$, $NaBaAsO_4 \cdot 9H_2O$, and $Ba_5Cl(AsO_4)_3$ give $-\log K_{SP}$ values of 5.60(5) for $BaHAsO_4 \cdot H_2O$, comparable to the previous literature, while for $NaBaAsO_4 \cdot 9H_2O$ and $Ba_5Cl(AsO_4)_3$ the previously unreported values are 10.8(3), and 35.3(4), respectively. Incongruent dissolution observed in $NaBaAsO_4 \cdot 9H_2O$ and $Ba_5Cl(AsO_4)_3$ dissolution systems is demonstrated to be due to the formation of

$Ba_3(AsO_4)_2$ phase which is confirmed by saturation index calculation. Thus, while $Ba_3(AsO_4)_2$ may be the preferred phase in the absence of other ions at high pH, the presence of sodium and chloride ions in the system can shift the equilibrium to prefer $NaBaAsO_4 \cdot 9H_2O$ and/or $Ba_5Cl(AsO_4)_3$ to precipitate. Based on the precipitation and dissolution study results, barium-arsenate precipitation is not suitable for arsenate precipitation from PEUF retentate stream.

Arsenate can be successfully removed by coprecipitation with low solubility calcium phosphate hydroxyapatite. Up to 99% arsenic removal was achieved from 25 ppm initial As concentration in both the absence and presence of QUAT in the system. Higher Ca/(P+As) and P/As mole ratios gave higher arsenic removal efficiencies with the highest arsenic removal efficiency obtained at Ca/(P+As) = 3 and P/As mole ratio = 5. The pH of the initial anionic solution has no significant effect on arsenic removal by this process. Semi-batch crystallization produces similar products to the batch precipitation experiment as demonstrated by XRD characterization, and further confirmed by TEM/EDX examination which confirms an arsenic constituent in the precipitation product. This work provides a basis for removing arsenic from QUAT-arsenate complex solution, freeing the QUAT for reuse.

School of Chemistry   Student's Signature _____

Academic Year 2010   Advisor's Signature _____

ACKNOWLEDGEMENTS

I would like to express sincere thanks to my research advisor, Assoc. Prof. Dr. Kenneth J. Haller, for his patience to teach me how to fish in a scientific context. I appreciate his advice, support, and help in both physical and psychological aspects throughout my time in his group. No words can cover all of my appreciation to him, thank you very much.

Very special thanks for my thesis coadvisor, Assoc. Prof. Dr. Adrian E. Flood, for his advice, and support in scientific ideas; my overseas coadvisor, Prof. John F. Scamehorn, for his kind support during my time to conduct research in his laboratory. Also thanks for Assoc. Prof. Dr. Malee Tangsathitkulchai who supported me from the first until the last day of my study at SUT.

Special thanks for my elder brother, Dr. Kittipong Chainok, for all of his sharing since the first day we met. I would also like to thank all of the alumni and current KJH group members for their mental support, wonderful friendships, and encouragements.

Finally, thanks to my mom, dad, and Ms. Kamonwan Wichai for their hands to hold me the rest of my and their life.

Winya Dungkaew

CONTENTS

CONTENTS (Continued)

CONTENTS (Continued)

CONTENTS (Continued)

LIST OF TABLES

LIST OF FIGURES

LIST OF FIGURES (Continued)

LIST OF FIGURES (Continued)

LIST OF ABBREVIATIONS

Å   Angstrom

ppb   part per billion

μg/L   microgram per liter

mg/kg   milligram per kilogram

WHO   World health organization

USEPA   United state environment protection agency

PEUF   Polyelectrolyte-enhanced ultrafiltration

QUAT   Poly(diallyldimethyl ammonium chloride)

IX   Ion exchange

GFH   Granular ferric hydroxide

C/MF   Coagulation/microfiltration

C/F   Coagulation/filtration

MCL   Maximum contaminant level

KHP   Potassium hydrogen phthalate

AAS   Atomic absorption spectroscopy

FAAS   Flame atomic absorption spectroscopy

ICP-MS   Inductively coupled plasma mass spectrometry

XRD   Powder X-ray diffraction

JCPDS   Joint committee on powder diffraction standards

kV   kilovolt

LIST OF ABBREVIATIONS (Continued)

mA	milliampere
SEM	Scanning electron microscope
TEM	Transmission electron microscope
EDX	Energy dispersive X-ray fluorescence
HDPE	High density polyethylene
K_{SP}	Solubility product constant
I	Ionic strength
LLNL	Lawrance Livermore National Laboratory
SI	Saturation index
IAP	Ion activity product
MWCO	Molecular weight cut-off
CaPHAP	Calcium phosphate hydroxyapatite
As-CaPHAP	Arsenate incorporated calcium phosphate hydroxyapatite
CaAsHAP	Calcium arsenate hydroxyapatite

CHAPTER I

GENERAL INTRODUCTION

1.1   Arsenic occurrence

Arsenic is the twentieth most abundant naturally occurring element in the earth's crust at 2×10^{-4} wt%. It occurs in more than 200 minerals of which arsenopyrite (FeAsS) is the most abundant (Smedley and Kinniburgh, 2002). Other common arsenic minerals are listed in Table 1.1.

Arsenic is also found as a constituent in other common rock-forming minerals in varying concentration (Arehart, Chryssoulis, and Kesler, 1993; Baur and Onishi, 1969; Boyle and Janasson, 1973; Dudas, 1984; Fleet and Mumin, 1997; Pichler, Veizer, and Hall, 1999; Smedley *et al.*, 2002; Stewart, 1963). High arsenic concentration is mainly found in sulfide minerals, perhaps due to similarity between the chemistry of arsenic and that of sulfur. High arsenic concentration is also found in oxide minerals, especially for Fe oxide which may due to sorption chemistry of arsenic species and its surface. Typical arsenic concentration found in common rock-forming minerals is listed in Table 1.2.

Table 1.1 Common arsenic minerals.

Mineral group	Mineral name	Formula
Arsenate	Olivenite	$Cu_2(AsO_4)OH$
	Scorodite	$FeAsO_4 \cdot 2H_2O$
Sulfides and sulfosalts	Arsenopyrite	$FeAsS$
	Cobaltite	$CoAsS$
	Enargite	Cu_3AsS_4
	Orpiment	As_2S_3
	Realgar	As_4S_4
	Tennantite	$(Cu,Fe)_{12}As_4S_{13}$
Arsenides	Nickeline	$NiAs_2$
	Safflorite	$(Co,Fe,Ni)As_2$
	Skutterudite	$CoAs_3$
Oxides	Arsenolite	As_2O_3
	Claudite	As_2O_3

Table 1.2 Typical arsenic concentration found in common rock-forming minerals.

Minerals	[As] range (mg/kg)	Minerals	[As] range (mg/kg)
Sulfide minerals:		**Carbonate Minerals:**	
Pyrite	100-77,000	Calcite	1-8
Marcasite	20-126,000	Dolomite	<3
Sphalerite	5-17,000	Siderite	<3
Charcopyrite	10-5,000	**Sulfate minerals:**	
Oxide minerals:		Gypsum/anhydrite	<1-6
Haematite	Up to 160	Barite	<1-12
Fe(III) oxyhydroxide	Up to 76,000	Jarosite	34-1,000
Silicate minerals:		**Other minerals:**	
Quartz	0.4-1.3	Apatite	<1-1,000
Feldspar	<0.1-2.1	Halite	<3-30
Biotite	1.4	Fluorite	<2

In addition to mineral sources, relatively small amounts of arsenic contamination can also be generated from other sources, including rocks, sediments, soils, volcanic activity, and human activity like agricultural activity, industrial operation, and fossil-fuel combustion. The average arsenic concentration in igneous rock types is 1.5 mg/kg (Ure and Berrow, 1982) while arsenic concentration in metamorphic rocks and sedimentary rocks are typically under 10 mg/kg (Webster, 1999). Arsenic concentration in sediment depends on texture and mineralogy but generally is in the range of 3-10 mg/kg (Smedley *et al.*, 2002) even in river sediments where arsenic concentration in groundwater is very high (Datta and Subramanian, 1997). Average arsenic concentration in soils is 5-10 mg/kg depending on the local

geological formations (Smedley *et al.*, 2002). Arsenic contamination from human activity is generally found near industrial and urban areas (WHO, 2001).

1.2 Arsenic contamination in natural water

Contamination around the world

Arsenic contamination in natural water has been a serious concern for some time due to the effects of arsenic on human health. Arsenic contamination in aquifers and surface water sources is found in many places throughout the world (Mandal and Suzuki, 2002; Smedley *et al.*, 2002; The World Bank, 2005). Typical arsenic concentrations found in surface water are 0.13-2.10 μg/L (Smedley *et al.*, 2002), and typical arsenic concentrations in groundwater in most countries is less than 10 μg/L. However, high arsenic concentrations are found under stimulate conditions including oxidizing condition, reducing condition, geothermal condition, and mining activity. As high as 50-10,000 μg/L arsenic contamination in mining contaminated groundwater (Welch, Lico, and Hughes, 1988; Williams, Fordyce, Paijitprapapon, and Charoenchaisri, 1996; Wilson and Hawkins, 1978) and <10-50,000 μg/L in geothermal groundwater (Baur *et al.*, 1969; White, Hem, and Waring, 1963) have been reported.

The most serious arsenic contamination in groundwater in terms of population exposed is in Bangladesh and West Bengal, India where arsenic concentrations in groundwater range from <0.5 to 3,200 μg/L (The World Bank, 2005). A study of about 140,000 people from the two areas (Rahman *et al.*, 2001) reported 12,195 patients with arsenical skin lesions. In addition up to 30-35 million people in

Bangladesh and about 6 million people in West Bengal are estimated to be at risk from arsenic contaminated drinking water above 50 ppb (Rahman *et al.*, 2001). Reported arsenic contaminations in groundwater in various parts of the world are represented in Figure 1.1 and summarized in Table 1.3.
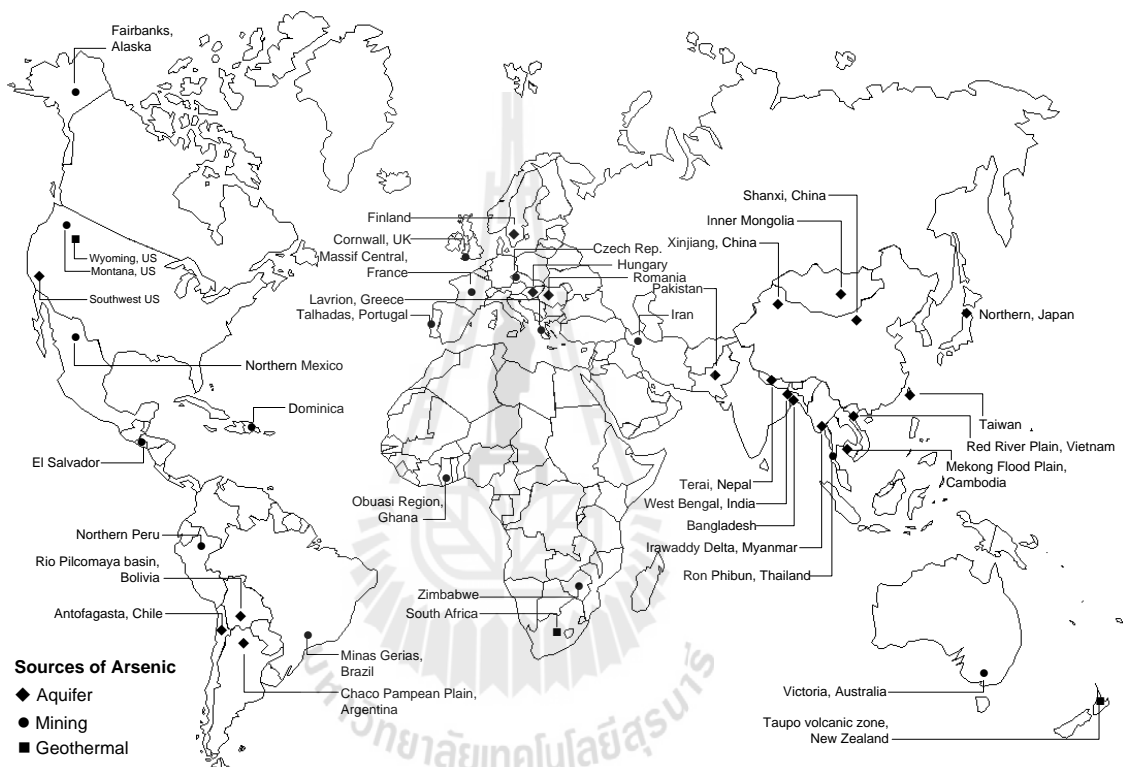
Figure 1.1 Arsenic contamination around the world.

Table 1.3 Summary of reported arsenic contaminations in groundwater and estimated
population at risk in various parts of the world.

Locations	[Arsenic], µg/L	Estimated population at risk
Bangladesh	<0.5-2,500	30-35 million
West Bengal, India	<10-3,200	6 million
Taiwan	10-1,820	5.6 million
Inner Mongolia	<1-2,400	100,000
Xinjiang, China	40-750	500
Nepal	<10-200	550,000
Red river, Vietnam	1-3,050	>1 million
Hungary	<2-176	29,000
Argentina	1-5,300	2 million
Northern Chile	100-1,000	500,000
Southwest USA (Arizona, California, Nevada)	Up to 2,600	350,000
Mexico	8-620	400,000

Contamination in Thailand

Arsenic contamination in Thailand has been reported associated with mining
activity in Ron Phibun district, Nakhon Si Thammarat province. Arsenic
concentrations in water from Ron Phibun (Williams *et al.*, 1996) are shown in Table
1.4. Arsenic concentrations greater than 50 ppb were common in surface water and
<15 meter shallow aquifer, but less common in aquifers deeper than 15 meters, where
arsenic concentration were generally less than 10 ppb. The highest arsenic

concentration found in surface water and the shallow aquifer were 580 μg/L and 5,100 μg/L, respectively.

Table 1.4 Arsenic concentrations in water from Ron Phibun, Nakhon Si Thammarat province, Thailand (Williams *et al.*, 1996).

Aquifers	Number of samples (%)			
	<10 μg/L	10-50 μg/L	>50 μg/L	Total
Surface water	1 (4)	2 (8)	20 (83)	24
<15 m shallow aquifer	7 (30)	7 (30)	9 (39)	23
>15 m deeper aquifer	9 (69)	2 (15)	2 (15)	13

In terms of health effects on humans, a sampling of adults from 58 households in the Ron Phibun area showed 9% with skin effects from arsenic poisoning (Foy, Tarmapai, Eamchan, and Metdilogkul, 1992), and by 1997 around 1,000 people in the Ron Phibun area had been diagnosed with arsenic related skin disorder (Choprapawon and Rodcline, 1997; Williams, 1997). No additional reports on arsenic effect on humans from this area are available.

Arsenic occurrence in the surface waters in the Chao Phraya basin, central Thailand, has also been studied (Kohnhorst, Allan, Pokethitiyoke, and Anyapo, 2002). Low arsenic concentrations in surface water from canals and ponds in the area in the range of 0-5 μg/L from 37 different surface waters were reported.

1.3   Effects of arsenic exposure on human health

Human arsenic exposure occurs by utilization of arsenic contaminated water. Exposure to high arsenic concentrations may create acute toxicity as arsenate interferes with ATP production and arsenite can bind and inactivate sulfhydryl-containing enzymes (Lantz, Parliman, Chen, and Carter, 1994). Arsenite is generally a more potent acute toxin than arsenate with LD50 values (in rat) of 15-110 mg/kg, and 110 mg/kg for arsenite and arsenate, respectively (ATSDR, 1993). Long term exposure to low concentration arsenic in drinking water can lead to a variety of skin, bladder, lung, liver, and kidney cancers (Chen and Wang, 1990; Chen, Chen, Wu, and Kuo, 1992; Chen, Kuo, and Wu, 1988). Ingestion of low levels of arsenic also induces cardiovascular disease, diabetes, and anemia as well as affecting the reproductive, developmental, immunological, and neurological processes in humans (Kapaj, Peterson, Liber, and Bhattacharya, 2006).

1.4   Regulations and guidelines for arsenic in drinking water

The first US national standard of 50 μg/L (50 ppb) for arsenic in public drinking water was adopted by the Public Health Service in 1942. On implementation of the national (US) Safe Drinking Water Act in 1975, regulation of arsenic in drinking water passed to the recently formed United States Environmental Protection Agency (USEPA) where it is vested today. There was general agreement that 50 ppb did not eliminate risks from chronic exposure to arsenic, and the level continued to be studied. By the late 1980s the US Congress had mandated a lower standard and the USEPA was grappling with the complicated health, feasible technology, and cost issues with study focusing on a range for the new maximum contaminant level

(MCL) from 3 μg/L to 20 μg/L. In 2001 the USEPA finally promulgated their new standard, setting the maximum contaminant level goal (MCLG) at 0 μg/L and the new MCL at 10 μg/L for arsenic in drinking water, effective in 2006 (USEPA, 2001). One of the lower standards of the world, 7 μg/L, was adopted in Australia in 1996 (NHMRC/AWRC, 1996) as the debate continued on the maximum safe levels.

The international drinking water standard for arsenic was issued by the World Health Organization (WHO) in 1958 for 200 μg/L. Later, WHO (1963) recommended the lower value of 50 μg/L. With the concerns regarding chronic and carcinogenic effects of arsenic compounds, especially regarding internal cancers, the WHO introduced provisional guideline recommendations (1993) lowering the value to 10 μg/L. The WHO guideline is not a mandatory limit but is to be used as a basis for setting up national standards to ensure safety of public health. Governments also consider local environment, social, economic, and cultural conditions in setting their own standards.

Most developed countries have adopted the WHO arsenic guideline of 10 ppb arsenic in public drinking water as their national standard while most developing countries including Thailand still use 50 ppb as arsenic standard in drinking water. The national standard of arsenic in drinking water of selected countries is shown in Table 1.5.

Table 1.5 National standards for arsenic in drinking water of selected countries.

Country	Standard, ppb	Country	Standard, ppb
Australia	7	Bangladesh	50
European Union	10	India	50
Japan	10	Pakistan	50
USA	10	Nepal	50
Vietnam	10	China	50
Canada	25	Lao PDR	50
		Myanmar	50
		Cambodia	50
		Thailand	50

1.5 Arsenic solution chemistry

Arsenic in water typically occurs from dissolution of minerals, rocks, and ores. It is generally found in oxidation states +3 (arsenite) and +5 (arsenate) forms which depend on oxidation-reduction conditions. Typically, arsenite forms are found in anoxic groundwater while arsenate forms are generally found in aerobic surface water. Arsenic acid can dissociate to provide a variety of oxyanions depending on the solution pH. Arsenic acid dissociation constants are provided below, and a speciation diagram of arsenic acid drawn based on these dissociation constants is shown in Figure 1.2.

Arsenic acid dissociation constants:

$$H_3AsO_4 \quad \rightleftharpoons \quad H^+ + H_2AsO_4^- \qquad\qquad pKa = 2.22$$

$$H_2AsO_4 \quad \rightleftharpoons \quad H^+ + HAsO_4^{2-} \qquad\qquad pKa = 6.89$$

$$HAsO_4^{2-} \quad \rightleftharpoons \quad H^+ + AsO_4^{3-} \qquad\qquad pKa = 11.53$$
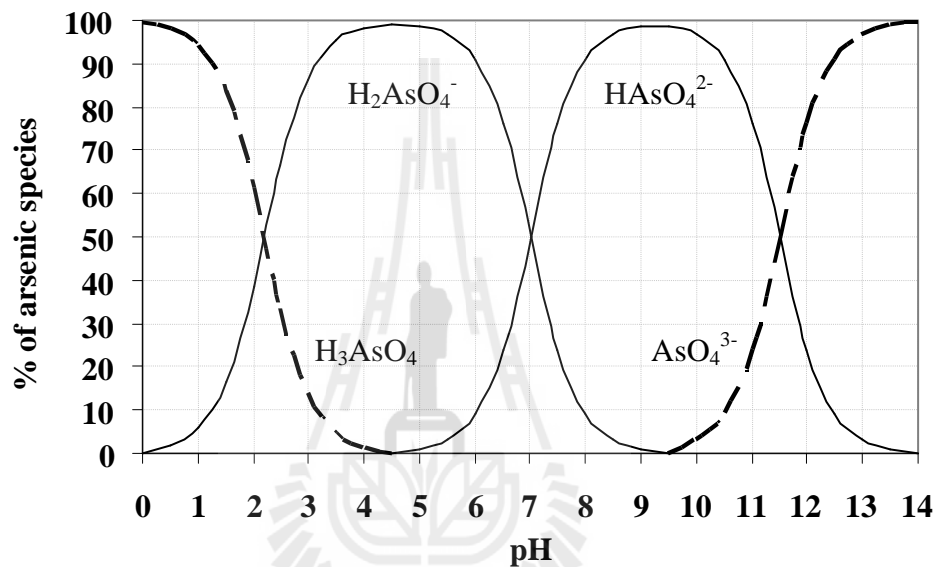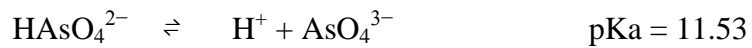
Figure 1.2 Speciation diagram of arsenic acid.

According to the speciation diagram, the neutral form of arsenic acid (H_3AsO_4) is the dominant species at pH less than 2.2. As pH increases deprotonated species of arsenic acid predominate, resulting in $H_2AsO_4^-$, $HAsO_4^{2-}$, and AsO_4^{3-} becoming predominant species at higher pH range of 2.2-6.9, 6.9-11.5, and >11.5, respectively.

1.6   Basics of crystallization

Crystallization is a process for particulate formation by changing the state of a solute in solution to a crystalline solid. It is widely used for separation and purification purposes, and can give solid products of high purity (Shan, Igarashi, Noda, and Ooshima, 2002). The most important crystallization process is crystallization from solution which is widely used in several industries including food, pharmaceutical, and chemical production.

For crystallization to occur requires suitable thermodynamic and kinetic conditions. A general crystallization process can be described in three steps:

Supersaturation: is the thermodynamic state of the system in which concentration of the solute in the solution is higher than the equilibrium (saturated) concentration (Myerson, 1999). It is the driving force for crystallization. When considering the crystallization reaction as a chemical equilibrium:

$$xA^{z+}(aq) + yB^{z-}(aq) \rightleftharpoons A_xB_y(s)$$
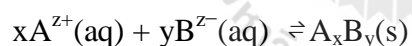
The saturation ratio (S) is defined as (Mersmann, 1995; Demopoulos, 2009):

$$S = a_{A^{z+}} a_{B^{z-}} / K_{SP} \qquad\qquad ……….(1)$$

where a_i denotes the thermodynamic activity of species i in solution, x and y are equal to the number of cation A and anion B, respectively, in the neutral compound, and K_{SP} is the solubility product constant, defined as:

$$K_{SP} = a^*_{A^{z+}} a^*_{B^{z-}} \qquad\qquad ……….(2)$$

where a^*_i denotes the thermodynamic activity of the species i at equilibrium. According to thermodynamics the crystallization of the solid phase will occur when

$$\Delta G = -RT\ln S < 0 \qquad\qquad ……….(3)$$

Where ΔG is the change in Gibbs free energy of the reaction, R is the gas constant, T is the absolute temperature, and S is the saturation ratio. When $S > 1$, then $\Delta G < 0$. This is the supersaturated state and crystallization is then spontaneous.

Considering the solubility curve of a typical single solute compound in Figure 1.3, the concentration of solute increased when temperature increased. Therefore, supersaturation can be achieved by many approaches, such as cooling (decreasing temperature), evaporating solvent (reducing the total volume, increasing concentration), and salting out (decreasing solubility) (Nyvlt, 1992).
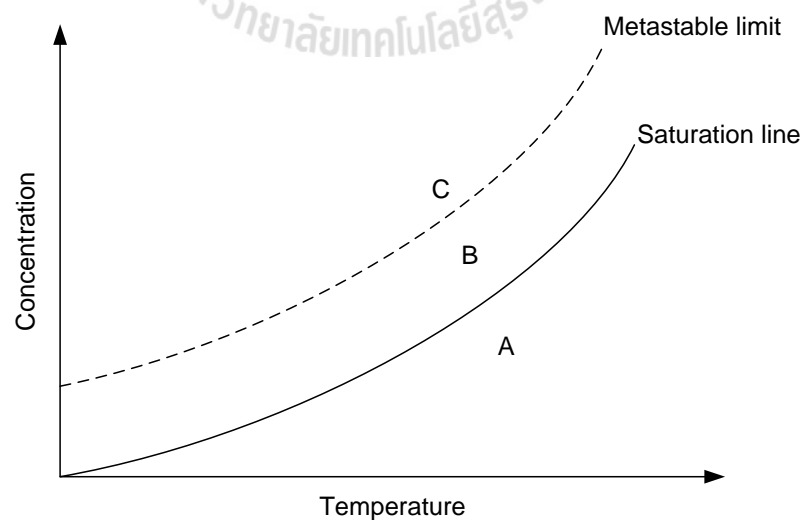
Figure 1.3 Solubility curve of typical single solute compound.

Region A in Figure 1 is under the saturation line which indicates the concentration at equilibrium in the solution, this region is called the "undersaturation" region. No crystallization occurs in this region. Above the saturation line, regions B and C, the concentration in the solution is greater than the concentration at equilibrium in the solution, this is called the "supersaturated" region. The difference in concentration between the solution and at equilibrium is the driving force for crystallization; crystallization can occur in both B and C regions. However, in region B the concentration is only a little larger than the equilibrium concentration (saturation) and nuclei do not immediately form, which is thus a "metastable zone". Once a nuclei is formed or introduced (seed crystal), crystallization proceeds in this region. In region C, there is a large enough driving force that crystallization immediately occurs spontaneously.

Nucleation: is the step for new crystal formation in a supersaturated phase. Crystal nuclei may form from various kinds of entities such as molecules, atoms, or ions into a small particle called a cluster. Clusters associate into an embryo, which is thermodynamically stable, and is the beginning of a lattice arrangement and the formation of a new separated phase (crystal).

Crystal growth: is the growth of a nucleus into a macroscopic crystal. The mechanism of crystal growth requires transport of solute to the crystal surface and then orientation into the crystal lattice. This is generally modeled as two required steps, a diffusion step, followed by a surface reaction (integration) step.

Precipitation

Typically crystallization from solution occurs at relatively low levels of supersaturation, therefore time is required for nuclei formation (nucleation) and growth of the crystal (crystal growth). In contrast, precipitation typically occurs at high supersaturation, therefore fast chemical reaction occurs resulting in nuclei formation and immediate growth of the crystals. However, crystallization and precipitation both occur based on the same theoretical concept. Both processes require a supersaturated state of the target compound in solution prior to the phenomenon occurring.

Effect on crystallization product

Certain crystal properties, especially high purity and uniform size and shape (morphology), can be obtained by a suitable crystallization technique. Size and shape strongly affect the separation of crystallized product from the solution. Many crystallization conditions affect the crystal size and shape such as supersaturation level, nucleation rate, agglomeration, breakage, growth rate, geometrical configuration of crystallizer (Shan *et al.*, 2002), crystal-impeller blade impacts (Synowiec, 2002), collisions between crystal-crystal and crystal-vessel (Pratora, Simons, and Jones, 2002), and mixing conditions (Kim and Tarbell, 1996; Marchisio, Barresi, and Garbero, 2002; Zauner and Jones, 2000). Therefore, crystallization process control is very important to achieve high quality of the crystallization product.

1.7   Polyelectrolyte-enhanced ultrafiltration (PEUF) for arsenic contamination treatment

The PEUF process using poly(diallyldimethyl ammonium chloride), QUAT, cationic polyelectrolyte (repeating unit shown in Figure 1.4) to bind with the arsenate anion and treating the solution using ultrafiltration with a 10 kDa molecular weight cut-off membrane has been demonstrated to achieve up to 99.95% arsenate removal from synthetic aqueous solutions with a starting arsenic concentration of 100 ppb (Pookrod, Haller, and Scamehorn, 2004). Thus, the PEUF process can produce water to meet the new 10 ppb MCL standard set by the USEPA and recommended by the WHO for arsenic in drinking water. A schematic diagram of their batch scale PEUF is shown in Figure 1.5.
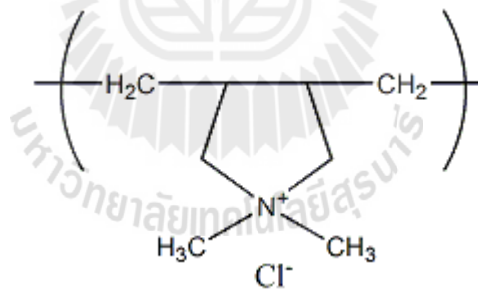
Figure 1.4 Poly(diallyldimethyl ammonium chloride), cationic polyelectrolyte repeating unit.
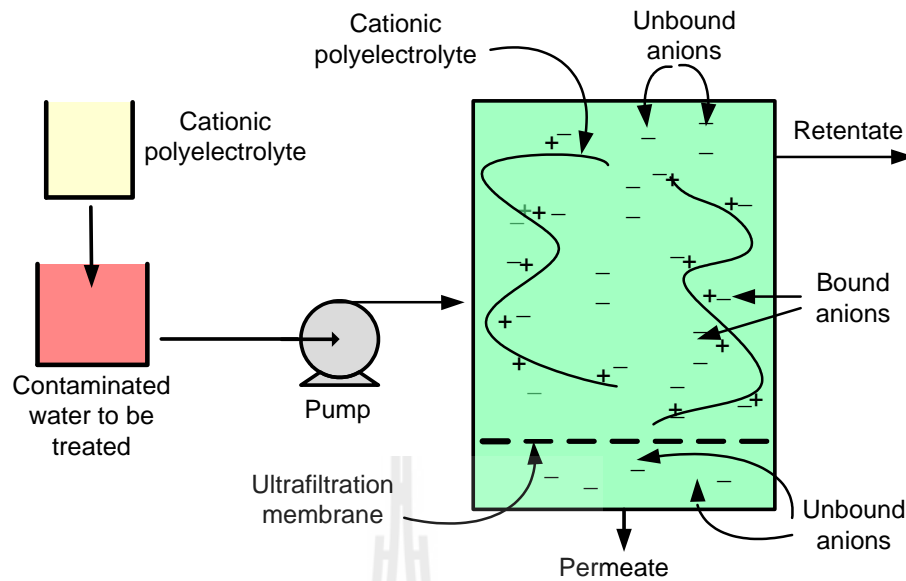
Figure 1.5 Schematic diagram of batch scale PEUF process.

Pilot scale-up, using the same polyelectrolyte and the PEUF concept for arsenic removal has been demonstrated and up to 95% arsenic removal was achieved (Gallo, Acosta, Scamehorn, and Sabatini, 2006). A schematic diagram of this pilot scale PEUF is shown in Figure 1.6.
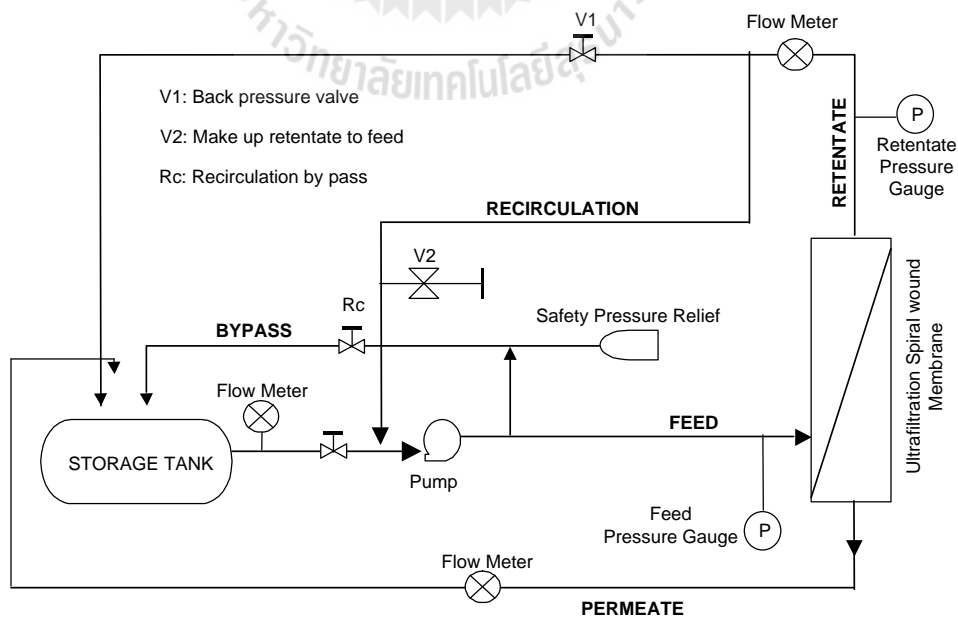
Figure 1.6 Schematic diagram of pilot scale PEUF process.

1.8 Current study: polyelectrolyte recovery for PEUF process

To make the PEUF process more economical and environmental friendly, the QUAT must be recovered for reuse in the process to save the chemical and minimize waste. Basis on 85% polyelectrolyte recovery let the PEUF provide lowest total unit cost/volume of produced water compare to ion exchange (IX), granular ferric hydroxide (GFH), coagulation/microfiltration (C/MF), and coagulation/filtration (C/F)) techniques as shown in comparison bar chart in Figure 1.7 (Gallo *et al.*, 2006).
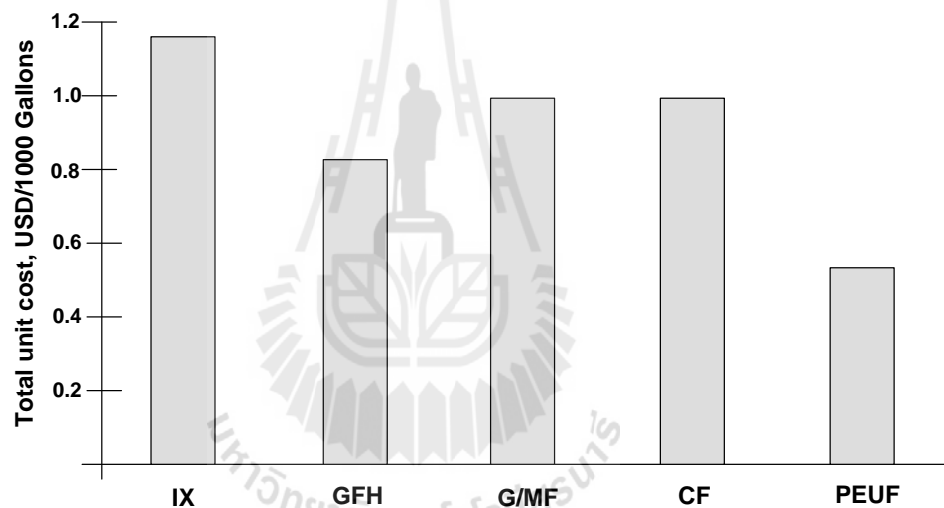
Figure 1.7 Total cost comparison of PEUF process versus other technologies.

The QUAT can be recovered by precipitation of the arsenate anion from the PEUF waste stream, QUAT-arsenate solution, by a metal cation. The precipitation process was considered due to its low cost and high feasibility. The best cation for arsenate precipitation must form a very low K_{SP} product with arsenate anion that should lead to a stable solid phase product even in a system that contains very low arsenic concentration.

The recovered QUAT to be reused in the PEUF process after the metal-arsenate compound is separated from the QUAT solution. The crystalline compounds formed can be separated by simple settling or gravity force if the particle size is suitable, or if high-density particles are formed. Centrifugation or hydrocyclone separation may be required if fine particles are formed. Different compounds have different physical properties, so it is important to know what compounds are formed as well as their precipitation properties to apply in crystallization experiments. The concept of this research is represented as a schematic diagram shown in Figure 1.8.
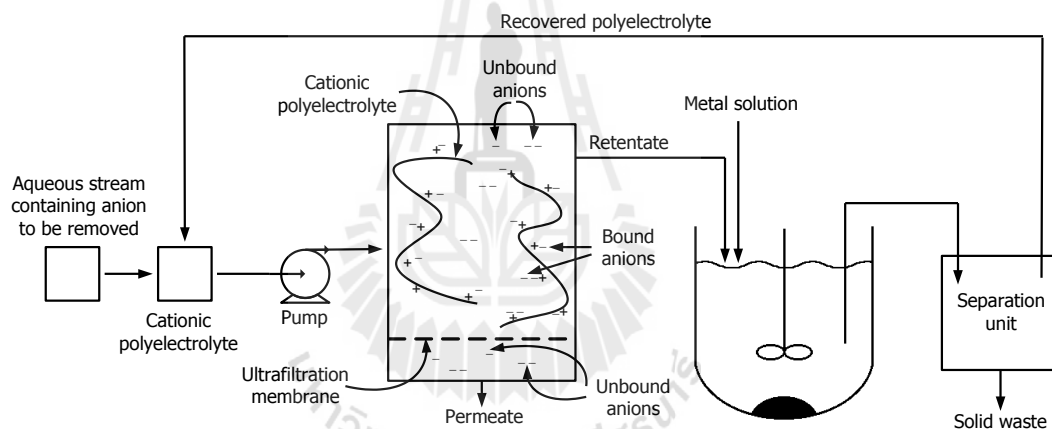
Figure 1.8 Conceptual schematic diagram of this research.

1.9   References

Arehart, G. B., Chryssoulis, S. L., and Kesler, S. E. (1993). Gold and Arsenic in Iron Sulfides from Sediment-hosted Disseminated Gold Deposits-Implications for depositional Processes. **Econ. Geol. Bull. Soc. Econ. Geol.** 88: 171-185.

ATSDR (Agency for Toxic Substances and Disease Registry). (1993). **Toxicological Profile for Arsenic.** U.S. Department of Health and Human Services.

Baur, W. H. and Onishi, B.-M. H. (1969). Arsenic. In: **Handbook of Geochemistry** (Edited by Wedepohl, K. H.). Springer-Verlag, Berlin. pp. 33-A-1-33-0-5.

Boyle, R. W. and Jonasson, I. R. (1973). The Geochemistry of As and Its Use as an Indicator Element in Geochemical Prospecting. **J. Geochem. Explor.** 2: 251-296.

Chen, C. J. and Wang, C. J. (1990). Ecological Correlation between Arsenic Level in Well Water and Age-adjusted Mortality from Maglignant Neoplasms. **Cancer Res.** 50: 5470-5474.

Chen, C. J., Chen, C. W., Wu, M. M., and Kuo, T. L. (1992). Cancer Potential in Liver, Lung, Bladder, and Kidney Due to Ingested Inorganic Arsenic in Drinking Water. **Br. J. Cancer.** 66: 888-892.

Chen, C. J., Kuo, T. L., and Wu, M. M. (1988). Arsenic and Cancers. **Lancet.** 1: 414-415.

Choprapawon, C. and Rodcline, A. (1997). Chronic Arsenic Poisoning in Ronpibool Nakhon Sri Thammarat, the Southern Province of Thailand. In: **Arsenic: Exposure and Health Effects** (Edited by: Abernathy C. O., Calderon R. L., Chappel, W. R.). Chapman and Hall, London. pp. 69-77.

Datta, D. K. and Subramanian, V. (1997). Texture and Mineralogy of Sediments from the Ganges-Brahmaputra-Meghna River System in the Bengal Basin, Bangladesh and Their Environmental Implications. **Environ. Geol.** 30: 181-188.

Demopoulos, G. P. (2009). Aqueous Precipitation and Crystallization for the Production of Particulate Solids with Desired Properties. **Hydrometallurgy.** 96: 199-214.

Dudas, M. J. (1984). Enriched Levels of Arsenic in Post-active Acid Sulfate Soils in Alberta. **Soil Sci. Soc. Am. J.** 48: 1451-1452.

Fleet, M. E. and Mumin, A. H. (1997). Gold-bearing Arsenian Pyrite and Marcasite and Arsenopyrite from Carlin Trend Gold Deposits and Laboratory Synthesis. **Am. Mineral.** 82: 182-193.

Foy, H. M., Tarmapai, S., Eamchan, P., and Metdilogkul, O. (1992). Chronic Arsenic Poisoning from Well Water in a Mining Area in Thailand. **Asia Pac. J. Public Health.** 6(3): 150-152.

Gallo, D., Acosta, E., Scamehorn, J. F., and Sabatini, D. A. (2006). Pilot Scale Study of Polyelectrolyte Enhanced Ultrafiltration for Arsenic Removal. **J. Am. Water Works Assoc.** 98(1): 106-116.

Kapaj, S., Peterson, H., Liber, K., and Bhattacharya, P. (2006). Human Health Effects from Chronic Arsenic Poisoning−A Review. **J. Environ. Sci. Health, Part A**. 41: 2399-2428.

Kim, W. S. and Tarbell, J. M. (1996). Micromixing Effects on Barium Sulfate Precipitation in an MSMPR Reactor. **Chem. Eng. Comm.** 146: 33-56.

Kohnhorst, A., Allan, L., Pokethitiyoke, P., and Anyapo, S. (2002). **Groundwater Arsenic in Central Thailand.** Proceedings of the 28th WEDC Conference, Kilkata (Calcutta), India.

Lantz, R. C., Parliman, G., Chen, G. J., and Carter, D. E. (1994). Effect of Arsenic Exposure on Alveolar Macrophage Function. I. Effect of Soluble As(III) and As(V). **Environ. Res.** 67: 183-195.

Mandal, B. K. and Suzuki, K. T. (2002). Arsenic Round the World: A Review. **Talanta.** 58(1): 201-35.

Marchisio, D. L., Barresi, A. A., and Garbero, M. (2002). Nucleation, Growth, and Agglomeration in Barium Sulfate Turbulent Precipitation. **AIChE.** 48(9): 2039-2050.

Mersmann, A. (2001). **Crystallization Technology Handbook.** 2nd edition, Marcel Dekker, New York.

Myerson, A. S. (1999). **Molecular Modeling Application in Crystallization.** Cambridge University Press, Cambridge, UK.

NHMRC/AWRC (National Health and Medical Research Council, and Agricultural and Resource Management Council of Australia and New Zealand). (1996). **Australian Drinking Water Guidelines,** Australia.

Nyvlt, J. (1992). **Design of Crystallizers.** CRC press, Florida.

Pichler, T., Veizer, J., and Hall, G. E. M. (1999). Natural Input of Arsenic into a Coral Reef Ecosystem by Hydrothermal Fluids and its Removal by Fe(III) Oxyhydroxides. **Environ. Sci. Technol.** 33: 1373-1378.

Pookrod, P., Haller, K. J., and Scamehorn, J. F. (2004). Removal of Arsenic Anions from Water using Polyelectrolyte-Enhanced Ultrafiltration. **Sep. Sci. Technol.** 39(4): 811-831.

Pratora, F., Simons, S. J. R., and Jones, A. G. (2002). A Novel Experimental Device for Measurement of Agglomerative Crystallization Forces. **Trans IChemE.** 80: 441-448.

Rahman, M. M., Chowdhury, U. K., Mukherjee, S. C., Mondal, B. K., Paul, K., Lodh, D., Biswas, B. K., Chanda, C. R., Basu, G. K., Saha, K. C., Roy, S., Das, R., Palit, S. K., Quamruzzaman, Q., and Chakraborti, D. (2001). Chronic Arsenic

Toxicity in Bangladesh and West Bengal, India−A Review and Commentary. **Clin. Toxic.** 39(7): 683-700.

Shan, G., Igarashi, K., Noda, H., and Ooshima, H. (2002). Production of Large Crystals with a Narrow Crystal Size Distribution by a Noval WWDJ Batch Crystallizer, **Chem. Eng. J.** 85: 161-167.

Smedley, P. L. and Kinniburgh, D. G. (2002). A Review of the Source, Behaviour, and Distribution of Arsenic in Natural Waters. **Appl. Geochem.** 17(5): 517-568.

Stewart, F. H. (1963). Data of Geochemistry, 6th ed. Chap. Y. Marine Evaporites. **US Geol. Surv. Prof. Pap.** 440-Y.

Synowiec, P. (2002). How to Improve the Crystal Size Distribution (CSD) in Crystallizers with the Inner Suspension Circulation, **Chem. Eng. Process.** 41: 585-593.

The World Bank (2005). **Towards a More Effective Operational Response Arsenic Contamination of Groundwater in South and East Asian Countries.** Volume 2, Technical Report, No. 31303.

Ure, A. and Berrow, M. (1982). Chapter 3. The Elemental Constituents of Soils. In: **Environmental Chemistry** (Edited by Bowen, H. J. M.). Royal Society of Chemistry, London, pp. 94-203.

Webster, J. G. (1999). Arsenic. In: **Encyclopedia of Geochemistry** (Edited by Marshall, C. P. and Fairbridge, R. W.). Chapman Hall, London, pp. 21-22.

Welch, A. H., Lico, M. S., and Hughes, J. L. (1988). Arsenic in Ground-water of the Western United States. **Ground Water.** 26: 333-347.

White, D. E., Hem, J. D., and Waring, G. A. (1963). Data of Geochemistry, 6th ed., M. Fleischer, (Ed). Chapter F. Chemical Composition of Sub-Surface Waters. **US Geol. Surv. Prof. Pap.** 440-F.

WHO (World Health Organization). (1958). **International Standards for Drinking-water,** World Health Organization, Geneva.

WHO (World Health Organization). (1963). **International Standards for Drinking-water,** 2nd ed., World Health Organization, Geneva.

WHO (World Health Organization). (1993). **Guidelines for Drinking-water Quality,** 2nd ed., vol.1, World Health Organization, Geneva.

WHO (World Health Organization). (2001). **Environmental Health Criteria 224: Arsenic Compounds**, 2nd ed., World Health Organization, Geneva.

Williams, M. (1997). Mining-related Arsenic Hazards: Thailand Case-study. Summary Report. **Brit. Geol. Surv. Tech. Rep.** WC/97/49.

Williams, M., Fordyce, F., Paijitprapapon, A., and Charoenchaisri, P. (1996). Arsenic Contamination in Surface Drainage and Groundwater in Part of the Southeast Asian Tin Belt, Nakhon Si Thammarat Province, Southern Thailand. **Environ. Geol.** 27: 16-33.

Wilson, F. H. and Hawkins, D. B. (1978). Arsenic in Streams, Stream Sediments and Ground Water, Fairbanks Area, Alaska**. Environ. Geol.** 2: 195-202.

Zauner, R. and Jones, A. G. (2000). Mixing Effects on Product Particle Characteristics from Semi-batch Crystal Precipitation. **Trans IChemE.** 78A: 894-902.

CHAPTER II

BARIUM-ARSENATE PRECIPITATION AND

SOLUBILITY STUDY

2.1   Introduction

Arsenic is a common contaminant in nature in both water and soil, and is of great concern due to it toxicity and wide exposure to living organisms (Mandal *et al.*, 2002; Oremland and Stolz, 2003; Smedley *et al.*, 2002). The interest in arsenic intensified with the widespread poisoning of Bangladeshi people due to the rapid development of shallow tube wells for drinking water (Smith, Lingas, and Rahman, 2000), followed by the promulgation of lowered maximum contaminant levels (MCL) for arsenic in drinking water (NHMRC/AWRC, 1996; United States Environmental Protection Agency, 2001; WHO, 1993).

Many processes have been studied and developed in recent decades in the attempt to solve this problem. Among the variety of techniques, polyelectrolyte-enhanced ultrafiltration (PEUF) has been studied as a process for removal of low concentrations of arsenic, and achievement of the most stringent MCL standard (Australia) for arsenic in drinking water of 7 ppb has been demonstrated using the PEUF process in both batch laboratory scale (Pookrod *et al.*, 2004) and continuous pilot scale process studies (Gallo *et al.*, 2006). For the PEUF process to be

economical as well as environmentally friendly, the polyelectrolyte used in the process must be recovered and reused.

The arsenic concentration in the PEUF waste stream is relatively low. Therefore, metal-arsenate compounds with low solubility product constant (K_{SP}) values are considered to be a target for precipitation. Among several metals, barium has been selected for arsenic precipitation study. The barium arsenate ($Ba_3(AsO_4)_2$) solubility product constant was first reported by Chukhlantsev (1956). Because of the extremely low K_{SP} value ($-\log K_{SP} = 50.11$) reported by Chukhlantsev, $Ba_3(AsO_4)_2$ became a target compound for arsenic removal by precipitation with barium, and several reports suggested that barium arsenate could be phase controlling for soluble arsenic in natural waters (Rai, Ainsworth, Eary, Mattigod, and Jackson, 1987; Turner, 1981; Wagemann, 1978). Essington (1988) reevaluated Chukhlantsev's value by correcting for ionic strength and found that barium arsenate is considerably more soluble ($-\log K_{SP} = 21.62$) than reported by Chukhlantsev. Essington also suggested that $Ba_3(AsO_4)_2$ might not be phase controlling for arsenic in natural systems due to possible phase transformations to sodium barium arsenate nonahydrate ($NaBaAsO_4 \cdot 9H_2O$) or barium chloride arsenate ($Ba_5Cl(AsO_4)_3$) in the presence of sodium or chloride ions, respectively. Later studies of the solubility product of $Ba_3(AsO_4)_2$ found good agreement with Essington's result (Davis, 2000; Zhu *et al.*, 2005). Pookrod (2004) studied precipitation of $Ba_3(AsO_4)_2$ as a potential way to recover polyelectrolyte from the PEUF process, a selection again based on the low K_{SP} value. The current work began as a follow up on that study, but extended to more detailed study of the precipitation of barium-arsenate compounds in the presence of sodium and chloride ions.

Stability of the phase is considerable in two aspects, thermodynamic stability and kinetic stability. For "chemical stability" is meaning to thermodynamically stable (IUPAC, 1997) which is an energetically stable state of a chemical system occurs when the energy of the system is in lowest state at chemical equilibrium with its surrounding. The stable state will persist indefinitely unless the system is changed. For other energy equilibrium state can either call "metastability" or "kinetic stability" which such phase can be converted to other phases containing lower energy at equilibrium if the energy barrier can be surmounted. Here, therefore, the metastability or kinetically stability phase is no longer stable (not stable anymore) if the system is disturbed adequately.

Chemical equilibrium is the thermodynamic property of the system which free energy (G) of the system is no change. Therefore, at equilibrium Gibss free energy change (ΔG) is equal to zero. ΔG is usually used to represent the spontaneity of the reaction. However, there is often ambiguity to relate (ΔG), K_{SP}, and stability of the phase. The stable phase in the given system is likely considering to contain lowest K_{SP} which also imply the lowest ΔG according to the relationship $\Delta G = -RT\ln K$, where R is a gas constant, T is thermodynamic temperature, and K is the equilibrium constant. It is suitable for such concept to consider stability of the interest phase if the phase is in the isolated system, the system with no interaction with other composition. The phase containing lowest ΔG should be the most stable phase in the isolated system. However, in the real solution with other compositions presented, the composition effect need also taken to account for stability consideration as well. The presence of other composition means the system is now changed, the system will arrange toward new equilibrium for the new system that may affect the stable phase in the system.

Therefore, the stability should be considered from the system point of view rather than only the property of the individual phase. Stability of the system is satisfy all equilibrium which arrange toward the lowest of Gibbs free energy of the system

Initially, the idea of stable phase and metastable phases, based on consideration of the Gibbs free energy of formation (ΔG_f) was explored and found to be inadequate to explain the phase precipitation region diagram. Subsequently, during the determination of K_{SP} values for the phases identified by Essington ($NaBaAsO_4 \cdot 9H_2O$ and $Ba_5Cl(AsO_4)_3$) it became apparent that a deeper understanding of the system equilibrium was necessary to understand the solid phases that precipitate as the composition of the system is varied. The effects of speciation as well as common/diverse ions on the solution equilibrium, and quintuple points and the incongruent dissolution phenomena that can be associated therewith were key elements in understanding the barium-arsenate precipitation system. This understanding will be important for further fundamental application and development of the precipitation model for better understanding of the arsenic distribution in a given system and the subsequent remediation thereof.

2.2   Experimental methods

Chemicals

The chemicals used in this work were analytical grade and used without further purification. Barium chloride dihydrate, $BaCl_2 \cdot 2H_2O$ (Carlo Erba, Milan, Italy), and disodium hydrogen arsenate heptahydrate, $Na_2HAsO_4 \cdot 7H_2O$ (Fluka, Buchs, Switzerland), were used as sources of barium and arsenate. 6 M hydrochloric acid, HCl (Merck, Darmstadt, Germany), and 6 M sodium hydroxide, NaOH (EKA

Chemicals, Bohus, Sweden), were selected for pH adjustment to accommodate very low and very high pH as well as to limit the total number of ions in the system (both of these chemicals are also commonly used in industrial processes for pH adjustment purposes). Potassium nitrate, KNO_3 (Carlo Erba, Milan, Italy), was used for ionic strength adjustment in dissolution experiments. Nitric acid, HNO_3 (Carlo Erba, Milan, Italy), was used to acidify the solution before composition analysis and silver nitrate, $AgNO_3$, for argentometric titration. Barium and arsenic standard solutions for atomic absorption spectroscopy, AAS (Merck, Darmstadt, Germany) were used for calibration of both flame atomic absorption spectroscopy, FAAS, and inductively coupled plasma-mass spectrometry, ICP-MS, analyses. Doubly-distilled water was used for all experiments.

The cationic polyelectrolyte, poly(diallyldimethyl ammonium chloride), QUAT, (trade name MERQUAT, Calgon Corp.) and treated by ultrafiltration using a 10 kDa molecular weight cut-off regenerated cellulose spiral wound membrane (Osomonics Inc.) prior to use to remove short chain QUAT using pilot scale ultrafiltration. The average molecular weight of about 240,000 Da corresponds to about 1400 units of the monomer, $(H_2C=CHCH_2)_2N(CH_3)_2Cl$, per molecule. QUAT concentrations were determined by total organic carbon measurement, standardized by potassium hydrogen phthalate (KHP) from Sigma. The concentration of carbon corresponds to QUAT concentration based on the QUAT polymer repeating formula unit.

Barium-arsenate precipitation in the absence of QUAT

Precipitation experiments were carried out in borosilicate screw-cap bottles. Barium and arsenate solutions were prepared such that when 10 mL of barium solution was added to 10 mL of arsenate solution the resulting Ba/As molar ratio was obtained in the range 0.5-3.0 with the starting arsenic concentration fixed at 0.08 M. Both solutions were adjusted to the target pH in the ranges 2.0-13.5 before mixing using either 6.0 M HCl or 6.0 M NaOH. After mixing, the solutions were allowed to react overnight at 24 $\pm 1°$C in a temperature controlled (air-conditioned) laboratory. The white precipitate was paper filtered, washed with distilled water, and air-dried at room temperature for 24 hr.

Barium-arsenate precipitation in the presence of QUAT

The barium-arsenate compound precipitation was carried out by preparation of arsenate-QUAT solution and barium solution in separate 50 mL cylinders. The arsenate and QUAT concentrations were fixed at 16 mM and 160 mM, corresponding to 8 mM arsenate and 80 mM QUAT, respectively, after dilution to 100 mL total volume. The barium solution was prepared in the concentrations varied to the desired Ba/As molar ratios 0.5-3.0 in steps of 0.5. The pH of both solutions was varied from 2.0-13.5 in steps of 0.5 pH units; HCl and NaOH solutions were used for pH adjustment. After adjustment to the desired pH value, the solutions were mixed in glass vials by pouring the barium solution into the QUAT-arsenate solution. The resulting solution was gently mixed and allowed to stand 1 day to equilibrate. The pH

of the supernatant was measured before separating the precipitate formed by filtration with filter paper. The compound was then air-dried at room temperature.

Characterization

Due to the limited amounts of sample obtained from the precipitation experiments, only small amounts (about 0.05 g) of precipitated samples were used in powder X-ray diffraction, XRD, characterizations for phase identification. The samples were ground using mortar and pestle to minimize preferred orientation of the crystallites, and then dusted onto the back side of a lightly greased XRD sample holder. The lightly greased sample holder was tested prior to use and no significant peaks in the range of 5.0-70.0° two theta were observed. Therefore, no blank subtraction was performed on the sample diffractogram prior to comparison with the Joint Committee on Powder Diffraction Standards, JCPDS, database for solid phase identification. XRD characterization used a Bruker Analytical X-ray Systems model D5005 X-ray diffractometer equipped with a Cu Kα sealed tube X-ray source operating at 40 kV and 35 mA. Data were collected in the range 5.0-70.0° two theta in steps of 0.02° and scan speed of 0.1 sec/step. XRD was the main technique used in this work for phase identification purposes. Low concentration minor phases present in a sample at the border regions in the precipitation diagram might not be identified by this technique due to limitation in quantity of the sample.

Scanning electron microscopy (JEOL model JSM-6400 SEM, equipped with a Microspec model WDX-100 EDX energy dispersive X-ray fluorescence attachment) was used to examine morphology and to verify heavy element composition in the precipitates.

Dissolution experiment for solubility study

Synthesis of starting compounds

Resyntheses of precipitates were performed to obtain single phases and larger amounts of sample for the dissolution study following a similar method as described above, keeping the same concentrations but using 5 times the volumes. Barium hydrogen arsenate monohydrate, $BaHAsO_4 \cdot H_2O$, and $NaBaAsO_4 \cdot 9H_2O$ were resynthesized with Ba/As = 1.0, and pH 9.0, and 12.5, respectively. $Ba_5Cl(AsO_4)_3$ was resynthesized with Ba/As = 3.0 and pH 12.3.

The pure phase precipitates were confirmed by XRD using the same sample preparation procedure and instrument conditions described above. The compositions of relevant species were confirmed by dissolving 0.01 g of solid in 0.2% nitric acid and then analyzing the resulting solutions by ICP-MS.

Dissolution and equilibration

Dissolution experiments were carried out in sealed 125 mL HDPE bottles by adding 0.15 g of the respective barium-arsenate compound into 100 mL of degassed (for 5 min in degas mode using CREST ultrasonic bath model 2800D) doubly-distilled water, and 0.01, 0.05, and 0.10 M KNO_3 solutions. The unagitated mixtures were allowed to equilibrate in a temperature controlled (air-conditioned) laboratory at 24°C ±1°C for 60 days to ensure thermodynamic equilibrium was reached. After equilibration, an adequate amount of supernatant solution was sampled by micropipette for elemental analysis, and the pH of each solution was measured by a buffer calibrated pH meter (Mettler Toledo with Inlab 413 electrode).

XRD was used to examine solid materials remaining after equilibration for phase changes of the barium-arsenate compounds during the dissolution experiments.

No new XRD peaks were observed in the remaining solid materials after any of the dissolution experiments in this study.

Determination of elemental concentration

Solution samples from dissolution experiments were diluted to 25 mL in borosilicate volumetric flasks and acidified by a few drops of concentrated nitric acid. The total elemental concentrations of barium, arsenic, and sodium in solutions were then analyzed by two techniques, FAAS (Varian model SpectrAA-250 plus) and ICP-MS (Agilent model 7500ce). Chloride ion concentrations in solutions were analyzed by argentometric titration with $AgNO_3$.

Arsenic concentrations were determined by two analytical techniques to avoid different potential interferences of each technique. When chloride ion is present in the sample, arsenic determination by the ICP-MS technique using an argon plasma, may exhibit interference from $ArCl^-$ which has a coincident mass (78) with arsenic (Hung, Nekrassova, and Compton, 2004). Therefore, in the study of $Ba_5Cl(AsO_4)_3$ solution analysis using FAAS is better. Similarly, the presence of an alkali earth metal in the flame may produce a chemical interference for barium determination by FAAS (Skoog and Leary, 1992). Therefore, for $NaBaAsO_4 \cdot 9H_2O$ dissolution experiment ICP-MS is deemed to be more suitable.

K_{SP} calculation

The solubility product constants, K_{SP}, of barium-arsenate compounds in this work were calculated from species thermodynamic activities based on the following dissolution equilibria:

$$BaHAsO_4 \cdot H_2O(s) \rightleftharpoons Ba^{2+}(aq) + HAsO_4^{2-}(aq) + H_2O(l)$$

$$K_{SP} = a^*_{Ba^{2+}} a^*_{HAsO_4^{2-}} \qquad \qquad ……….(1)$$

$$Ba_3(AsO_4)_2(s) \rightleftharpoons 3Ba^{2+}(aq) + 2AsO_4^{3-}(aq)$$

$$K_{SP} = (a^*_{Ba^{2+}})^3 (a^*_{AsO_4^{3-}})^2 \qquad\qquad ....(2)$$

$$NaBaAsO_4 \cdot 9H_2O(s) \rightleftharpoons Na^+(aq) + Ba^{2+}(aq) + AsO_4^{3-}(aq) + 9H_2O(l)$$

$$K_{SP} = a^*_{Na^+} a^*_{Ba^{2+}} a^*_{AsO_4^{3-}} \qquad\qquad ....(3)$$

$$Ba_5Cl(AsO_4)_3(s) \rightleftharpoons 5Ba^{2+}(aq) + Cl^-(aq) + 3AsO_4^{3-}(aq)$$
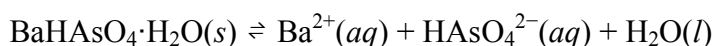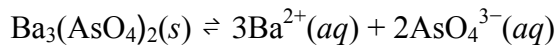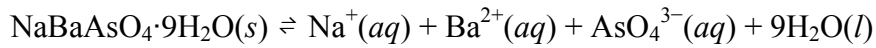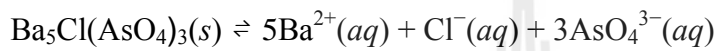
$$K_{SP} = (a^*_{Ba^{2+}})^5 a^*_{Cl^-} (a^*_{AsO_4^{3-}})^3 \qquad\qquad ....(4)$$

Where a^*_i denotes thermodynamic activity of the species i at equilibrium, and the

$$a^*_{H_2O} = 1$$

As concentration increases in a given solution, the interactions of ions and/or uncharged molecules in solution become significant leading to deviations from ideal solution behavior such that the thermodynamic activity of a given species is usually smaller than the concentration of the species. The thermodynamic activities of species in aqueous solutions are calculated from relationships

$$a_i = \gamma_i m_i \qquad\qquad ....(5)$$

where γ_i is the activity coefficient and m_i is the molality of species i.

The geochemical calculation computer program, PhreeqC version 2.11.00 (Parkhurst and Appelo, 1999) was used to calculate ion speciation and

thermodynamic activity in the aqueous solutions. In practice, nonideal aqueous solution activity coefficients are derived from an activity coefficient model. This work uses the default program parameters for the activity coefficient calculation where charged species are predicted by the Davis equation

$$\log \gamma_i = -Az_i^2 \left(\frac{\sqrt{I}}{1+\sqrt{I}} - 0.3I \right) \qquad\qquad \ldots\ldots\ldots(6)$$

where z_i is the ionic charge of aqueous species i, and A is a constant that depends only on temperature ($A = 0.51$ at 25°C in water), and I is the ionic strength of the solution, defined as

$$I = \frac{1}{2} \sum_i m_i z_i^2 \qquad\qquad \ldots\ldots\ldots(7)$$

If ion-specific parameters are specified in the database, another extended form of the Debye-Hückel equation, the Wateq equation will be employed for those species

$$\log \gamma_i = -\frac{Az_i^2 \sqrt{I}}{1 + Ba_i^o \sqrt{I}} + b_i I \qquad\qquad \ldots\ldots\ldots(8)$$

where B is a constant that depends only on temperature ($B = 0.33$ at 25°C in water), and a_i^0 and b_i are ion-specific parameters fitted from mean-salt activity-coefficient

data. For uncharged species the first term of Wateq equation is zero and the activity coefficient equation is reduced to the Setchenow equation

$$\log \gamma_i = b_i I \qquad\qquad ....(9)$$

where the default value for b_i is assumed to be 0.1 for all uncharged species in the PhreeqC calculations.

The Debye-Hückel aqueous model used in PhreeqC is adequate with small deviations in the ionic strength range studied in this work. The Davis equation can give a possible error of 3% at $I = 0.1$ M, while the Setchenow equation for uncharged species is valid as high as $I = 5$ M (Butler, 1998).

The PhreeqC calculations are based on the equilibrium chemistry of aqueous solutions for all known equilibria existing in the database. PhreeqC is distributed with a PhreeqC default internal database, Minteq, MinteqV4, Wateq4f, and LLNL databases. The LLNL (Lawrence Livermore National Lab) database was used in the calculations since it is more complete for the relevant equilibria for this study when compared to the default PhreeqC and other databases. Even so, some relevant equilibria were still incorrect or missing and have to be added as input to the program. Input data for the program consists of properties and compositions of equilibrated solutions, including pH, temperature, and total concentrations of barium, arsenic, sodium, chloride, potassium, and nitrate ion in the supernatant solutions, and equilibria data for incorrect and missing values in the LLNL database.

Saturation Indices (SI) Calculation

SI calculation is done by the PhreeqC program based on input datasimilar to that used for speciation and thermodynamic activity calculations. Three new K_{SP} values of $BaHAsO_4 \cdot H_2O$, $NaBaAsO_4 \cdot 9H_2O$, and $Ba_5Cl(AsO_4)_3$ determined from this work were included in the input data. SI is calculated by the equation

$$SI = \log (IAP/K_{SP}) \qquad\qquad\qquad ....(10)$$

and compares the ion activity product, IAP, to the K_{SP} to indicate saturation state with respect to a particular phase in the system. When SI < 0, the solution is undersaturated and when SI = 0, the solution is in equilibrium for the solute under consideration; when SI > 0, the solution is supersaturated and precipitation is thermodynamically spontaneous. As SI increases above zero the solution becomes more supersaturated with respect to that solid phase. The solution may be in a metastable supersaturated state, but a larger value of SI implies a greater driving force for crystallization of that phase and crystallization is thermodynamically spontaneous.

2.3   Results and discussion

Barium-arsenate precipitation in the absence of QUAT

Three pure species, $BaHAsO_4 \cdot H_2O$, $NaBaAsO_4 \cdot 9H_2O$, and $Ba_5Cl(AsO_4)_3$, and their three binary mixtures were observed as crystallization products in different regions of pH and Ba/As molar ratio. The XRD patterns of pure and mixed phases are shown in Figure 2.1. All the peaks in a "pure phase" pattern correspond to peaks in

one JCPDS pattern and all the peaks in a "mixed phase" pattern correspond to peaks

in a combination of two JCPDS patterns.
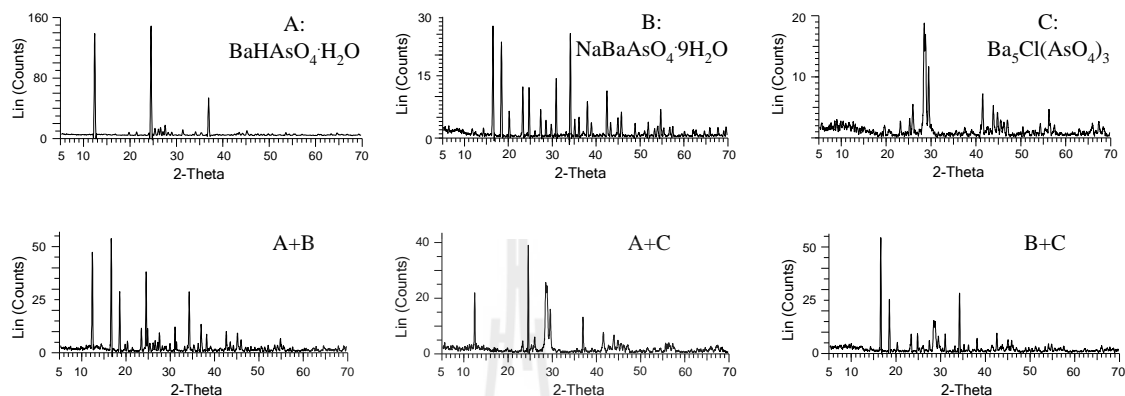
Figure 2.1 Selected XRD patterns of formed precipitates.

$BaHAsO_4 \cdot H_2O$ forms large plate-like crystals, $NaBaAsO_4 \cdot 9H_2O$ forms cube-

like crystals with edges having lengths in the order of 10 μm, and $Ba_5Cl(AsO_4)_3$ forms

spherical crystals with a diameter of about 1 μm. Mixed phases show mixed

morphologies consistent with the above (Figure 2.2). The heavy element compositions

from EDX examination also agree with the XRD results (Figure 2.2).

A: BaHAsO$_4$·H$_2$O   B: NaBaAsO$_4$·9H$_2$O   C: Ba$_5$Cl(AsO$_4$)$_3$

A+B   A+C   B+C
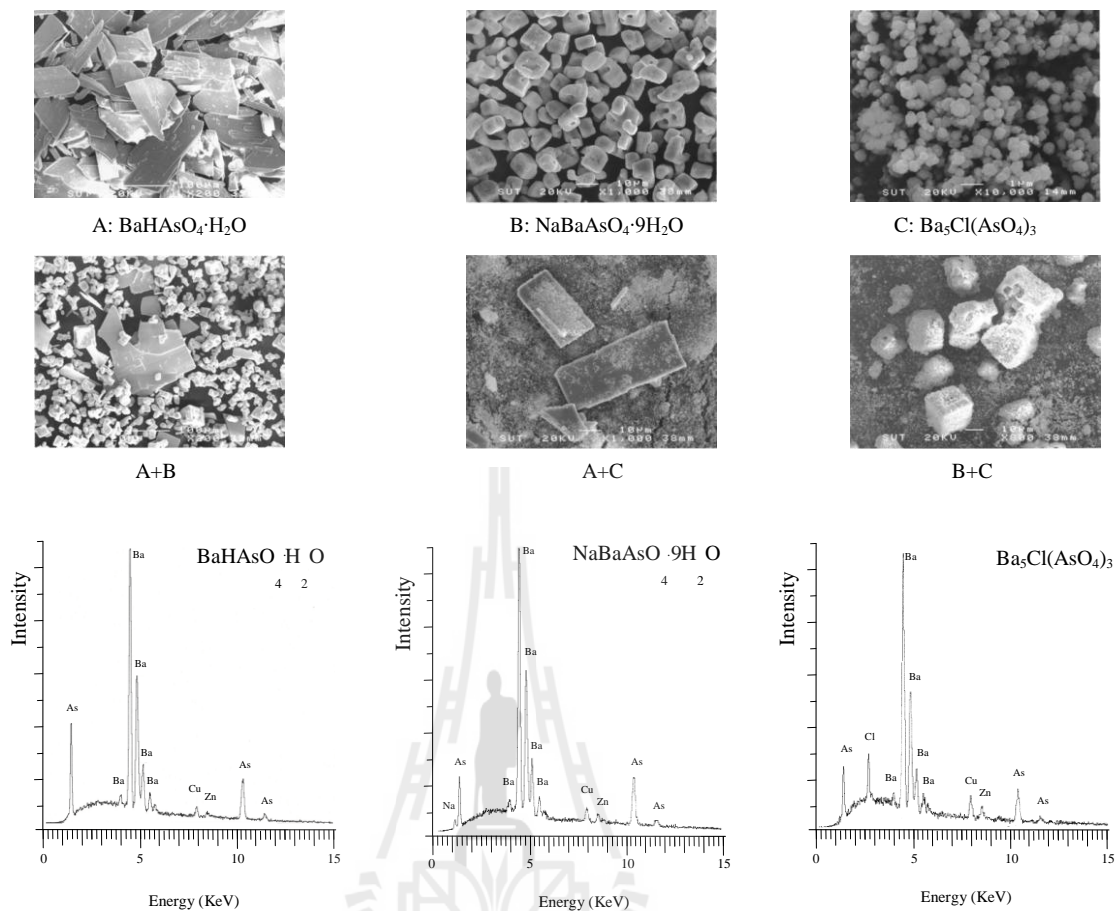
Figure 2.2 Selected SEM micrographs and EDX spectra of formed precipitates.

BaHAsO$_4$·H$_2$O, NaBaAsO$_4$·9H$_2$O, Ba$_5$Cl(AsO$_4$)$_3$, and the mixtures thereof that precipitate are represented in a phase precipitation region diagram plotted between pH versus Ba/As molar ratio (Figure 2.3). No precipitate was found at pH 2.0-5.5 for any Ba/As molar ratio studied in this work. BaHAsO$_4$·H$_2$O formed at pH 6.0-11.5, while NaBaAsO$_4$·9H$_2$O and Ba$_5$Cl(AsO$_4$)$_3$ formed at pH > 10.5. Ba$_5$Cl(AsO$_4$)$_3$ is more likely to form at higher Ba/As molar ratios which contain high barium (and consequently even higher chloride from BaCl$_2$·2H$_2$O used as the source for barium in our experiments) concentrations as might be expected from stoichiometry considerations. At the boundaries of two regions, a mixture of two phases is observed.
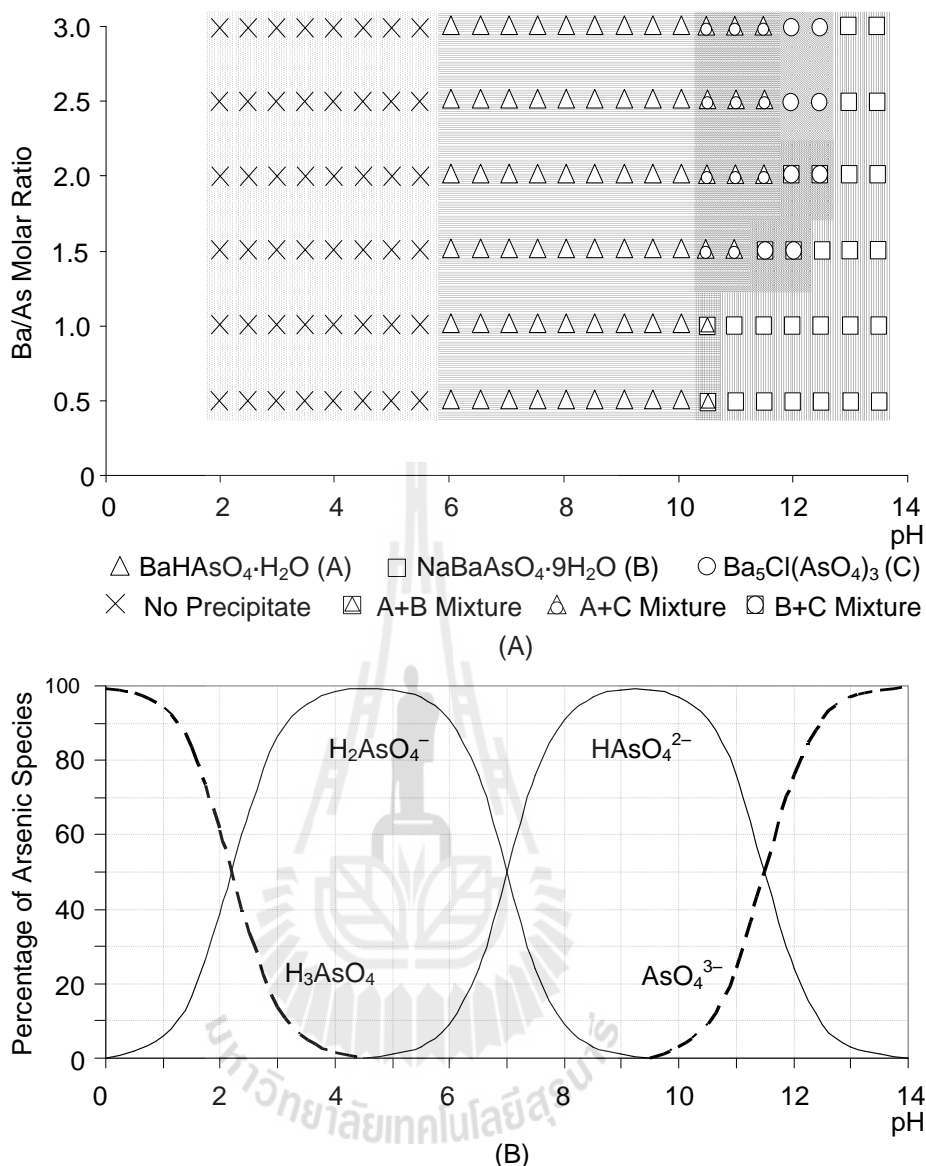
Figure 2.3 Phase precipitation region diagram of barium-arsenate (A) and speciation

diagram of arsenic acid (B).

Effect of QUAT on barium-arsenate precipitation

In the presence of QUAT, the phases formed were three pure species, $BaHAsO_4 \cdot H_2O$, $NaBaAsO_4 \cdot 9H_2O$, and $Ba_5Cl(AsO_4)_3$, and a mixture of $BaHAsO_4 \cdot H_2O / NaBaAsO_4 \cdot 9H_2O$ as represented in the precipitation region diagram in Figure 2.4.
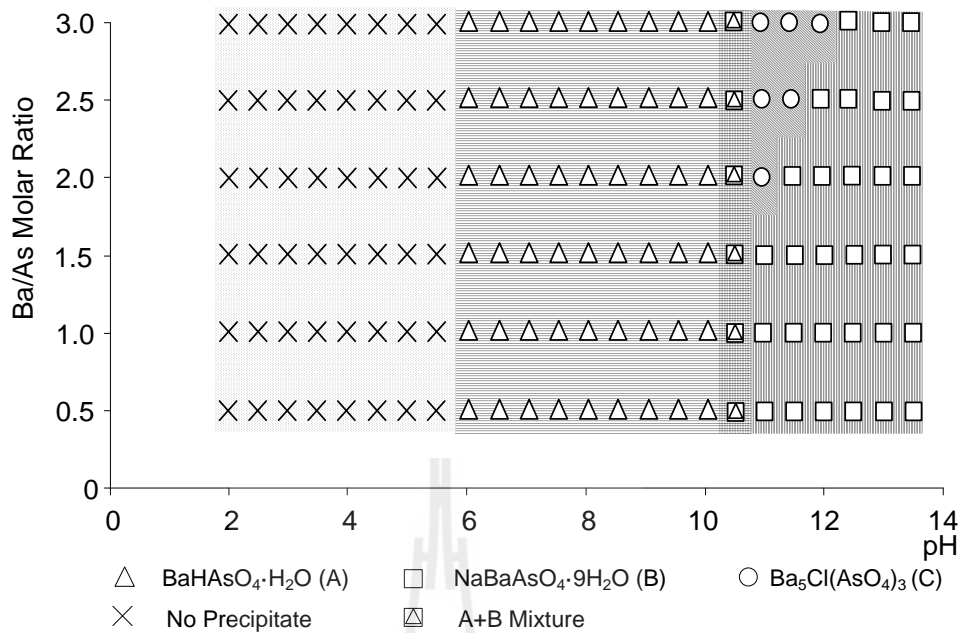
Figure 2.4 Phase precipitation region diagram of barium-arsenate compounds in the presence of QUAT.

The phase precipitation region diagram of barium-arsenate precipitates formed in the presence of QUAT shows differences with the phase diagram in the absence of QUAT. The $BaHAsO_4 \cdot H_2O$ region was reduced from pH 5.5-11.0 in the absence of QUAT to pH 5.5-10.0 in the presence of QUAT. The phase mixture regions ($BaHAsO_4 \cdot H_2O/Ba_5Cl(AsO_4)_3$, and $NaBaAsO_4 \cdot 9H_2O/Ba_5Cl(AsO_4)_3$) disappeared in the presence of QUAT. Pookrod *et al.* (2004) demonstrated that the arsenate rejection was greater than 99% at pH 6.5-8.5, which indicates that the $HAsO_4^{2-}$ specie shows stronger binding with QUAT. At pH higher than 10.0, both $HAsO_4^{2-}$ and AsO_4^{3-} occur in the system. Both species will be strongly bound by the QUAT, altering the precipitation equilibrium. Presumably the phase formed under these conditions would favor one with higher lattice stabilization energy, perhaps helping to account for reduction of the $BaHAsO_4 \cdot H_2O$ region and the disappearance of the mixtures of

BaHAsO$_4$·H$_2$O/Ba$_5$Cl(AsO$_4$)$_3$ and NaBaAsO$_4$·9H$_2$O/Ba$_5$Cl(AsO$_4$)$_3$ from the phase precipitation region diagram, leading to its apparent simplification in the presence of QUAT.

The SEM micrographs (Figure 2.5) show morphologies and sizes of pure phases and mixtures of barium-arsenate compounds. The morphology of BaHAsO$_4$·H$_2$O crystals formed in the absence of QUAT was plate-like with size about 20 × 100 μm (width × length). The crystals are very thin, and in the filtration step they stack and adhere together on the surface of the filter paper and become a large stacked plate cake. The SEM micrograph shows the stacked plates of BaHAsO$_4$·H$_2$O rather than a single crystal. The morphologies of NaBaAsO$_4$·9H$_2$O and Ba$_5$Cl(AsO$_4$)$_3$ particles are cube-like with a hole inside and sphere-like, with sizes about 10 × 10 μm and less than 1 μm, respectively.

In the presence of QUAT, the morphologies and sizes of BaHAsO$_4$·H$_2$O and Ba$_5$Cl(AsO$_4$)$_3$ were different. BaHAsO$_4$·H$_2$O changes to needle-like crystals, greater than 1,000 μm long at pH 10.0. Ba$_5$Cl(AsO$_4$)$_3$ changes to rod-like particles, about 5 μm long. Changes in morphology are known to occur when additives, which may have different interactions with different faces of the crystals, are included in a crystallization system. Larger crystal size when QUAT is added to the system suggests a lower supersaturation driving force and consequently a decrease in the number of crystal nuclei formed, presumably due to reduced activity of arsenate on binding to QUAT. The different concentrations may also relate to changes in crystal size, because the concentration is related directly to the supersaturation, which is the driving force for crystallization.
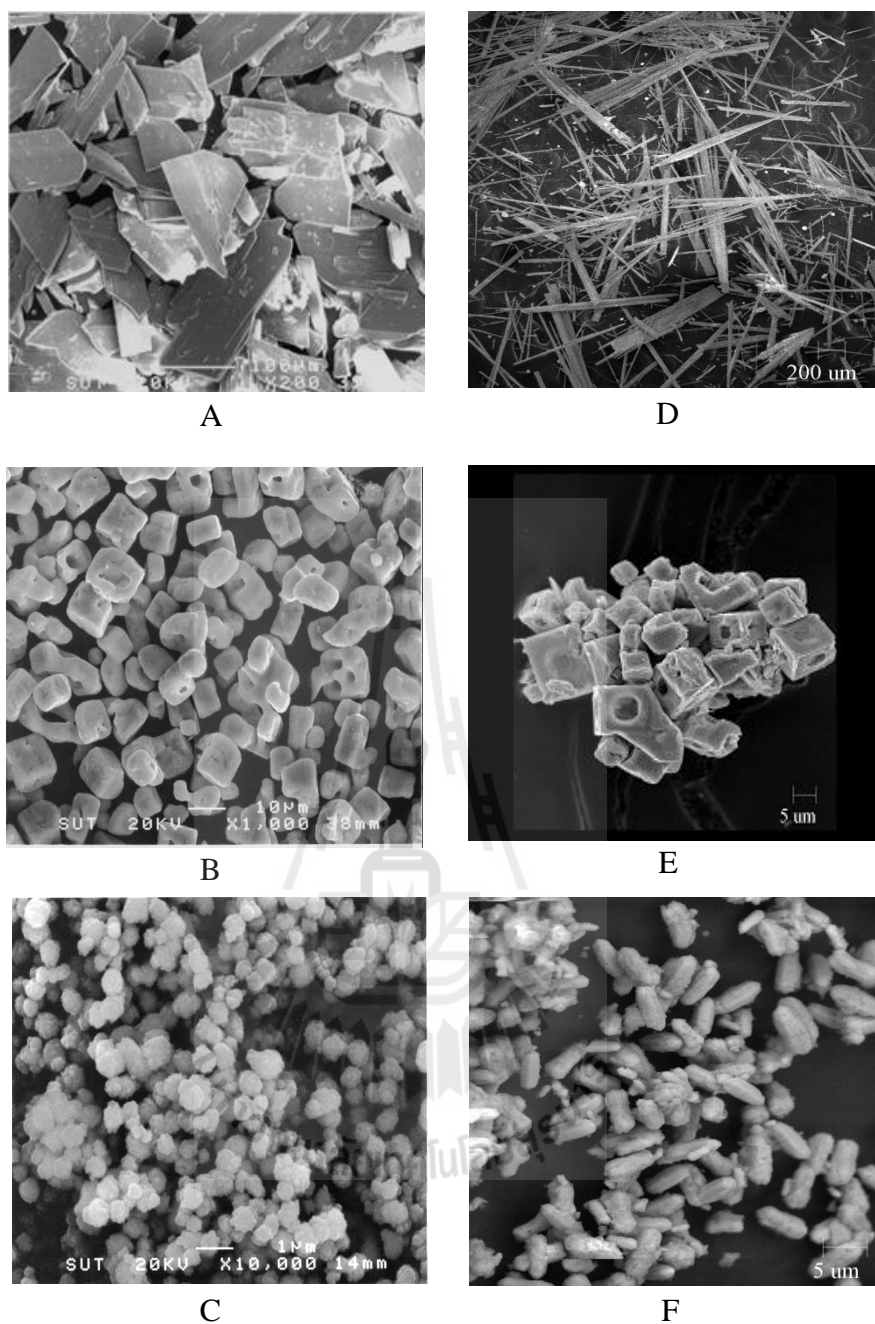
Figure 2.5 SEM micrographs of barium-arsenate compounds precipitated in the absence (A-C) and presence (D-F) of QUAT. Various compounds $BaHAsO_4 \cdot H_2O$ (A, D), $NaBaAsO_4 \cdot 9H_2O$ (B, E), $Ba_5Cl(AsO_4)_3$ (C, F), were formed.

Effect of pH and arsenic speciation on phase precipitation region diagrams

The formation of barium-arsenate compounds observed in the phase precipitation region diagrams corresponds to the relationship of arsenic acid, pH, and speciation. According to the speciation diagram (Figure 2.3B) of arsenic acid, $H_2AsO_4^-$ is a principal component at low to moderate pH ($0 < pH < 9.5$), $HAsO_4^{2-}$ is a principal component in the moderate to high pH region ($4.5 < pH < 14.0$), and AsO_4^{3-} is a principal component at high pH ($9.5 < pH < 14.0$). Thus, at high pH the highly charged AsO_4^{3-} anion forms charge stabilized crystals of $NaBaAsO_4 \cdot 9H_2O$ and $Ba_5Cl(AsO_4)_3$ and as the pH is reduced to the medium range where $H_2AsO_4^-$ dominates in solution those phases are augmented by the $BaHAsO_4 \cdot H_2O$ phase. Then as pH reaches 10 and the quantity of AsO_4^{3-} in solution becomes insignificant $BaHAsO_4 \cdot H_2O$ is the only observed phase. The monoanionic $H_2AsO_4^-$ and neutral H_3AsO_4 were not observed in solid phases with Ba^{2+} in this study.

Effect of common and diverse ions on the phase precipitation region diagrams

The common ions (ions involved in the equilibrium reaction) and diverse ion (ions not involved in the equilibrium reaction) present in solution play an important role in barium-arsenate compound precipitation. The presences of high Na^+ concentration (from arsenate precursor and NaOH used for pH adjustment) induce $NaBaAsO_4 \cdot 9H_2O$ to crystallize in the high pH region. At high Ba/As molar ratios, more $BaCl_2 \cdot 2H_2O$ was required to be added to achieve the desired ratio, and hence the Cl^- content is also high. Under high pH much of the arsenic acid is in the AsO_4^{3-} state. These conditions drive $Ba_5Cl(AsO_4)_3$ to precipitate.

In this study Na^+ and Cl^- can be both common and diverse ions in the barium-arsenate system. Na^+ is common ion for $NaBaAsO_4 \cdot 9H_2O$, while it is a diverse ion for $Ba_3(AsO_4)_2$, $BaHAsO_4 \cdot H_2O$, and $Ba_5Cl(AsO_4)_3$. On the other hand, Cl^- is a common ion for $Ba_5Cl(AsO_4)_3$, while it is a diverse ion for $Ba_3(AsO_4)_2$, $BaHAsO_4 \cdot H_2O$, and $NaBaAsO_4 \cdot 9H_2O$. If considering increasing pH and the Ba/As = 1.5 system in the phase precipitation region diagram, $BaHAsO_4 \cdot H_2O$ precipitates first as arsenic speciation effects dominate. Then at pH 10.5 $Ba_5Cl(AsO_4)_3$ begins to precipitate due to the arsenic speciation shift and sufficiently high Cl^- concentrations. By adding more NaOH to achieve higher pH, arsenic speciation for $HAsO_4^{2-}$ is reduced, while Na^+ concentration is increased, finally overcoming the excess Cl^- resulting in pure $NaBaAsO_4 \cdot 9H_2O$ precipitating from pH 12.5. The Cl^- concentration is more significant at the higher Ba/As molar ratios (2.5 and 3.0) resulting in $Ba_5Cl(AsO_4)_3$ becoming dominant over a wider range of pH. Higher Na+ concentration is required to overcome the excess Cl^- resulting in pure $NaBaAsO_4 \cdot 9H_2O$ precipitating only at pH 13.0 and higher.

The effect of Na^+ and Cl^- common/diverse ions on the precipitation results agrees with Essington's observation (Essington, 1988) of formation of $NaBaAsO_4 \cdot 9H_2O$ or $Ba_5Cl(AsO_4)_3$ instead of $Ba_3(AsO_4)_2$ when Na^+ or Cl^- ions are present in the systems, respectively. It should be noted from this result that simple ions like Na^+ and Cl^- can create large effects on the precipitation in the barium-arsenate system, therefore such simple ions, which are ubiquitous in nature and in industrial process systems, must be carefully considered in real environmental or industrial systems also.

K_{SP} of Barium-arsenate compounds

The K_{SP} of the three pure barium-arsenate compounds *i.e.* $BaHAsO_4 \cdot H_2O$, $NaBaAsO_4 \cdot 9H_2O$, and $Ba_5Cl(AsO_4)_3$ found in this work were studied. The result of composition analysis of the initial compounds by ICP-MS and complete data of the barium-arsenate solubility product constant calculations are available in supporting information at the end of the chapter. Summary data at four different solution ionic strengths are given in Table 2.1.

Table 2.1 Summary data of the barium-arsenate solubility product constants study.

Compounds	pH	Temp (°C)	KNO₃ (M)	Total concentration at equilibrium (mM) Barium	Arsenic	Sodium	Chloride	Ba/As ratio	−log K_{SP}	−log K_{SP} Ba₃(AsO₄)₂	SI Ba₃(AsO₄)₂
BaHAsO₄·H₂O	7.78(5)†	25.1(2)	0.00	2.65(7)	2.32(4)	NA‡	NA	1.14(3)	5.61(2)	21.56(9)	0.06(9)
(FAAS)	7.81(2)	24.7(4)	0.01	2.96(7)	2.82(7)	NA	NA	1.05(1)	5.61(2)	21.58(8)	0.04(4)
	7.86(2)	25.1(3)	0.05	4.90(15)	4.30(37)	NA	NA	1.14(6)	5.52(4)	21.25(8)	0.37(8)
	8.07(3)	24.7(3)	0.10	5.01(5)	4.96(9)	NA	NA	1.01(3)	5.64(1)	21.18(5)	0.44(5)
								Average	**5.60(5)**	**21.39(20)**	**0.23(21)**
NaBaAsO₄·9H₂O	9.31(32)	24.9(3)	0.00	0.49(20)	2.11(3)	3.12(10)	NA	0.23(8)	11.14(16)	20.67(10)	0.96(11)
(ICP-MS)	9.66(16)	25.0(1)	0.01	0.57(8)	2.29(22)	3.48(9)	NA	0.25(1)	10.82(7)	20.10(6)	1.52(7)
	9.98(6)	24.1(2)	0.05	0.70(1)	2.45(6)	3.96(22)	NA	0.29(1)	10.70(6)	19.99(5)	1.63(5)
	10.14(1)	25.0(3)	0.10	0.94(2)	2.86(14)	6.38(2.43)	NA	0.33(2)	10.43(15)	19.77(3)	1.85(3)
								Average	**10.77(30)**	**20.13(38)**	**1.49(38)**
Ba₅Cl(AsO₄)₃	9.72(15)	24.4(2)	0.00	0.89(4)	0.23(4)	NA	0.62(3)	3.93(46)	35.82(26)	20.67(19)	0.95(19)
(FAAS)	10.07(2)	24.1(3)	0.01	1.05(5)	0.27(5)	NA	0.57(4)	3.99(71)	35.27(26)	20.25(17)	1.37(17)
	10.25(4)	24.7(0)	0.05	1.33(1)	0.43(2)	NA	0.57(3)	3.13(17)	35.17(16)	20.12(12)	1.50(12)
	10.43(4)	24.5(8)	0.10	1.93(1)	0.46(2)	NA	0.46(4)	4.20(15)	34.94(2)	19.91(3)	1.71(3)
								Average	**35.30(37)**	**20.24(32)**	**1.38(32)**

†The number in parentheses are the estimate standard deviations (ESD) in the least significant digits. ESDs on individual values for FAAS are from three replicate measurements and for ICP-MS are from two replicate measurements. ESDs on average values are based on variance within the four ionic strength values averaged.
‡NA = Not applicable

Consistent −log K_{SP} values are obtained over a large range of ionic strengths for all three compounds. The value of −log K_{SP} for $BaHAsO_4 \cdot H_2O$ is 5.60(5), comparable to that previously reported (Zhu *et al.*, 2005). The previously unreported values of −log K_{SP} for $NaBaAsO_4 \cdot 9H_2O$ and $Ba_5Cl(AsO_4)_3$ are 10.8(3) and 35.3(4), respectively.

Considering from the obtained K_{SP} of this study and use simple-mind solubility calculation suggest solubility of $BaHAsO_4 \cdot H_2O$ > $NaBaAsO_4 \cdot 9H_2O$ > $Ba_5Cl(AsO_4)_3$ (Table 2.2). However, all of these phases are more soluble when compared to $Ba_3(AsO_4)_2$. Due to low in solubility suggested by $-\log K_{SP}$ value, $Ba_3(AsO_4)_2$.was proposed to be a precipitating phase for arsenic immobilization purpose. However, from this work, it is to be noted that the ions present in the system is a very important factor for phase precipitation in the system as discussed above in the section on the effect of common and diverse ions in the equilibrium system. Even through $Ba_3(AsO_4)_2$ was suggested to have the lowest solubility based on the K_{SP} values and was expected to be easiest to precipitate, the presence of Na^+ and Cl^- in the system makes $NaBaAsO_4 \cdot 9H_2O$ and $Ba_5Cl(AsO_4)_3$ also likely to form.

K_{SP} values of compounds are also generally used for calculation of ΔG_f, and then, sometimes somewhat naively, to predict relative thermodynamic stability within a group of compounds. This interpretation is widely used, especially in geochemistry (Krauskopf and Bird, 1995). When ΔG_f is negative, it indicates that the reaction may spontaneously go to the products. In a thermodynamic stability context, the more negative value of ΔG_f may also indicate a more stable phase, but only in the context of the two phases having the same reactants. This study demonstrates the inadequacy of such an interpretation to judge which is the stable phase in a system. Calculated ΔG_f values suggest stability of $Ba_5Cl(AsO_4)_3$ > $NaBaAsO_4 \cdot 9H_2O$ > $Ba_3(AsO_4)_2$ > $BaHAsO_4 \cdot H_2O$. As discussed above, in this work the effect of pH, and type and concentration of ions present in the system play an important role in phase precipitation selection, and the precipitating phase is more likely to be driven by solution equilibrium rather than by ΔG_f. $BaHAsO_4 \cdot H_2O$ is formed at lower pH region

even through it is highest in ΔG_f but the pH of the solution is suitable for $HAsO_4^{2-}$ formation which is most suitable for $BaHAsO_4 \cdot H_2O$ formation.

Table 2.2 Solubility and ΔG_f of barium-arsenate calculated from this work.

Phases	$-\log K_{SP}$	Solubility, M	ΔG_r, kJ/mol	ΔG_f, kJ/mol
$Ba_3(AsO_4)_2$	21.62	1.86×10^{-5}	123.41	-3077.57
$BaHAsO_4 \cdot H_2O$	5.60	1.60×10^{-3}	31.96	-1544.49
$NaBaAsO_4 \cdot 9H_2O$	10.77	3.71×10^{-4}	61.48	-3654.86
$Ba_5Cl(AsO_4)_3$	35.30	3.39×10^{-5}	201.49	-5044.30

Effect of measurement technique

Errors in analytical techniques are another concern which needs careful consideration. This work used two analytical techniques, FAAS and ICP-MS, for determining arsenic concentrations of dissolution supernatant solutions (the results are given in the supporting information). The reason is to cover limitation of each technique for the best analytical result to be discussed. $ArCl^-$ interference occurring in the argon plasma on arsenic determination when analyzed by ICP-MS technique, therefore, the FAAS result was used for $Ba_5Cl(AsO_4)_3$ case. For $NaBaAsO_4 \cdot 9H_2O$ dissolution experiment, ICP-MS result was used to avoid sodium interference on the barium determination when using FAAS techniques. Error in analytical techniques can create large doubts in scientific results. Since the error in analytical technique was carefully taken care of, the disagreement of analytical data with the theoretical value must arise from another effect.

Effect of speciation on K_{SP} study

The aqueous solutions present in this study are very complex systems with many chemical equilibrium involved. Failing to include any significant equilibrium will interfere with understanding of the system and produce incorrect results. Solubility products must be calculated from equilibrium ion activity values. The quality of calculated K_{SP} values, therefore, depends on the accuracy of the ion activity calculation and also the completion of the speciation of all key complex ions were accounted for. In this work not only the speciation of arsenic acid, but also the formation of various complex ions in solution and compounds containing barium ion with arsenate ion (from existing species in solution), hydroxide ion, and nitrate ion (from ionic strength adjustment) were also considered. By considering so found consumption of barium and arsenate ions through the formation of barium arsenate in the system leading to disagreement of Ba/As ratio to initial dissolution phase (incongruent dissolution, which is to be discussed later). By ignore all key equilibriums we may not able to figure out the incongruent dissolution in this study. This work using LLNL database in the calculation by update relevant value to more reasonable value, relevant equilibrium and its constant is listed in Table 2.3.

Table 2.3 List of relevant compounds and species in the barium-arsenate system under study.

Equilibriums	LLNL log $K^{\ddagger}$	Amended Log K	Sources
$H_3AsO_4 = H_2AsO_4^- + H^+$	-2.25	-	
$H_2AsO_4^- = HAsO_4^{2-} + H^+$	-6.76	-	
$HAsO_4^{2-} = AsO_4^{3-} + H^+$	-11.60	-	
$Cl^- + Ba^{2+} = BaCl^+$	-0.50	-	
$H_2O + Ba^{2+} = BaOH^+ + H^+$	-13.47	-	
$NO_3^- + Ba^{2+} = BaNO^{3+}$	$+0.90$	-	
$K^+ + Cl^- = KCl$	-1.49	-	
$H^+ + Cl^- = HCl$	-0.67	-	
$NO_3^- + H^+ = HNO_3$	-1.30	-	
$K^+ + H_2O = KOH + H^+$	-14.46	-	
$H_2O = OH^- + H^+$	-14.00	-	
$Ba_3(AsO_4)_2(s) = 3Ba^{2+} + 2AsO_4^{3-}$	-	-21.62	Essington, 1988
$BaHAsO_4 \cdot H_2O(s) = Ba^{2+} + HAsO_4^{2-} + H_2O$	-	-5.60	Zhu *et al.*, 2005
$Ba(OH)_2 \cdot 8H_2O(s) = Ba^{2+} + 2OH^- + 8H_2O$	-	-3.59	PhreeqC Database
$Ba(OH)_2(s) = Ba^{2+} + 2OH^-$	-	-2.30	PhreeqC Database
$Ba(NO_3)_2(s) = Ba^{2+} + 2NO_3^-$	-	-2.33	PhreeqC Database

‡values of log K in the distributed LLNL database (reference)

Effect of activity coefficient model on K_{SP}

Correction for the effect of total ionic strength on activity coefficients is another point requiring careful consideration. There are several activity coefficient models and each has its own strengths, limitations, and inherent errors. Most of the activity coefficient models are extensions of the Debye-Hückel limiting model which assumes that ions in solution behave like point charges in a continuous dielectric medium moving as a result of electrostatic interactions and Boltzman's energy, intended to account for nonidealities. The extended Debye-Hückel, Davis equation,

used in this work is generally regarded to produce an error of 3% in ionic strength up to 0.1 M which is a suitable ionic strength range for this work. This is to be noted that (1) without carefully consideration of activity coefficient model, the high error may be obtained, (2) within 3% error from Davis equation may create a significant impact on the calculated K_{SP}, the observed deviation of Ksp in each ionic strength concentrations are within error of activity coefficient model we used.

Incongruent dissolution and the barium-arsenate system

During determination of K_{SP} values by dissolution, deviations of the Ba/As molar ratios (and Ba or As to Na or Cl as relevant) in supernatant solutions from those in the starting compounds were observed in $NaBaAsO_4 \cdot 9H_2O$ (Ba/As ratio varying 0.17-0.34 in the equilibrium solutions) and in $Ba_5Cl(AsO_4)_3$ (Ba/As ratio varying 2.95-4.81 in the equilibrium solutions); values lower than the expected value of 1.00 (1:1 ratio) and higher than the expected value of 1.67 (5:3 ratio), respectively, based on the stoichiometry of the starting solid phase materials. Similar observations of deviations of ion ratios in supernatants at equilibrium with a single solid starting phase have been previously noted for a number of compounds, including $FeAsO_4 \cdot 2H_2O$ (Langmuir, Mahoney, and Rowson, 2006; Zhu and Merkel, 2001). In these cases it was suggested to be due to imperfect starting compound or the presence of an impurity in the starting compound, either of which could account for deviation from stoichiometric ratios in the supernatant compared to the starting compounds.

Another explanation for such deviations has been incongruent dissolution which occurs due to phase transformations mediated by solution of the solid followed by precipitation of a new phase (or phases) in the system. Incongruent dissolution is

offered as a rational explanation when such disagreement occurs; however, often without giving evidence to prove the formation of the secondary phase or other investigation of the total system. Previous use of the incongruent dissolution concept thus seems unclear; we do not find a suitable definition in the literature.

Therefore, before going further a definition will be useful. Incongruent dissolution is the phenomenon wherein as dissolution progresses the trajectory of the elemental composition of the supernatant deviates from that expected from the composition of the starting compound. A graphical illustration of the concept of incongruent dissolution of a binary compound is shown in Figure 2.6.
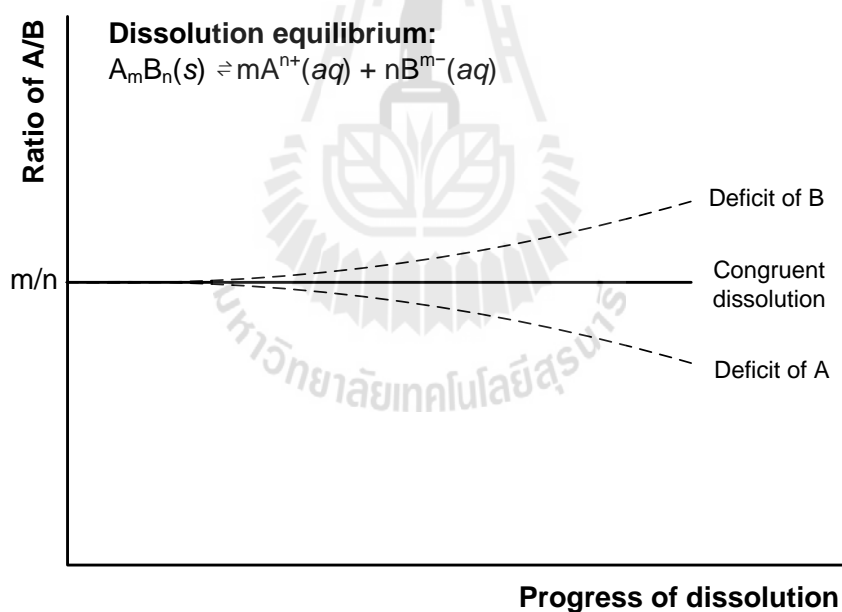
Figure 2.6 Trajectories of ion ratios as dissolution of a pure species occurs.

Incongruent dissolution is thus an observable fact in the systems noted above. The cause of incongruent dissolution is that at least one additional nonsolution phase of different stoichiometry is in equilibrium with the solution at saturation. Each of

these phases contributes or consumes the species present in the solution resulting in deviations from values predicted only on the basis of dissolution of a single solid species.

The incongruent dissolution observed for the $NaBaAsO_4 \cdot 9H_2O$ dissolution experiment in water can be understood as consumption of solute species Ba^{2+} and AsO_4^{3-} from the solution to form another solid phase, $Ba_3(AsO_4)_2$, thereby shifting the equilibrium. The process is illustrated in Figure 2.6 assuming that only two nonsolution phases are present during the entire dissolution process. The dissolution of $NaBaAsO_4 \cdot 9H_2O$ gives suitable pH for the AsO_4^{3-} species to be stable, and at the same time gives adequate Ba^{2+} to initiate $Ba_3(AsO_4)_2$ formation. The saturation index of $Ba_3(AsO_4)_2$ reaches zero when the ion product for $NaBaAsO_4 \cdot 9H_2O$ is significantly less than the K_{SP} value and therefore not yet a saturated solution of $NaBaAsO_4 \cdot 9H_2O$ (see Figure 2.7A, congruent dissolution region). As more $NaBaAsO_4 \cdot 9H_2O$ dissolves, the solution becomes supersaturated in $Ba_3(AsO_4)_2$, *i.e.* SI for $Ba_3(AsO_4)_2$ increases above zero and $Ba_3(AsO_4)_2$ crystals are forced to nucleate and grow (see Figure 2.7A, right-hand boundary of congruent dissolution region). Formation of $Ba_3(AsO_4)_2$ results in a decrease in Ba^{2+} relative to AsO_4^{3-} in the ratio 3:2 in the system, thereby leading to deviation to an average Ba/As ratio of 0.27 as observed for equilibrium Ba/As ratios in the $NaBaAsO_4 \cdot 9H_2O$ dissolution experiments. The quantity of $Ba_3(AsO_4)_2$ present at equilibrium will be determined by the volume of water used and can be calculated from the K_{SP} values. The maximum quantity of $Ba_3(AsO_4)_2$ produced in our dissolution experiments would be 1.26 mg when the final Ba/As ratio was 0.17.

A similar analysis, illustrated in Figure 2.7B, can be used to understand the incongruent dissolution of $Ba_5Cl(AsO_4)_3$. Again, the dissolution gives suitable pH for the AsO_4^{3-} species to be stable, and at the same time gives adequate Ba^{2+} to initiate $Ba_3(AsO_4)_2$ formation as shown in Figure 2.7B as the progress of the saturation index of $Ba_3(AsO_4)_2$ from negative to zero, then with a brief excursion to the positive, creating a metastable supersaturated solution of $Ba_3(AsO_4)_2$ to complete the congruent dissolution region. The formation of $Ba_3(AsO_4)_2$ (Ba/As ratio 3:2) from $Ba_5Cl(AsO_4)_3$ (Ba/As ratio 5:3) dissolution results in a relative increase of Ba^{2+} relative to AsO_4^{3-} in the supernatant solution, thereby leading to an average Ba/As ratio of 3.67, compared to the expected value of 1.67 based on the Ba/As stoichiometric ratio in $Ba_5Cl(AsO_4)_3$. Once again, the quantity of $Ba_3(AsO_4)_2$ present at equilibrium will be determined by the volume of water used and can be calculated from the K_{SP} values. The maximum quantity of $Ba_3(AsO_4)_2$ produced in our dissolution experiments would be 1.14 mg when the final Ba/As ratio was 4.81.

NaBaAsO₄·9H₂O Dissolution

$$NaBaAsO_4 \cdot 9H_2O(s) \rightleftharpoons Na^+(aq) + Ba^{2+}(aq) + AsO_4^{3-}(aq) + 9H_2O(l)$$

$$Ba_3(AsO_4)_2(s)$$

Ba₅Cl(AsO₄)₃ Dissolution

$$Ba_5Cl(AsO_4)_3(s) \rightleftharpoons 5Ba^{2+}(aq) + 3AsO_4^{3-}(aq) + Cl^-(aq)$$
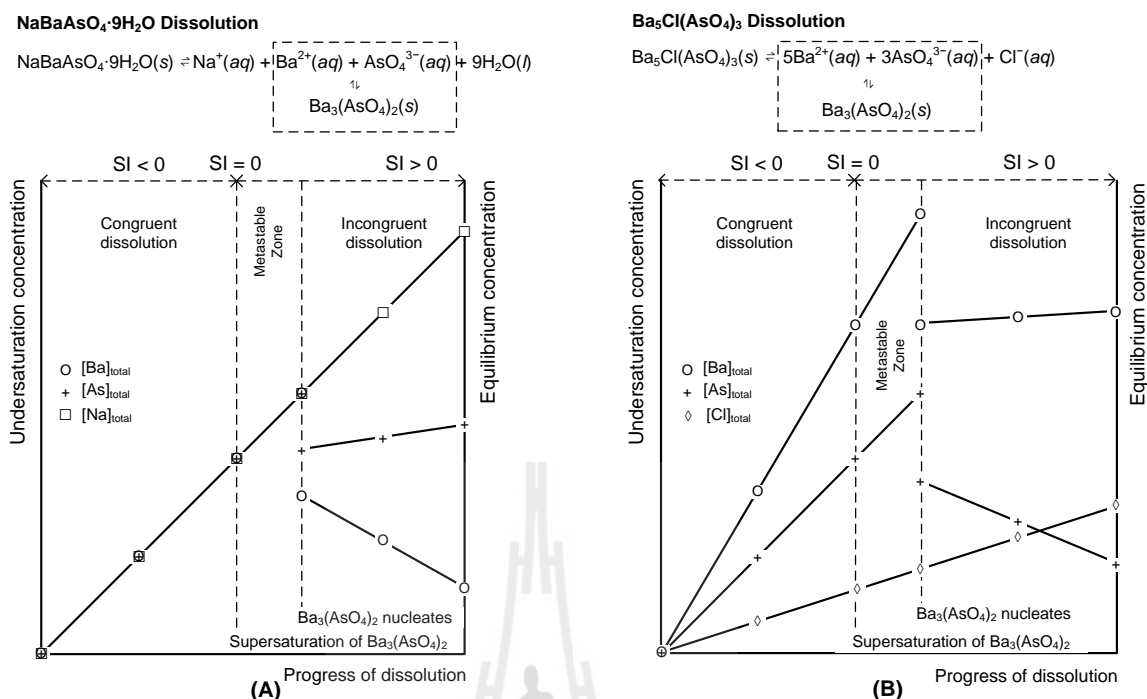
$$Ba_3(AsO_4)_2(s)$$

Figure 2.7 Conceptual diagrams representing dissolution equilibria of NaBaAsO₄·9H₂O (A) and Ba₅Cl(AsO₄)₃ (B) and formation of Ba₃(AsO₄)₂.

NaBaAsO₄·H₂O and Ba₅Cl(AsO₄)₃ show incongruent dissolution with deviation in the Ba/As ratio due to the formation of solid Ba₃(AsO₄)₂. The directions of the deviations are opposite due to the Ba/As stoichiometric ratios bracketing that of Ba₃(AsO₄)₂. The preceding analysis is of course simplified. There is no reason to restrict the number of nonsolution phases as dissolution progresses or when the system reaches equilibrium (geochemistry and ground water for example). Another complication occurs when more than one nonsolution phase has the same stoichiometry for the elements being analyzed in which case incongruent dissolution would not be noted, but different apparent solubilities might occur (calcium phosphate systems for example).

PhreeqC calculation of the saturation index (SI) and formation amount of $Ba_3(AsO_4)_2$ based on the relevant equilibria and equilibrium constants is shown in Table 2.4.

Table 2.4 Calculated saturation index values and formed amounts of $Ba_3(AsO_4)_2$ in $NaBaAsO_4 \cdot 9H_2O$ and $Ba_5Cl(AsO_4)_3$ dissolution equilibria.

Dissolution Systems	$-\log K_{SP}$	Calculated values for $Ba_3(AsO_4)_2$		
	(This work)	SI	$-\log$ IAP	mg formed (IAP based)
$BaHAsO_4 \cdot H_2O$	5.60(05)	0.23(21)	21.39(20)	-
$NaBaAsO_4 \cdot 9H_2O$	10.77(30)	1.49(38)	20.13(38)	1.26
$Ba_5Cl(AsO_4)_3$	35.30(37)	1.38(32)	20.24(32)	1.14

The calculations indicate that $Ba_3(AsO_4)_2$ has reached saturation in both $NaBaAsO_4 \cdot 9H_2O$ and $Ba_5Cl(AsO_4)_3$ dissolution experiments, SI = 1.49(38), and 1.38(32), respectively. Therefore, thermodynamically spontaneous precipitation of $Ba_3(AsO_4)_2$ can occur. The XRD diffractogram of remaining compound suggests only starting compound with no $Ba_3(AsO_4)_2$ formed from the dissolution equilibria in both dissolution experiments (the XRD spectra available in supporting information). The amount of $Ba_3(AsO_4)_2$ formed is very small (1.26 and 1.14 mg for $NaBaAsO_4 \cdot 9H_2O$ and $Ba_5Cl(AsO_4)_3$ dissolution experiments, respectively) relative to the bulk undissolved phase therefore, XRD examination may not be suitable for detection of $Ba_3(AsO_4)_2$in the solids remaining after the dissolution experiment.

In the $BaHAsO_4 \cdot H_2O$ dissolution experiment, the Ba/As ratio of 1.09 agrees reasonably well to the expected value of 1.00 (1:1 ratio) indicating that there is no significant competing solid of different stoichiometric ratio to consume Ba^{2+} and

AsO_4^{3-}. This system may not show incongruent dissolution (due to formation of $Ba_3(AsO_4)_2$) because the equilibrium pH in the range 7.47-8.09 is not favorable to forming AsO_4^{3-} species, therefore, insufficient AsO_4^{3-} is available to drive $Ba_3(AsO_4)_2$ formation. SI calculation of $Ba_3(AsO_4)_2$ in this system shows a small positive value (0.23) indicating that $Ba_3(AsO_4)_2$ is supersaturated, but perhaps still within the metastable region with no nucleation or spontaneous precipitation occurring. Furthermore, the observed Ba/As ratio deviates in the opposite direction expected from formation of $Ba_3(AsO_4)_2$.

Figure 2.8 gives a schematic diagram representing the important species affecting precipitation in the barium-arsenate system discussed herein.
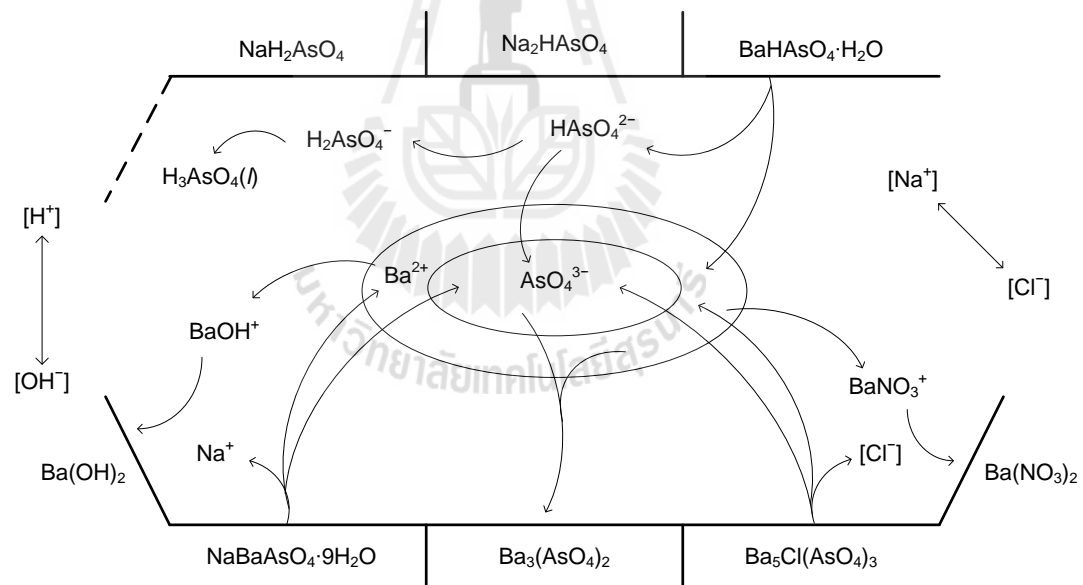
Figure 2.8 Representation diagram of barium-arsenate system incongruent dissolution.

The more soluble phases in the system provide Ba^{2+} and AsO_4^{3-} by dissolution resulting in increased Ba^{2+} and AsO_4^{3-} concentrations in the system until it reaches equilibrium. Meanwhile, depending on the pH and common/diverse ions in the

system, more than one phase reaches supersaturation simultaneously, and thus more than one solid phase may be present in simultaneous equilibrium with the solution.An interesting consequence of this can be seen in the dissolution of relatively simple low solubility salts such as $NaBaAsO_4 \cdot 9H_2O$ and $Ba_5Cl(AsO_4)_3$, as discussed previously. As dissolution proceeds ion concentrations higher than the $Ba_3(AsO_4)_2$ saturation level are reached and $Ba_3(AsO_4)_2$ becomes supersaturated and precipitates, creating incongruent dissolution in both systems. At equilibrium in these systems two solid phase dissolution equilibriums connect two solid phases with a single solution giving a quintuple point on a phase diagram.

2.4   Conclusions

Precipitation of barium-arsenate compounds is affected by pH, Ba/As molar ratio, and the presence of common/diverse ions (sodium and chloride). Three single phases of $BaHAsO_4 \cdot H_2O$, $NaBaAsO_4 \cdot 9H_2O$, and $Ba_5Cl(AsO_4)_3$ and their three binary mixtures were formed as the dominant solid phases in different regions of pH, Ba/As molar ratio, and common ion concentration. The pH of the initial solution has a great effect on the precipitates formed due to pH determining the speciation of the arsenate ion. The availability of diverse ions in the system induces formation of species containing those diverse ions and barium or arsenate, thereby reducing their activities and inhibiting the formation of $Ba_3(AsO_4)_2$. Thus, while in the absence of other ions, $Ba_3(AsO_4)_2$ may be the stable phase, in some real environmental systems containing ions such as sodium and chloride, $NaBaAsO_4 \cdot 9H_2O$ or $Ba_5Cl(AsO_4)_3$ may become the stable phase.

QUAT added to the precipitation reaction results in crystal morphology and size changes. For $BaHAsO_4 \cdot H_2O$ the shape changes from plate-like crystals to needle-like crystals with a length increase of about 10 times. $Ba_5Cl(AsO_4)_3$ crystals change from spherical to rod-like crystals with a length increase of about 5 times. The increase in crystal size is suggested to be due to inhibition of nucleation due to decreased activity of the divalent cation on binding to the polyelectrolyte. Reduced nucleation leads to means a smaller number of crystals were produced so they grow to larger size. The adsorption of QUAT molecules onto the crystal surface can inhibit crystal growth in some direction, resulting in differences in crystal morphology.

Previously unreported values for $-\log K_{SP}$ for $NaBaAsO_4 \cdot 9H_2O$ and $Ba_5Cl(AsO_4)_3$ of 10.8(3), and 35.3(4), respectively, were determined. The value of 5.60(5) determined for $BaHAsO_4 \cdot H_2O$ is comparable to the previously reported value.

The incongruent dissolution of two barium-arsenate compounds was explored in this study. Incongruent dissolution occurs with $NaBaAsO_4 \cdot 9H_2O$ and $Ba_5Cl(AsO_4)_3$. Formation of $Ba_3(AsO_4)_2$ phase is demonstrated in both systems leading to incongruent dissolution with deviations in the expected Ba/As ratio in opposite directions. PhreeqC calculations show that $Ba_3(AsO_4)_2$ reaches supersaturation in both cases, enabling formation of solid phase $Ba_3(AsO_4)_2$ in both systems. Moreover, calculating values for $-\log K_{SP}$ for $Ba_3(AsO_4)_2$ from the equilibrium activities of Ba^{2+} and AsO_4^{3-} in the $NaBaAsO_4 \cdot 9H_2O$ and $Ba_5Cl(AsO_4)_3$ dissolution systems gives values of 20.1(4) and 20.57(27), respectively, both identical within experimental error to the previously determined value.

2.5   Supporting information

Composition analysis using ICP-MS of Barium-arsenate compounds for K_{SP} study

Sample	ppm		mmol		mol ratio	Ave	%Recovery	
	Arsenic	Barium	Arsenic	Barium	Ba/As	(SD)	Arsenic	Barium
$BaHAsO_4 \cdot H_2O\_1$	0.54	0.93	7.22E-03	6.80E-03	0.94			
$BaHAsO_4 \cdot H_2O\ \_2$	0.55	0.94	7.38E-03	6.82E-03	0.92	0.93(0.01)	101.29	104.12
$BaHAsO_4 \cdot H_2O$ +0.2ppm std	0.75	1.14	1.00E-02	8.33E-03	-			
$NaBaAsO_4 \cdot 9H_2O\_1$	0.37	0.64	4.95E-03	4.69E-03	0.95			
$NaBaAsO_4 \cdot 9H_2O\ \_2$	0.38	0.65	5.13E-03	4.75E-03	0.93	0.94(0.01)	103.38	104.65
$NaBaAsO_4 \cdot 9H_2O$ +0.2ppmstd	0.58	0.86	7.80E-03	6.25E-03	-			
$Ba_5Cl(AsO_4)_3\_1$	0.38	1.10	5.08E-03	7.99E-03	1.57			
$Ba_5Cl(AsO_4)_3\_2$	0.41	1.15	5.50E-03	8.37E-03	1.52	1.55(0.04)	100.94	93.50
$Ba_5Cl(AsO_4)_3$+0.2ppm std	0.60	1.31	7.98E-03	9.54E-03	-			

K_{SP} calculation using FAAS data

K_{SP} Calculation of BaHAsO$_4$·H$_2$O compound using FAAS data

Sample No.	Rep	Temp (°C)	pH	[Ba]total ppm	[Ba]total mM	[As]total ppm	[As]total mM	Ba/As	[K]tot mM	[NO$_3$]tot mM	Activity from PhreeqC Ba^{2+}	Activity from PhreeqC HAsO$_4^{2-}$	$-\log K_{SP}$	Average	Stdev
Added KNO$_3$ 0 M															
1	1	25.3	7.75	375.21	2.73	176.39	2.35	1.16	-	-	1.83E-03	1.44E-03	5.60		
2	2	25.2	7.75	355.17	2.59	174.32	2.33	1.11	-	-	1.74E-03	1.44E-03	5.61	5.61	0.02
3	3	24.9	7.84	360.97	2.63	170.18	2.27	1.16	-	-	1.77E-03	1.42E-03	5.63		
Added KNO$_3$ 0.01 M															
4	1	24.6	7.81	411.61	3.00	216.8	2.89	1.04	10	10	1.66E-03	1.54E-03	5.60		
5	2	25.2	7.79	410.87	2.99	211.63	2.82	1.06	10	10	1.65E-03	1.50E-03	5.61	5.61	0.02
6	3	24.4	7.82	395.88	2.88	206.14	2.75	1.05	10	10	1.60E-03	1.47E-03	5.63		
Added KNO$_3$ 0.05 M															
7	1	25.1	7.88	659.08	4.80	312.36	4.17	1.15	50	50	1.77E-03	1.63E-03	5.54		
8	2	25.4	7.85	662.87	4.83	300.9	4.02	1.20	50	50	1.78E-03	1.57E-03	5.55	5.52	0.05
9	3	24.9	7.84	696.94	5.07	353.33	4.72	1.08	50	50	1.86E-03	1.83E-03	5.47		
Added KNO$_3$ 0.1 M															
10	1	24.4	8.08	680.92	4.96	378.92	5.06	0.98	100	100	1.40E-03	1.65E-03	5.64		
11	2	24.7	8.09	688.16	5.01	365.38	4.88	1.03	100	100	1.42E-03	1.59E-03	5.65	5.64	0.01
12	3	24.9	8.03	695.41	5.06	371.08	4.95	1.02	100	100	1.43E-03	1.61E-03	5.64		

K_{SP} Calculation of NaBaAsO$_4$·9H$_2$O compound using FAAS data

Added KNO$_3$ 0 M

Sample No.	Rep	Temp (°C)	pH	[Ba]total ppm	mM	[As]total ppm	mM	Ba/As	[Na]tot ppm	mM	[K]tot mM	[NO$_3$]tot mM	Activity from PhreeqC Na$^+$	Ba^{2+}	AsO$_4^{3-}$	K_{SP}	$-\log K_{SP}$	Average	Stdev
13	1	24.7	10.75	25.28	0.18	76.71	1.02	0.18	96.09	4.18	-	-	3.87E-03	1.33E-04	8.84E-05	4.54E-11	10.34		
14	2	24.7	10.77	23.76	0.17	60.56	0.81	0.21	88.35	3.84	-	-	3.57E-03	1.28E-04	7.47E-05	3.40E-11	10.47	10.36	0.10
15	3	24.4	10.76	29.67	0.22	72.74	0.97	0.22	94.37	4.10	-	-	3.80E-03	1.63E-04	8.54E-05	5.27E-11	10.28		

Added KNO$_3$ 0.01 M

Sample No.	Rep	Temp (°C)	pH	[Ba]total ppm	mM	[As]total ppm	mM	Ba/As	[Na]tot ppm	mM	[K]tot mM	[NO$_3$]tot mM	Activity from PhreeqC Na$^+$	Ba^{2+}	AsO$_4^{3-}$	K_{SP}	$-\log K_{SP}$	Average	Stdev
16	1	24.4	10.84	32.84	0.24	80.69	1.08	0.22	101.23	4.40	10	10	3.88E-03	1.40E-04	8.56E-05	4.66E-11	10.33		
17	2	24.4	10.82	35.26	0.26	82.32	1.10	0.23	95.74	4.16	10	10	3.67E-03	1.52E-04	8.43E-05	4.70E-11	10.33	10.32	0.01
18	3	24.4	10.87	36.11	0.26	78.25	1.04	0.25	98.05	4.26	10	10	3.76E-03	1.52E-04	8.69E-05	4.97E-11	10.30		

Added KNO$_3$ 0.05 M

Sample No.	Rep	Temp (°C)	pH	[Ba]total ppm	mM	[As]total ppm	mM	Ba/As	[Na]tot ppm	mM	[K]tot mM	[NO$_3$]tot mM	Activity from PhreeqC Na$^+$	Ba^{2+}	AsO$_4^{3-}$	K_{SP}	$-\log K_{SP}$	Average	Stdev
19	1	23.6	10.81	106.36	0.77	81.63	1.09	0.71	101.93	4.43	50	50	3.61E-03	2.94E-04	5.10E-05	5.42E-11	10.27		
20	2	23.5	10.81	113.05	0.82	75.95	1.01	0.81	98.85	4.30	50	50	3.50E-03	3.14E-04	4.73E-05	5.20E-11	10.28	10.27	0.01
21	3	24	10.84	99.78	0.73	76.33	1.02	0.71	107.25	4.67	50	50	3.80E-03	2.79E-04	5.04E-05	5.35E-11	10.27		

Added KNO$_3$ 0.1 M

Sample No.	Rep	Temp (°C)	pH	[Ba]total ppm	mM	[As]total ppm	mM	Ba/As	[Na]tot ppm	mM	[K]tot mM	[NO$_3$]tot mM	Activity from PhreeqC Na$^+$	Ba^{2+}	AsO$_4^{3-}$	K_{SP}	$-\log K_{SP}$	Average	Stdev
22	1	24.7	10.83	298.54	2.17	103.89	1.39	1.57	62.53	2.72	100	100	2.11E-03	6.24E-04	4.91E-05	6.45E-11	10.19		
23	2	24.4	10.80	309.26	2.25	108.59	1.45	1.55	52.38	2.28	100	100	1.77E-03	6.47E-04	4.89E-05	5.59E-11	10.25	10.21	0.04
24	3	24.6	10.85	289.76	2.11	108.16	1.44	1.46	62.25	2.71	100	100	2.10E-03	6.06E-04	5.22E-05	6.64E-11	10.18		

K_{SP} Calculation of $Ba_5Cl(AsO_4)_3$ compound using FAAS data

Added KNO₃ 0 M

Sample No.	Rep	Temp (°C)	pH	[Ba]total ppm	mM	[As]total ppm	mM	Ba/As	[Cl⁻] M	[K]tot	[NO₃]tot	Activity from PhreeqC Ba²⁺	Cl⁻	AsO₄³⁻	K_{SP}	−log K_{SP}	Average	Stdev
25	1	24.3	9.56	129.67	0.94	19.95	0.27	3.55	6.52E-04	-	-	7.49E-04	6.15E-04	1.94E-06	1.05E-36	35.98		
26	2	24.6	9.75	120.09	0.87	14.75	0.20	4.44	6.23E-04	-	-	7.00E-04	5.89E-04	2.25E-06	1.13E-36	35.95	35.82	0.26
27	3	24.2	9.85	119.57	0.87	17.21	0.23	3.79	5.85E-04	-	-	6.99E-04	5.53E-04	3.20E-06	3.03E-36	35.52		

Added KNO₃ 0.01 M

Sample No.	Rep	Temp (°C)	pH	[Ba]total ppm	mM	[As]total ppm	mM	Ba/As	[Cl⁻] M	[K]tot mM	[NO₃]tot mM	Activity from PhreeqC Ba²⁺	Cl⁻	AsO₄³⁻	K_{SP}	−log K_{SP}	Average	Stdev
28	1	24.3	10.08	147.53	1.07	22.92	0.31	3.51	5.78E-04	10	10	6.49E-04	5.13E-04	5.59E-06	1.03E-35	34.99		
29	2	24.3	10.09	136.61	0.99	20.42	0.27	3.65	5.21E-04	10	10	6.03E-04	4.63E-04	5.00E-06	4.60E-36	35.34	35.27	0.26
30	3	23.8	10.05	148.25	1.08	16.81	0.22	4.81	6.03E-04	10	10	6.57E-04	5.36E-04	3.68E-06	3.27E-36	35.49		

Added KNO₃ 0.05 M

Sample No.	Rep	Temp (°C)	pH	[Ba]total ppm	mM	[As]total ppm	mM	Ba/As	[Cl⁻] M	[K]tot mM	[NO₃]tot mM	Activity from PhreeqC Ba²⁺	Cl⁻	AsO₄³⁻	K_{SP}	−log K_{SP}	Average	Stdev
31	1	24.7	10.21	181.64	1.32	31.25	0.42	3.17	5.66E-04	50	50	5.12E-04	4.56E-04	6.78E-06	5.00E-36	35.30		
32	2	24.7	10.29	184.29	1.34	34.03	0.45	2.95	5.43E-04	50	50	5.20E-04	4.38E-04	8.54E-06	1.03E-35	34.99	35.17	0.16
33	3	24.7	10.24	182.83	1.33	30.42	0.41	3.28	6.01E-04	50	50	5.16E-04	4.85E-04	7.04E-06	6.17E-36	35.21		

Added KNO₃ 0.1 M

Sample No.	Rep	Temp (°C)	pH	[Ba]total ppm	mM	[As]total ppm	mM	Ba/As	[Cl⁻] M	[K]tot mM	[NO₃]tot mM	Activity from PhreeqC Ba²⁺	Cl⁻	AsO₄³⁻	K_{SP}	−log K_{SP}	Average	Stdev
34	1	24.2	10.41	263.92	1.92	34.44	0.46	4.18	4.48E-04	100	100	5.58E-04	3.40E-04	8.32E-06	1.06E-35	34.97		
35	2	25.5	10.41	264.54	1.93	35.56	0.47	4.06	4.30E-04	100	100	5.60E-04	3.26E-04	8.70E-06	1.19E-35	34.93	34.94	0.03
36	3	24.2	10.48	265.96	1.94	33.33	0.44	4.35	5.15E-04	100	100	5.64E-04	3.91E-04	8.07E-06	1.18E-35	34.93		

K_{SP} calculation using ICP-MS data

K_{SP} Calculation of BaHAsO$_4$ H$_2$O compound using ICP-MS data

Added KNO$_3$ 0 M

Sample No.	pH	Temp	I (M)	conc (ppm) Ba	As	mmol Ba	As	Ba/As	Activities from PhreeqC Ba^{2+}	HAsO$_4^{2-}$	p(Ba2+)	p(HAsO42-)	$-\log K_{SP}$	Ave	Stdev
1	7.47	24.7	0.00	512.21	276.42	3.73	3.69	1.01	2.34E-03	1.99E-03	2.63	2.70	5.33	5.31	0.02
2	7.58	24.6	0.00	531.18	285.91	3.87	3.82	1.01	2.41E-03	2.10E-03	2.62	2.68	5.30		

Added KNO$_3$ 0.01 M

Sample No.	pH	Temp	I (M)	conc (ppm) Ba	As	mmol Ba	As	Ba/As	Activities from PhreeqC Ba^{2+}	HAsO$_4^{2-}$	p(Ba2+)	p(HAsO42-)	$-\log K_{SP}$	Ave	Stdev
3	7.63	24.9	0.01	575.13	308.25	4.19	4.11	1.02	2.22E-03	2.03E-03	2.65	2.69	5.35	5.33	0.02
4	7.63	25.2	0.01	592.02	322.81	4.31	4.31	1.00	2.27E-03	2.12E-03	2.64	2.67	5.32		

Added KNO$_3$ 0.05 M

Sample No.	pH	Temp	I (M)	conc (ppm) Ba	As	mmol Ba	As	Ba/As	Activities from PhreeqC Ba^{2+}	HAsO$_4^{2-}$	p(Ba2+)	p(HAsO42-)	$-\log K_{SP}$	Ave	Stdev
5	7.65	25.2	0.05	631.82	364.38	4.60	4.86	0.95	1.69E-03	1.85E-03	2.77	2.73	5.51	5.50	0.00
6	7.62	24.9	0.05	638.45	367.53	4.65	4.91	0.95	1.71E-03	1.85E-03	2.77	2.73	5.50		

Added KNO$_3$ 0.1 M

Sample No.	pH	Temp	I (M)	conc (ppm) Ba	As	mmol Ba	As	Ba/As	Activities from PhreeqC Ba^{2+}	HAsO$_4^{2-}$	p(Ba2+)	p(HAsO42-)	$-\log K_{SP}$	Ave	Stdev
7	7.52	25.2	0.10	783.64	432.67	5.71	5.78	0.99	1.52E-03	1.78E-03	2.82	2.75	5.57	5.81	0.34
8	7.72	24.2	0.10	436.19	228.53	3.179	3.050	0.99	9.13E-04	9.90E-04	3.04	3.00	6.04		

K_{SP} Calculation of NaBaAsO$_4$ 9H$_2$O compound using ICP-MS data

Added KNO$_3$ 0 M

Sample No.	pH	temp	I (M)	conc (ppm) Ba	As	Na	mmol Ba	As	Na	Ba/As	Activities from PhreeqC Ba^{2+}	AsO$_4$$^{3-}$	Na$^+$	K_{SP} calculation p(Ba^{2+})	p(AsO$_4$$^{3-}$)	p(Na$^+$)	$-$log K_{SP}	Ave	Stdev
9	9.08	25.1	0.00	85.98	159.67	70.01	0.63	2.13	3.05	0.29	4.43E-04	4.58E-06	2.79E-03	3.35	5.34	2.55	11.25	11.14	0.15
10	9.53	24.7	0.00	48.41	156.39	73.31	0.35	2.09	3.19	0.17	2.52E-04	1.26E-05	2.93E-03	3.60	4.90	2.53	11.03		

Added KNO$_3$ 0.01 M

Sample No.	pH	temp	I (M)	conc (ppm) Ba	As	Na	mmol Ba	As	Na	Ba/As	Activities from PhreeqC Ba^{2+}	AsO$_4$$^{3-}$	Na$^+$	K_{SP} calculation p(Ba^{2+})	p(AsO$_4$$^{3-}$)	p(Na$^+$)	$-$log K_{SP}	Ave	Stdev
11	9.55	24.9	0.01	84.54	183.17	78.45	0.62	2.44	3.41	0.25	3.52E-04	1.28E-05	2.99E-03	3.45	4.89	2.52	10.87	10.82	0.07
12	9.77	25.1	0.01	70.50	159.58	81.48	0.51	2.13	3.54	0.24	2.95E-04	1.85E-05	3.11E-03	3.53	4.73	2.51	10.77		

Added KNO$_3$ 0.05 M

Sample No.	pH	temp	I (M)	conc (ppm) Ba	As	Na	mmol Ba	As	Na	Ba/As	Activities from PhreeqC Ba^{2+}	AsO$_4$$^{3-}$	Na$^+$	K_{SP} calculation p(Ba^{2+})	p(AsO$_4$$^{3-}$)	p(Na$^+$)	$-$log K_{SP}	Ave	Stdev
13	9.94	24.2	0.05	97.81	186.67	87.39	0.71	2.49	3.80	0.29	2.71E-04	2.18E-05	3.09E-03	3.57	4.66	2.51	10.74	10.70	0.05
14	10.02	23.9	0.05	94.17	180.86	94.55	0.69	2.41	4.11	0.28	2.61E-04	2.49E-05	3.34E-03	3.58	4.60	2.48	10.66		

Added KNO$_3$ 0.1 M

Sample No.	pH	temp	I (M)	conc (ppm) Ba	As	Na	mmol Ba	As	Na	Ba/As	Activities from PhreeqC Ba^{2+}	AsO$_4$$^{3-}$	Na$^+$	K_{SP} calculation p(Ba^{2+})	p(AsO$_4$$^{3-}$)	p(Na$^+$)	$-$log K_{SP}	Ave	Stdev
15	10.13	25.2	0.10	129.88	206.53	185.99	0.95	2.76	8.09	0.34	2.70E-04	2.86E-05	6.25E-03	3.57	4.54	2.20	10.32	10.42	0.15
16	10.14	24.8	0.10	125.84	221.92	107.24	0.92	2.96	4.66	0.31	2.63E-04	3.13E-05	3.61E-03	3.58	4.50	2.44	10.53		

K_{SP} Calculation of $Ba_5Cl(AsO_4)_3$ compound using ICP-MS data

Added KNO$_3$ 0 M

Sample No	pH	Temp	I (M)	conc (ppm) Ba	As	mmol Ba	As	Cl^{-*}	Ba/As	Activities from PhreeqC Ba^{2+}	AsO$_4^{3-}$	Cl$^-$	K_{SP} calculation p(Ba^{2+})	p(AsO$_4^{3-}$)	p(Cl$^-$)	$-\log K_{SP}$	Ave	Stdev
17	8.96	25.3	0.00	326.57	137.05	2.38	1.83	0.48	1.30	1.63E-03	2.90E-06	4.31E-04	2.79	5.54	3.37	33.92	33.81	0.17
18	9.13	24.4	0.00	302.87	127.80	2.21	1.71	0.44	1.29	1.53E-03	3.96E-06	4.01E-04	2.82	5.40	3.40	33.69		

Added KNO$_3$ 0.01 M

Sample No	pH	Temp	I (M)	conc (ppm) Ba	As	Mmol Ba	As	Cl^{-*}	Ba/As	Activities from PhreeqC Ba^{2+}	AsO$_4^{3-}$	Cl$^-$	K_{SP} calculation p(Ba^{2+})	p(AsO$_4^{3-}$)	p(Cl$^-$)	$-\log K_{SP}$	Ave	Stdev
19	9.21	24.9	0.01	338.23	145.26	2.46	1.94	0.49	1.27	1.39E-03	4.62E-06	4.28E-04	2.86	5.34	3.37	33.66	33.61	0.07
20	9.22	25.2	0.01	347.43	144.69	2.53	1.93	0.51	1.31	1.43E-03	4.73E-06	4.40E-04	2.85	5.33	3.36	33.56		

Added KNO$_3$ 0.05 M

Sample No	pH	Temp	I (M)	conc (ppm) Ba	As	Mmol Ba	As	Cl^{-*}	Ba/As	Activities from PhreeqC Ba^{2+}	AsO$_4^{3-}$	Cl$^-$	K_{SP} calculation p(Ba^{2+})	p(AsO$_4^{3-}$)	p(Cl$^-$)	$-\log K_{SP}$	Ave	Stdev
21	9.62	25.1	0.05	395.59	174.86	2.88	2.33	0.58	1.23	1.09E-03	1.02E-05	4.60E-04	2.96	4.99	3.34	33.13	33.02	0.16
22	9.76	24.9	0.05	382.46	162.61	2.78	2.17	0.56	1.28	1.05E-03	1.29E-05	4.45E-04	2.98	4.89	3.35	32.90		

Added KNO$_3$ 0.10 M

Sample No	pH	Temp	I (M)	conc (ppm) Ba	As	Mmol Ba	As	Cl^{-*}	Ba/As	Activities from PhreeqC Ba^{2+}	AsO$_4^{3-}$	Cl$^-$	K_{SP} calculation p(Ba^{2+})	p(AsO$_4^{3-}$)	p(Cl$^-$)	$-\log K_{SP}$	Ave	Stdev
23	9.64	24.7	0.10	450.58	202.47	3.28	2.70	0.66	1.21	9.41E-04	9.80E-06	4.95E-04	3.03	5.01	3.31	33.46	33.28	0.26
24	9.84	25.2	0.10	430.26	188.34	3.13	2.51	0.63	1.25	8.99E-04	1.43E-05	4.73E-04	3.05	4.85	3.32	33.09		

* Cl concentration is calculate from assumption that 1 mol total chloride is equivalent to 5 mol total barium

2.6 References

Butler, B. N. (1998). **Ionic Equilibrium: Solubility and pH Calculations.** John Wiley & Sons, Toronto, Canada.

Chukhlantsev, V. G. (1956). Solubility Product of Arsenates. **J. Inorg. Chem. (USSR).** 1: 1975-1982.

Davis, J. (2000). Stability of Metal-Arsenic Solids in Drinking Water Systems. **Pract. Periodical Haz. Toxic Radioactive Waste Mgmt.** 4(1): 31-35.

Essington, M. E. (1988). Solubility of Barium Arsenate. **Soil Sci. Soc. Am. J.** 52: 1566-1570.

Gallo, D., Acosta, E., Scamehorn, J. F., and Sabatini, D. A. (2006). Pilot Scale Study of Polyelectrolyte Enhanced Ultrafiltration for Arsenic Removal. **J. Am. Water Works Assoc.** 98(1): 106-116.

Hung, D. Q., Nekrassova, O., and Compton, R. G. (2004). Analytical Methods for Inorganic Arsenic in Water: A Review. **Talanta.** 64: 269-277.

IUPAC. (1997). **Compendium of Chemical Terminology,** 2nd ed. the Gold Book, (Compiled by McNaught, A. D., and Wilkinson, A.). Blackwell Scientific Publications, Oxford.

Krauskopf, K. B. and Bird, D. K. (1995). **Introduction to Geochemistry,** 3rd ed., McGraw-Hill, New York.

Langmuir, D., Mahoney, J., and Rowson, J. (2006). Solubility Products of Amorphous Ferric Arsenate and Crystalline Scorodite ($FeAsO_4 \cdot 2H_2O$) and Their Application to Arsenic Behavior in Buried Mine Tailing. **Geochem. Cosmochim. Acta.** 70: 2942-2956.

Mandal, B. K. and Suzuki, K. T. (2002). Arsenic Round the World: A Review. **Talanta.** 58(1): 201-235.

NHMRC/AWRC (National Health and Medical Research Council, and Agricultural and Resource Management Council of Australia and New Zealand). (1996). **Australian Drinking Water Guidelines,** Australia.

Oremland, R. S. and Stolz, J. F. (2003). The Ecology of Arsenic**. Science.** 300: 939-944.

Parkhurst, D. L. and Appelo, C. A. J. (1999). **User's Guide to PHREEQC: A Computer Program for Speciation, Batch-reaction, One-dimensional Transport, and Inverse Geochemical Calculations,** Version 2, Water-Resources Investigations Report 99-4259, U.S. Geological Survey.

Pookrod, P., Haller, K. J., and Scamehorn, J. F. (2004). Removal of Arsenic Anions from Water using Polyelectrolyte-Enhanced Ultrafiltration. **Sep. Sci. Technol.** 39(4): 811-831.

Rai, D., Ainsworth, C. C., Eary, L. E., Mattigod, S. V., and Jackson, D. R. (1987). **Inorganic and Organic Constituents in Fossil Fuel Combustion Residues.** Vol 1. A Critical Review. EPRI Rep. EA-5176. Electric Power Research Institute, Palo Alto, CA.

Skoog, D. A. and Leary, J. L. (1992). **Principles of Instrumental Analysis,** 4th ed., Saunders College Publishing pp. 219-221.

Smedley, P. L. and Kinniburgh, D. G. (2002). A Review of the Source, Behaviour and Distribution of Arsenic in Natural Waters. **Appl. Geochem.** 17(5): 517-568.

Smith, A. H., Lingas, E. O., and Rahman, M. (2000). Contamination of Drinking-water by Arsenic in Bangladesh: a Public Health Emergency. **B. World Health Organ.** 78(9): 1093-1103.

Turner, T. R. (1981). Oxidation State of Arsenic in Coal Ash Leachate. **Environ. Sci. Technol.** 15: 1062-1066.

United States Environmental Protection Agency. (2001), **EPA to Implement 10 ppb Standard for Arsenic in Drinking Water,** EPA 815-F-01-010.

Wagemann, R. (1978). Some Theoretical Aspects of Stability and Solubility of Inorganic Arsenic in the Freshwater Environment. **Water Res.** 12: 139-145.

WHO (World Health Organization). (1993). **Guidelines for Drinking-water Quality,** 2nd ed., vol.1, World Health Organization, Geneva.

Zhu, Y. and Markel, B. J. (2001). The Dissolution and Solubility of Scorodite, $FeAsO_4 \cdot 2H_2O$ Evaluation and Simulation with PHREEQC2. **Wiss. Mitt. Inst. Fur. Geologie.** 18: 1-12.

Zhu, Y., Zhang, X., Xie, Q., Chen, Y., Wang, D., Liang, Y., and Lu, J. (2005). Solubility and Stability of Barium Arsenate and Barium Hydrogen Arsenate at 25°C. **J. Hazard. Mater.** 120: 37-44.

CHAPTER III

ARSENATE REMOVAL BY COPRECIPITATON WITH

CALCIUM PHOSPHATE HYDROXYAPATITE

3.1   Introduction

Arsenic removal by precipitation with calcium is a topic of increasing interest. Low arsenic concentration can be obtained by formation of various low solubility calcium-arsenate compounds *e.g.* $Ca_3(AsO_4)_2$, $CaHAsO_3$, $Ca_4(OH)_2(AsO_4)_2 \cdot 4H_2O$, and $Ca_5(AsO_4)_3OH$ (Bothe and Brown, 1999a, 1999b; Dutre and Vandecasteele, 1995, 1998; Moon, Dermatas, and Menounou, 2004; Vandecasteele, Dutre, Geysen, and Wauters, 2002). However, these calcium-arsenate compounds are unstable at high pH when they can convert to calcium carbonate in the presence of atmospheric carbon dioxide releasing the arsenic back to the environment. Because of this, arsenic immobilization by simple precipitation with calcium may not be acceptable. Apatite is a class of mineral with formula $M_5(BO_4)_3X$ where M is a divalent metal ion, *e.g.* Ca^{2+}, Ba^{2+}, or Pb^{2+}; BO_4 is a trivalent oxyanion, *e.g.* PO_4^{3-} or VO_4^{3-}; and X is a monovalent anion, generally OH^-, Cl^-, or F^-. The structure of calcium phosphate hydroxyapatite, CaPHAP, is shown in Figure 3.1. The structure can accept replacements in M, B, and X positions, as indicated by the Ca^{2+} and PO_4^{3-} positions in Figure 3.1, when the replacements are of similar size or coordination geometry. Consequently, apatites are widely studied for heavy metal immobilization purposes.

Exchangeable Ca^{2+} position

[001] view

Exchangeable PO$_4^{3-}$ position

[010] view
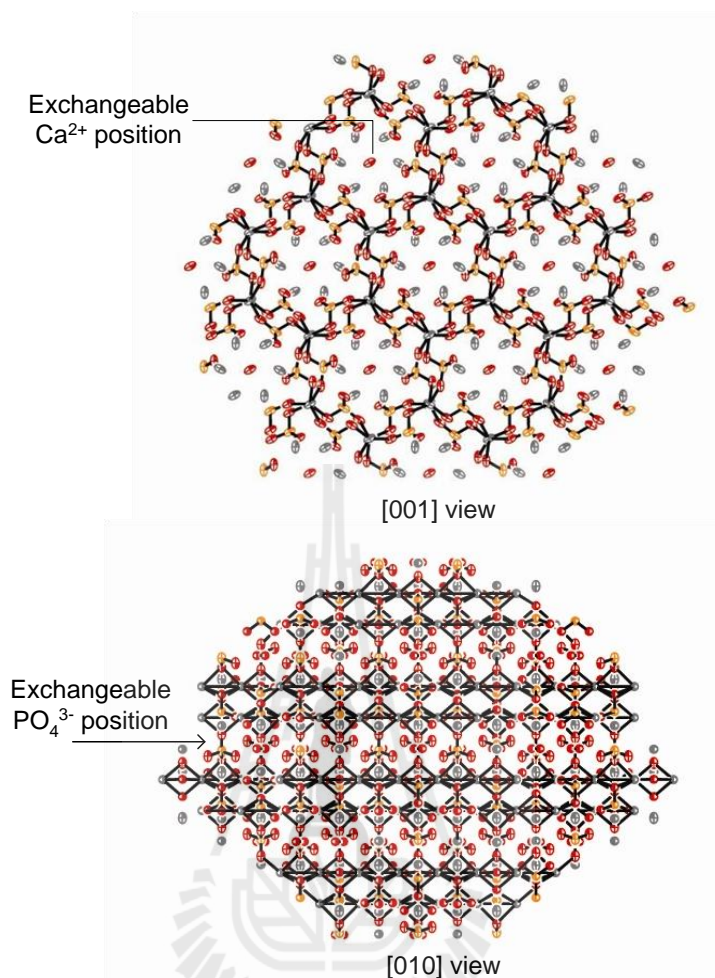
Figure 3.1 CaPHAP structure and Ca^{2+} and PO$_4^{3-}$ exchangeable positions.

CaPHAP, Ca$_5$(PO$_4$)$_3$(OH), is a naturally occurring apatite mineral that is a major component of animal bones and teeth. Due to the special chemical properties of CaPHAP to tolerate substitution in the structure, it has been used as the host for cations and anions such as Cd^{2+}, Zn^{2+} (Gomez del Rio, Sanchez, Morando, and Cicerone, 2006; Marchat, Bernache-Assollant, and Champion, 2006; Peld, Tonsuaadu, and Bender, 2004; Yasukawa, Yokoyama, Kandori, and Ishikawa, 2007), Pb^{2+} (Chen, Wright, Conca, and Peurrung, 1997), VO$_4^{3-}$ (Vega, Pedregosa, Narda, and Morando, 2003), U^{6+} (Fuller, Bargar, Davis, and Piana, 2002; Krestou, Xenidis,

and Panias, 2004). Substitutions of metal cation and oxyanion occur in the apatite structure at Ca^{2+} and PO_4^{3-} positions, respectively, resulting in the toxic substances being removed into a chemically very stable structural form. Moreover, the resulting compounds appear to be stable under atmospheric conditions with no transformation to calcium carbonate observed.

The present study examines arsenic removal from an arsenate containing PEUF waste stream by coprecipitating arsenate with phosphate under conditions that result in the formation of CaPHAP. Presumably, based on the similarity of phosphate and arsenate (atomic radius 0.47 Å for As and 0.34 Å for P; arsenate and phosphate are tetrahedral), the arsenate substitutes for a fraction of the phosphate in a calcium phosphate hydroxyapatite host allowing formation of a stable calcium phosphate/arsenate hydroxyapatite compound.

3.2   Experimental

Chemicals

All chemicals used were analytical grade and used without further purification. Disodium hydrogen phosphate dodecahydrate, $Na_2HPO_4 \cdot 12H_2O$, (Carlo Erba, Milan, Italy) and disodium hydrogen arsenate heptahydrate, $Na_2HAsO_4 \cdot 7H_2O$, (Fluka, Buchs, Switzerland) were used as sources of phosphate and arsenate. Calcium hydroxide, $Ca(OH)_2$ (Carlo Erba, Milan, Italy) was used as the source of calcium. Sodium hydroxide, NaOH, (EKA Chemicals, Bohus, Sweden) and hydrochloric acid, HCl, (Merck, Darmstadt, Germany) were used for pH adjustments.

The cationic polyelectrolyte, QUAT, (tradename MERQUAT, Calgon Corp., Pittsburgh PA) with the average molecular weight of 240 kDa was prepurified by

removing short chain polyelectrolyte using a 10 kDa ultrafiltration membrane (Osmonics Inc., Minnetonka MN). QUAT concentrations were determined by total organic carbon measurement (Leco CNS-2000 analyzer) using Leco soil standard. The concentrations of carbon and nitrogen correspond to QUAT concentration based on the polymer repeating unit formula. Deionized water was used for all experiments.

Coprecipitation of arsenate with calcium phosphate hydroxyapatite

Precipitation in the absence of QUAT

Solutions of mixed anions (50 mL) were prepared from $Na_2HAsO_4 \cdot 7H_2O$ and $Na_2HPO_4 \cdot 12H_2O$ with arsenic concentrations fixed at 25 ppm and phosphate concentrations varied to give P/As mole ratios of 0 (no P), 1, 3, and 5. The pH of the anionic solutions was varied to 4.5, 7.0, 9.5, and 11.5 before mixing with 50 mL of $Ca(OH)_2$ with concentrations varied to Ca/(P+As) = 1, 2, and 3 without pH adjustment. The mixed solutions were allowed to stand at 24 $\pm$1°C for 24 hr in a temperature controlled laboratory. The product was filtered off and air-dried.

Precipitation in the presence of QUAT

The precipitation in the presence of QUAT was conducted by a procedure similar to that described above except with the addition of QUAT (monomer concentration 100 times the arsenic concentration) to the anion solution prior to mixing with the $Ca(OH)_2$ solution.

Characterization

Filtrates were analyzed for arsenic concentration using an AAS spectrometer (Perkin-Elmer AAnalyst 100) equipped with a flow injection hydride generation

system (Perkin Elmer FIAS-400). Solid precipitates were characterized by XRD using a Bruker Analytical X-ray Systems model D5005 X-ray diffractometer equipped with a Cu K_α sealed tube X-ray source operating at 40 kV and 35 mA. The data were collected in the range of 5.0-60.0° two theta in steps of 0.02° and a scan speed of 0.4 sec/step. Particle morphologies and heavy elemental compositions of the solid samples were examined by SEM/EDX.

3.3   Results and discussion

Formation of coprecipitate

Calcium arsenate hydroxyapatite, CaAsHAP, was formed in a preliminary study of calcium arsenate precipitation at high arsenic concentration. However, this phase does not form at the low arsenic concentration levels used in the no phosphate (P/As = 0) experiments here. Precipitation immediately occurs creating a turbid solution when phosphate is present and the two solutions are mixed at the certain condition. The white precipitates were characterized by XRD for phase identification.

Typical XRD patterns of the precipitation products are very low in intensity as can be seen in the lower of each pair of curves in Figure 3.2. This may be due to low crystallinity or very small crystallite size of the precipitate. The precipitates were heat treated at 600°C for 4 hr to improve the sharpness of the XRD pattern before comparing d-spacing. The comparison of d-spacing of CaPHAP, a material formed by coprecipitation of arsenate with CaPHAP, and CaAsHAP are shown in Figure 3.3 and Table 3.1. The results here are consistent with those reported on formation of solid solutions incorporating arsenate into CaPHAP, which results in expansion of the d-spacings of CaPHAP due to the larger radius of arsenic compared to phosphorous.

We can conclude that arsenate can be removed from solutions containing arsenate anion by forming a coprecipitate with CaPHAP.
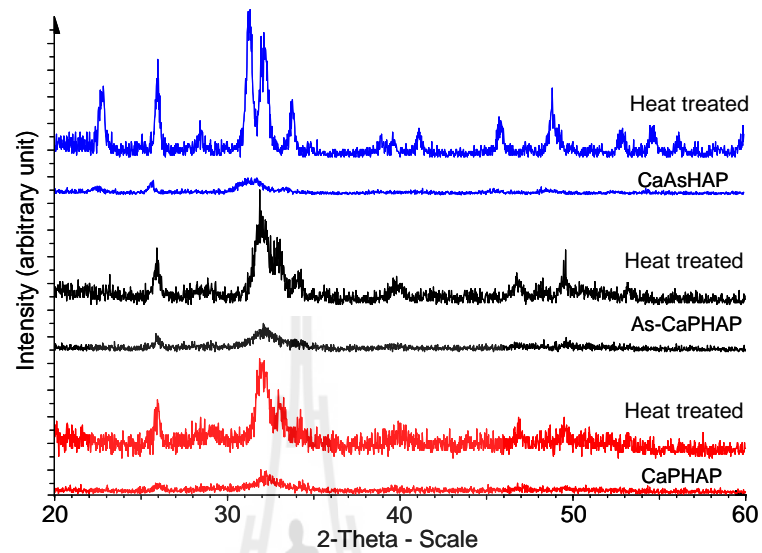
Figure 3.2 Typical XRD patterns of CaPHAP, As-CaPHAP, and CaAsHAP before

and after heat treatment.
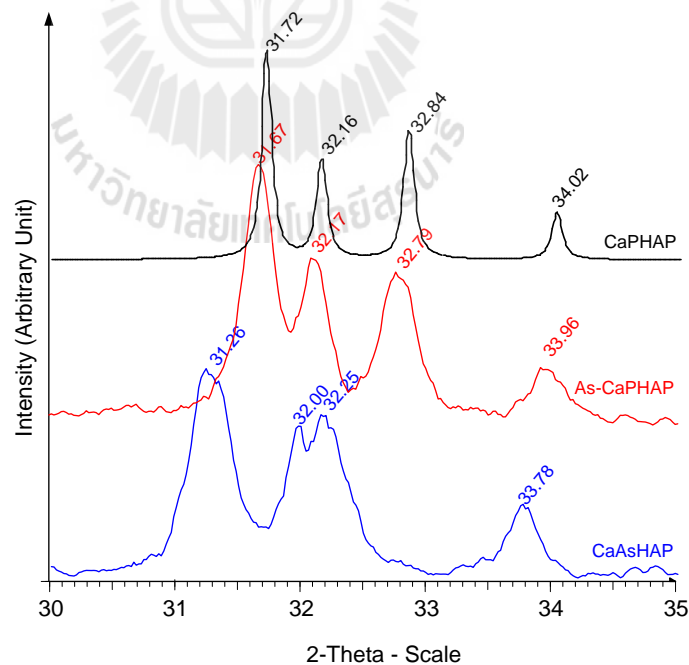
Figure 3.3 XRD patterns showing shift of d-spacing in CaPHAP, As-CaPHAP, and

CaAsHAP.

Table 3.1 d-spacings of CaPHAP, As-CaPHAP, and CaAsHAP.

Compound	2-Theta (d-spacing)			
CaPHAP	31.72	32.16	32.84	34.02
	(2.8175)	(2.7800)	(2.7240)	(2.6321)
As-CaPHAP	31.67	32.17	32.79	33.96
	(2.8219)	(2.7792)	(2.7280)	(2.6374)
CaAsHAP	31.26	32.00	32.25	33.78
	(2.8579)	(2.7935)	(2.7724)	(2.6503)

The SEM micrograph of broken filter cake of As-CaPHAP (Figure 3.4) shows the particle size to be very small, making the SEM technique unsuitable for morphological studies of these samples. However, elemental analysis from EDX suggests that arsenic is found in the CaPHAP precipitates from arsenate-containing solutions supporting the contention that arsenic coprecipitates with CaPHAP.
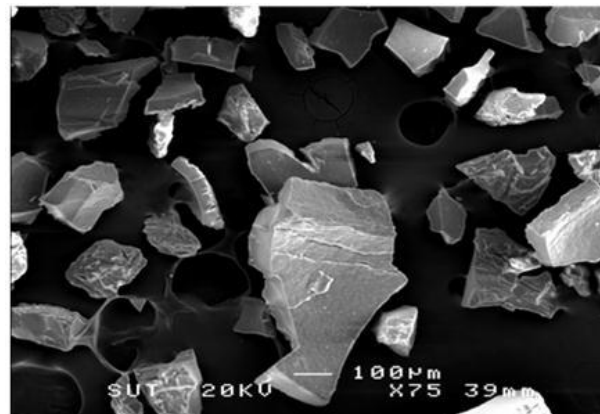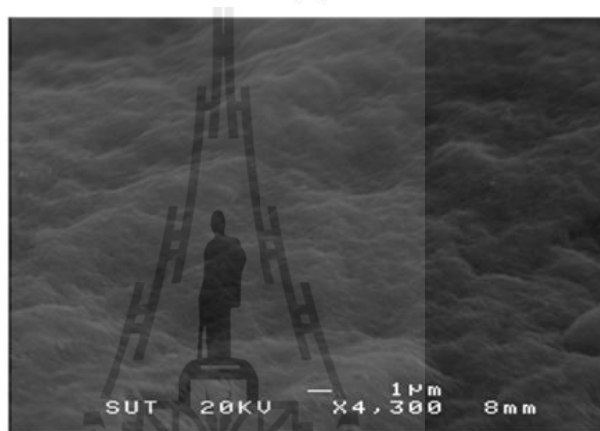
Figure 3.4 SEM micrographs of broken filter cake of As-CaPHAP.
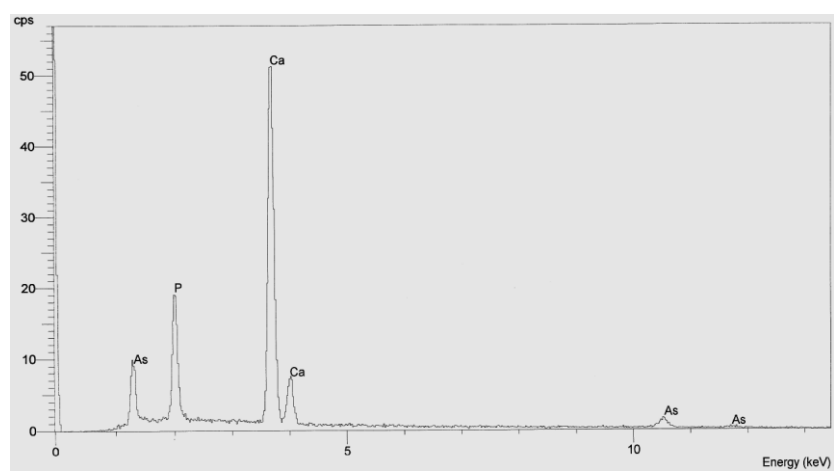
Figure 3.5 EDX of As-CaPHAP.

When phosphate and arsenate are both present in the solution in the presence of QUAT, turbidity occurs immediately on mixing the two solutions together. The precipitates formed in the presence of QUAT settle to the bottom of the vessel more slowly than those formed in the absence of QUAT. After 24 hr the QUAT containing solutions are still turbid even as most of the precipitate had settled, indicating that there are still extremely fine particles dispersed in the solution. XRD characterization of the white precipitates gave similar results to those formed in the absence of QUAT discussed above.

Arsenate removal efficiency without polyelectrolyte

The relationship of arsenic removal by coprecipitation with CaPHAP in the absence of QUAT and precipitation parameters (pH of anion solution, P/As ratio, and Ca/(P+As) ratio) is represented in Figure 3.6. Ca/(P+As) and P/As mole ratios play an important role for arsenate removal in this study. At Ca/(P+As) = 1 poor arsenate removal was achieved (in every P/As mol ratio, and pH of anion studied) due to a lack of precipitation within the 24 hr reaction time of this study. Neither a calcium arsenate phase nor a calcium phosphate phase formed in these conditions indicating that Ca/(P+As) = 1 is not kinetically preferred to force the precipitation to occur in a short period of time. On the other hand, the higher Ca/(P+As) ratios of 2, and 3 create a large enough driving force to cause precipitation to occur immediately. CaPHAP is found as the precipitate compound (as mentioned in characterization result) in the solution when the phosphate anion is available (P/As is not 0). The precipitation of CaPHAP with arsenate anions available in the same solution induces coprecipitation of arsenate anion with CaPHAP resulting in arsenate anions being removed from the

solution. The removed arsenate anions are presumed to incorporate in the CaPHAP structure in $PO_4{}^{3-}$ positions as discussed previously, forming As-CaPHAP. Therefore, arsenate removals were obtained in both Ca/(P+As) ratios of 2, and 3, with higher arsenate removal efficiency in Ca/(P+As) = 3 at the same P/As ratio and pH. This might be due to larger driving force in the Ca/(P+As) = 3 system to drive CaPHAP precipitation resulting in higher amount of CaPHAP precipitated, consequently both phosphate and arsenate anions removed more complete, hence higher arsenic removal achieved.

The P/As mole ratio plays an important role for CaPHAP precipitation, hence P/As is a significant parameter for removal of arsenate from the solution. No precipitation occurs without phosphate ion (P/As = 0) in any Ca/(P+As) or pH in this study. No calcium-arsenate phases are observed in all of these conditions, therefore no arsenate removal is obtained. When phosphate is available in the solution even in low concentration (P/As = 1) at suitable Ca/(P+As) ratio (2, or 3), the CaPHAP is able to precipitate and arsenic removal was achieved. The removal of arsenate at low phosphate concentration is not high in both Ca/(P+As) = 2, or 3 due to a limited amount of CaPHAP precipitate forming, thereby limiting the sites for arsenate anion to be incorporated. Dramatic reductions of arsenic concentration in the supernatant were achieved when phosphate concentration in solution increased (P/As = 3, or 5), indicating that as a larger amount of CaPHAP precipitates more sites are available for arsenate anion to incorporate.
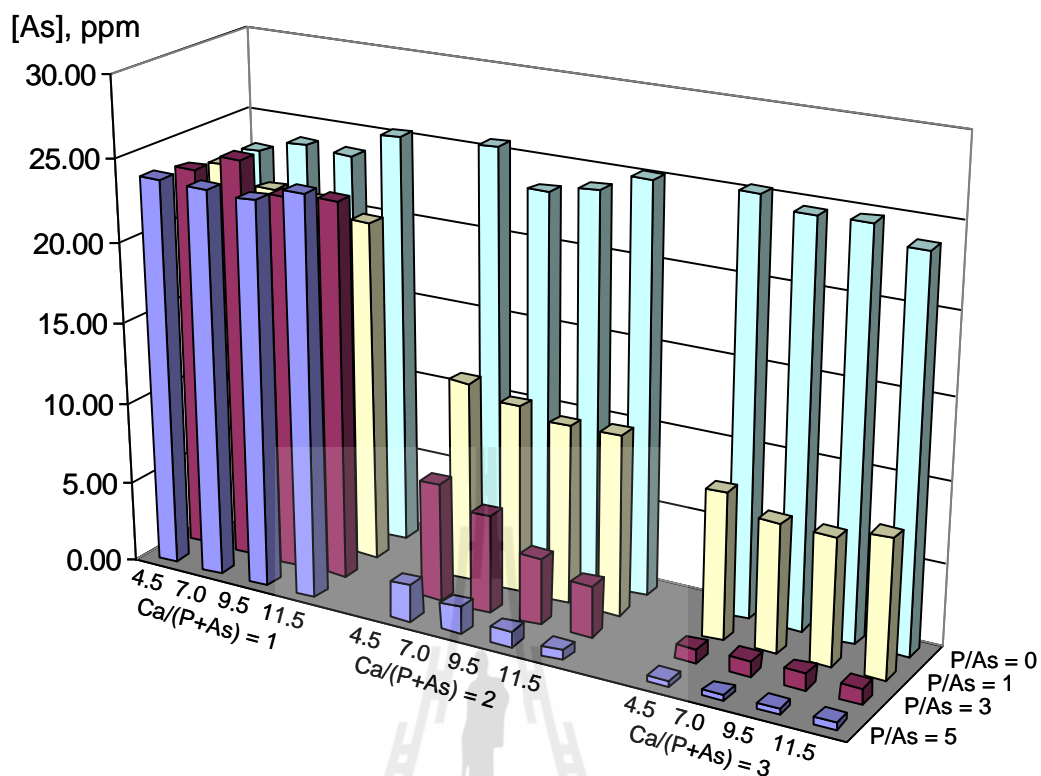
Figure 3.6 Arsenate removal efficiency without QUAT.

The pH of the anion solution does not significantly affect the arsenate removal efficiency in this approach. At Ca/(P+As) = 1 where low calcium cation concentration is inadequate to drive the CaPHAP precipitation, no arsenate removal was achieved for any P/As ratio or pH studied. At Ca/(P+As) = 3 enough calcium cation concentration is available to drive a large amount of CaPHAP to precipitate when phosphate is available in the solution, and similar arsenate removal levels are achieved at the same P/As mole ratio at every pH condition studied. Arsenate removal seems to depend on Ca/(P+As) and P/As mole ratios rather than on pH in these conditions. However, as the relative Ca concentration decreases, Ca/(P+As) = 2, the arsenate removal is affected by the pH as observed in P/As = 1, 3, and 5 experiments. Higher arsenate removals were achieved with increasing pH for all three

ratios, indicating that AsO_4^{3-} is the most preferred species to incorporate into CaPHAP structure since high pH is suitable for AsO_4^{3-} speciation consistent with the arsenic speciation diagram in Figure 3.7. As pH becomes more acidic the protonated forms of AsO_4^{3-} will dominate; $HAsO_4^{2-}$, and $H_2AsO_4^{-}$ are the dominant species at pH 7.0-11.5, and 2.2-7.0, respectively. Neither $HAsO_4^{2-}$ or $H_2AsO_4^{-}$ can incorporate in CaPHAP, therefore lower arsenic removal efficiencies are observed when the pH decreases.
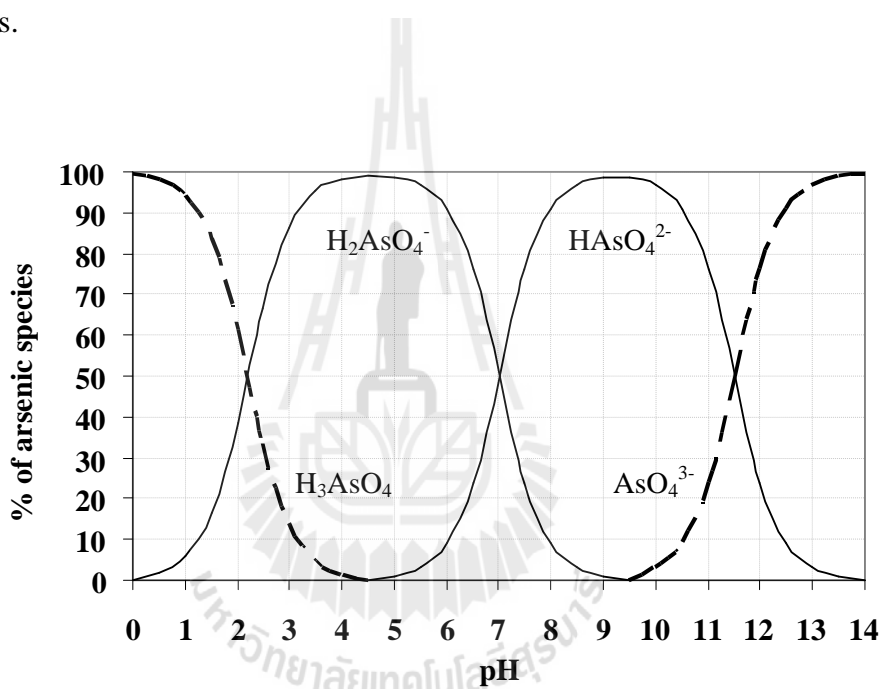
Figure 3.7 Speciation diagram of arsenic acid.

Arsenate removal efficiency by coprecipitation with CaPHAP is found to correlate with the precipitation of CaPHAP as discussed previously. Better CaPHAP precipitation provides higher arsenate removal efficiency. This work found highest arsenate removal efficiency at Ca/(P+As) = 3 and P/As = 5 in all pH, where arsenic concentration is reduced from 25 ppm to about 0.3 ppm or up to 99% arsenate removal.

Arsenate removal efficiency in the presence of polyelectrolyte

The relationship of arsenate removal by coprecipitation with CaPHAP in the presence of QUAT and precipitation parameters (pH of anion solution, P/As ratio, and Ca/(P+As) ratio) is represented in Figure 3.8.
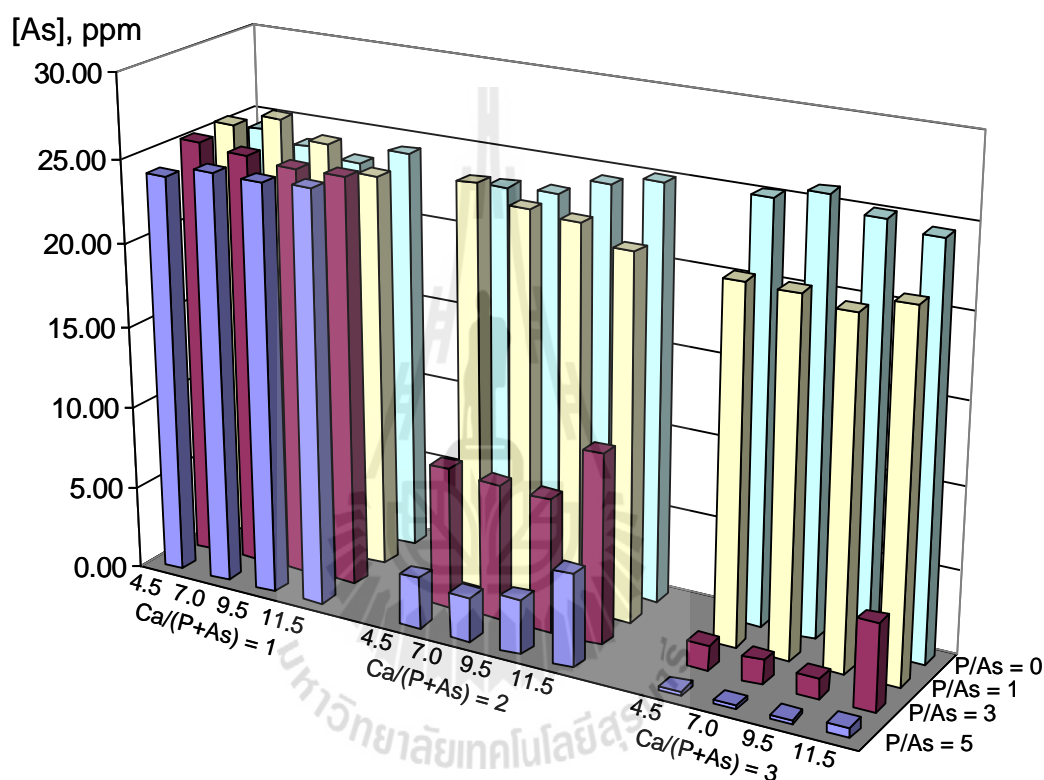
Figure 3.8 Arsenate removal efficiency in the presence of QUAT.

A similar result to systems without QUAT is obtained, Ca/(P+As) and P/As mole ratios play an important role for CaPHAP formation. Higher Ca/(P+As) and P/As ratios improve arsenate removal. Up to 99% arsenate removal was found at P/As = 5 and Ca/(P+As) = 3 in every pH condition indicating that high arsenate removal from QUAT-arsenate complex solution can be achieved by coprecipitating arsenate with CaPHAP. The presence of QUAT in the system inhibits the

precipitation in P/As = 1 at Ca/(P+As) = 2, and 3 resulting in poor arsenate removal in these conditions when compared to no QUAT system. In contrast with the no QUAT system, the pH of the starting anion solution affects arsenate removal efficiency at Ca/(P+As) = 2, and P/As = 3, and 5 in the opposite way, the lower arsenate removal obtained at the higher pH. This is due to higher pH shifting the phosphoric acid equilibrium to favor PO_4^{3-} which binds to QUAT forming QUAT-phosphate complex and thus reducing the activity of PO_4^{3-} in solution at the higher pH. This in turn decreases both the driving force for precipitation of CaPHAP and the amount of CaHAP that can form, hence lower arsenate removal is observed.

3.4 Conclusions

Arsenic in solution can be successfully removed by coprecipitation with low solubility calcium phosphate hydroxyapatite forming As-CaHAP materials. The arsenic removal proposed by incorporation of arsenate into the calcium phosphate hydroxyapatite structure. Up to 99% arsenic removal was achieved from 25 ppm As initial concentration in both the absence and presence of QUAT. The Ca/(P+As) and P/As mole ratios play an important role in arsenic removal efficiency. The higher Ca/(P+As) and P/As mole ratios, the higher the arsenic removal efficiency. The pH of the initial anionic solution does not significantly affect the arsenic removal by this process.

The advantage of this approach is that precipitation can occur at low arsenic concentration implying an easy and inexpensive process for arsenic removal could be based on this method. QUAT interaction on the product surface may disperse small particles in the solution resulting in retardation of the settling of precipitates.

3.5 References

Bothe, J. V. and Brown, P. W. (1999a). Arsenic Immobilization by Calcium Arsenate Formation. **Environ. Sci. Technol.** 33: 3806-3811.

Bothe, J. V. and Brown, P. W. (1999b). The Stabilities of Calcium Arsenates at 23 ±1°C. **J. Hazard. Mater.** B69: 197-207.

Chen, X. B., Wright, J. V., Conca, J. L., and Peurrung, L. M. (1997). Effects of pH on Heavy Metal Sorption on Mineral Apatite. **Environ. Sci. Technol.** 31(3): 624-631.

Dutre, V. and Vandecasteele, C. (1995). Solidification/stabilization of Arsenic-containing Waste: Leach Tests and Behavior of Arsenic in the Leachate. **Waste Manage.** 15: 55-62.

Dutre, V. and Vandecasteele, C. (1998). Immobilization Mechanism of Arsenic in Waste Solidified using Cement and Lime. **Environ. Sci. Technol.** 32: 2782-2787.

Fuller, C. C., Bargar, J. R., Davis, J. A., and Piana, M. J. (2002). Mechanisms of Uranium Interactions with Hydroxyapatite: Implications for Groundwater Remediation. **Environ. Sci. Technol.** 36(2): 158-165.

Gomez del Rio, J., Sanchez, P., Morando, P. J., and Cicerone, D. S. (2006). Retention of Cd, Zn and Co on Hydroxyapatite Filters. **Chemosphere.** 64(6): 1015-1020.

Krestou, A., Xenidis, A., and Panias, D. (2004). Mechanism of Aqueous Uranium(VI) Uptake by Hydroxyapatite. **Miner. Eng.** 17(3): 373-81.

Marchat, D., Bernache-Assollant, D., and Champion, E. (2007). Cadmium Fixation by Synthetic Hydroxyapatite in Aqueous Solution--Thermal Behaviour. **J. Hazard. Mater.** 139(3): 453-60.

Moon, D. H., Dermatas, D., and Menounou, N. (2004). Arsenic immobilization by calcium–arsenic precipitates in lime treated soils, **Sci. Total Environ.** 330: 171-185.

Peld, M., Tonsuaadu, K., and Bender, V. (2004). Sorption and Desorption of Cd^{2+} and Zn^{2+} Ions in Apatite-Aqueous Systems. **Environ. Sci. Technol.** 38(21): 5626-5631.

Vandecasteele, C., Dutre, V., Geysen, D., and Wauters, G. (2002). Solidification/stabilization of Arsenic Bearing Fly Ash from the Metallurgical Industry. Immobilization Mechanism of Arsenic. **Waste Manage.** 22: 143-146.

Vega, E. D., Pedregosa, J. C., Narda, G. E., and Morando, P. J. (2003). Removal of Oxovanadium(IV) from Aqueous Solutions by Using Commercial Crystalline Calcium Hydroxyapatite. **Water Res.** 37(8): 1776-1782.

Yasukawa, A., Yokoyama, T., Kandori, K., and Ishikawa, T. (2007). Reaction of Calcium Hydroxyapatite with Cd^{2+} and Pb^{2+} Ions. **Colloids Surf. A Physicochem. Eng. Asp.** 299(1-3): 203-208.

CHAPTER IV

POLYELECTROLYTE RECOVERY FROM

POLYELECTROLYTE-ARSENATE COMPLEX

SOLUTION

4.1 Introduction

Arsenic contamination in water supplies is a serious problem in various parts of the world (Mandal *et al.*, 2002; Smedley *et al.*, 2002), and has been concern for long time due to the carcinogenic, mutagenic, and teratogenic effect of arsenic on humans. In 2001, the United States Environmental Protection Agency (USEPA) set a new maximum concentration level (MCL) for arsenic in drinking water of 10 ppb which came into effect in 2006 to replace the old MCL of 50 ppb, a level at which arsenic still exhibits chronic effects (USEPA, 2001). Compliance with this new MCL makes a serious problem, especially for small communities with less financial support, to reach the new standard since expensive technologies are often required.

The technology called polyelectrolyte-enhanced ultrafiltration, PEUF, is one technology being explored to remediate low level arsenic contamination to meet this new standard. Pookrod and co-workers (2004) using poly(diallyldimethyl ammonium chloride), QUAT, cationic polyelectrolyte and a 10 kDa molecular weight cut-off, MWCO, ultrafiltration membrane can achieved up to 99.95% arsenic removal from 100 ppb synthetic arsenic solution. Scale-up of the PEUF process for arsenic removal

using QUAT and a 10 kDa MWCO spiral wound ultrafiltration module demonstrated 95% arsenic removal from synthetic 50 ppb feed inlet solution (Gallo *et al*., 2006), further demonstrating that PEUF is a useful technology to remove low concentration arsenic from water. Gallo and co-worker (2006) also performed cost analysis for using the PEUF process for arsenic removal. Their estimation based on the assumption of 85% polyelectrolyte recovery and recycle found that the PEUF technology has lower total unit cost compared to ion exchange (IX), granular ferric hydroxide adsorbents (GFH), coagulation/microfiltration (C/MF), coagulation/filtration (C/F), and nanofiltration (NF) technologies. Therefore, the polyelectrolyte recovery to be reuse in the PEUF process is the key step to make the PEUF more economical and environmental friendly by reduce and reuse of chemical waste.

The polyelectrolyte recovery to be reused in PEUF process has been studied by Soponvuttikul and coworker (2003) in QUAT-chromate system. Precipitate out of chromate anion from QUAT-chromate complex solution by using barium cation was reported. Low solubility barium chromate can formed resulting to chromate was precipitated out from the complex solution and free polyelectrolyte to be able to reuse. However, the present of QUAT in the precipitation system affect settling ability due to particle dispersion resulting in barium chromate precipitate is difficult to remove by gravimetric settling.

The similar idea to Soponvuttikul's work by using barium cation to precipitate out arsenate anion from QUAT-arsenate complex solution was studied in the previous work (Chapter II). This is aim that low solubility barium-arsenate compound will be formed and leave free polyelectrolyte to be reused. However, barium-arsenate

precipitation system does not appear to be suitable due to precipitation is not occur at low initial arsenate concentration, and the fact that barium itself may have an effect on human health (USEPA, 1998).

The arsenate removal from QUAT-arsenate solution for QUAT removal purpose was succeed by co-precipitate arsenate anion with calcium phosphate hydroxyapatite, the high percent arsenate removal result at low arsenic concentration was obtained (Chapter III). The QUAT recovery from PEUF waste stream solution through simple and inexpensive precipitation of arsenate incorporated calcium phosphate hydroxyapatite is now becomes achievable.

To make the precipitation more suitable with the continuous pilot scale PEUF process, this work study continuous precipitation of arsenate-calcium phosphate hydroxyapatite coprecipitation. The crystallization basic will be applied to this work to control the continuous precipitation process which suitable product for simple separation from the solution is expected. The QUAT recovery to be reused in PEUF process from realistic QUAT-arsenate concentration level from PEUF operation will be demonstrated and discussed.

4.2   Experimental

PEUF steady state operation

The steady state of PEUF operation was studied to get an idea about QUAT and arsenic concentration in PEUF waste stream for further use in continuous precipitation experiment. The study of the PEUF steady state operation is performed by a spreadsheet calculation based on actual construction of PEUF process. The PEUF process use in this study is based on pilot scale PEUF process set up at the

University of Oklahoma by Gallo and coworker (2006) which the similar pilot scale PEUF process has also set up at Suranaree University of Technology (SUT). The schematic diagram of the studied PEUF process is shown in Figure 4.1, and a pilot scale PEUF set up at SUT is shown in Figure 4.2
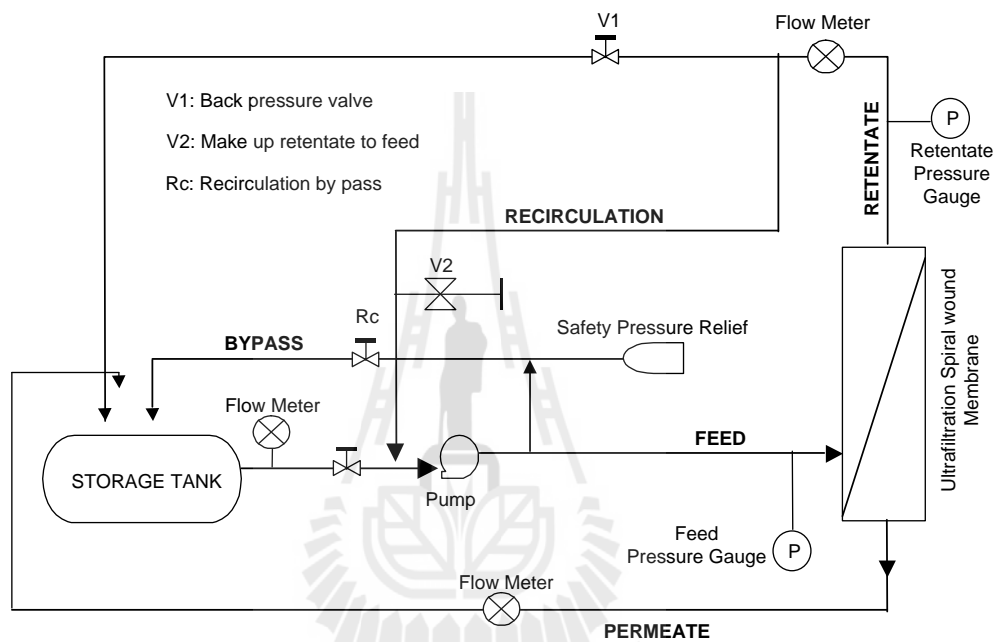
Figure 4.1 Schematic diagram of pilot scale PEUF process studied by Gallo and coworker at the University of Oklahoma (2006).

(A)
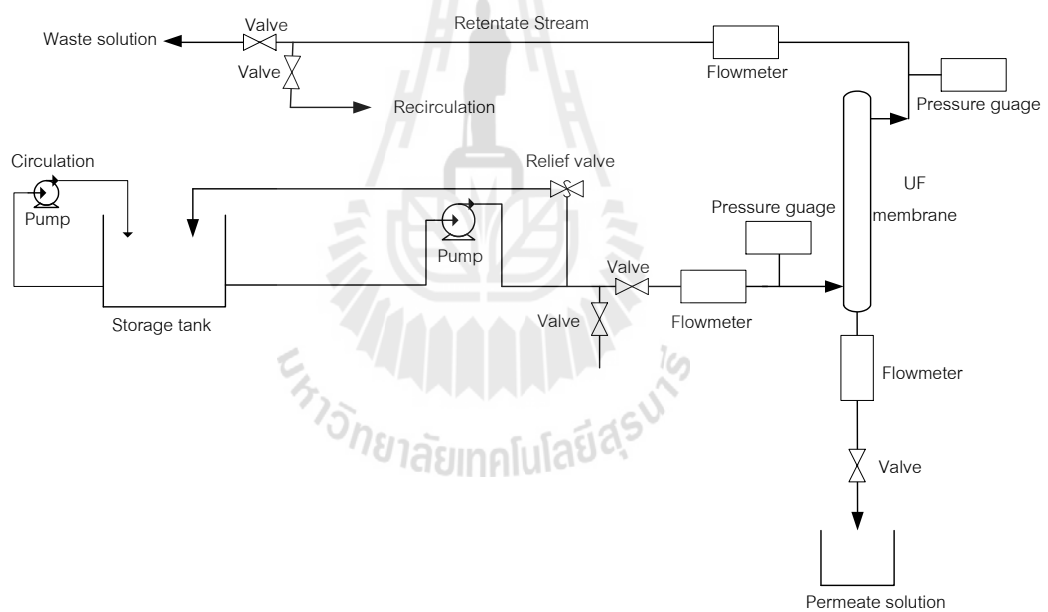
(B)

Figure 4.2 Photo (A) and schematic diagram (B) of pilot scale PEUF set up at Suranaree University of Technology.

Continuous arsenate-calcium phosphate hydroxyapatite coprecipitation

Chemicals

Disodium hydrogen phosphate dodecahydrate ($Na_2HPO_4 \cdot 12H_2O$) and disodium hydrogen arsenate heptahydrate ($Na_2HAsO_4 \cdot 7H_2O$) from Carlo Erba (Milan, Italy) and Fluka (Buchs, Switzerland), respectively, were used as the source of phosphate and arsenate anion. Calcium hydroxide ($Ca(OH)_2$) from Carlo Erba for calcium source.

Poly(diallyldimetyl ammonium chloride), QUAT, cationic polyelectrolyte with the average molecular weight of 240 kDa was purchased from Calgon Corp. (Pittsburgh, PA) under the trade name MERQUAT. Short chain polyelectrolyte was removed before use using SUT pilot scale PEUF process with a 10 kDa ultrafiltration membranes from Osmonic (Minnetonka, MN) as filter. QUAT concentrations were determined by a LECO CNS-2000 analyzer using Leco soil standard. Deionized water was used for all experiments.

Pilot scale crystallization experiment

The crystallization experiment is very important to control quality of the crystallized product. In this work, require to obtain right target compound with uniform size and shape due to it effect directly to the removal efficiency and settling ability of the product from the solution. Many crystallization conditions play an important role in crystal size and shape including supersaturation level, geometry of the crystallizer (Shan *et al.*, 2002), impact of the crystal-impeller (Synowiec, 2002), collisions between crystal-crystal and crystal-vessel (Pratora *et al.*, 2002), and mixing conditions (Zauner *et al.*, 2000; Kim *et al.*, 1996; Marchisio *et al.*, 2002). Therefore,

the pilot scale crystallization experiments were performed using a 500 mL semi-batch borosilicate crystallizer equipped with MasterFlex L/S peristaltic pump and CAT R50D overhead stirrer. The crystallizer in this work is designed to have round surface throughout the vessel, no kink site to create stuck flow. The bottom of the vessel is design to have a baffle to prevent dead zone and to enhance particle dispersion. The draft tube is inserted to the crystallizer to create top-down flow direction enhancing similar particle dispersion in different height of the crystallizer. The injection points of both cation and anion feeds is just above the impeller which located just above the baffle at the bottom. This is to let the impeller to disperse both solutions immediately after its come out from the nozzles to prevent local supersaturation may occur. A schematic diagram of experimental set up is shown in Figure 4.3. 500 mL of anion and cation solutions were prepared in separate storage before being introduced simultaneously into the crystallizer by peristaltic pump with equal flow rates of 8.3 mL/min. The agitation speed was fixed at 100 RPM throughout the experiment. This is the agitation speed able to disperse the suspension to the top level of the draft tube creating gentle top-down flow in the crystallizer. The solution level in the crystallizer was maintained at 500 mL by setting the outlet line to remove the mixed-product solution to the product storage at this level. The reaction time in the crystallizer was 30 min from start until the mixed product started to be removed to the product storage, and the reaction finished within 60 min of the start. The mixed products were filtered, air-dried, and then characterization. Initial arsenic concentration was fixed at 25 ppm, QUAT/As mol ratio was 100, P/As mol ratio was 5, and no arsenic, and Ca/(P+As) used in this experiment was 3.

(A)

(B)
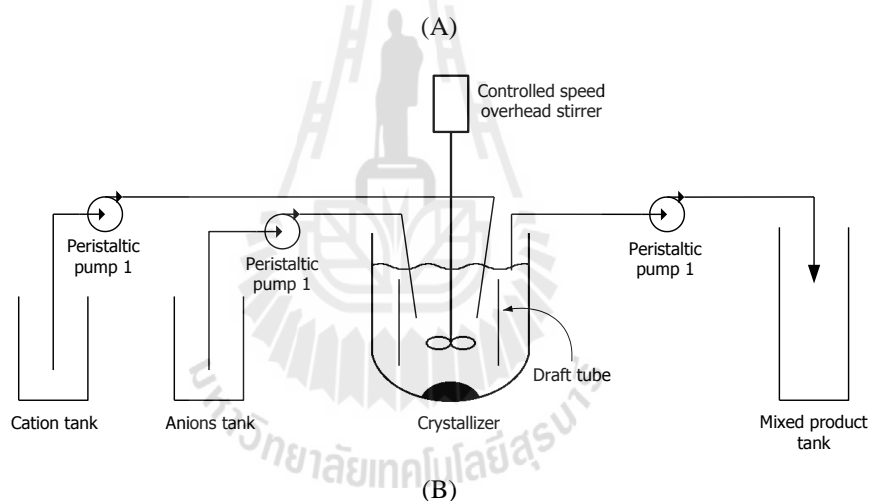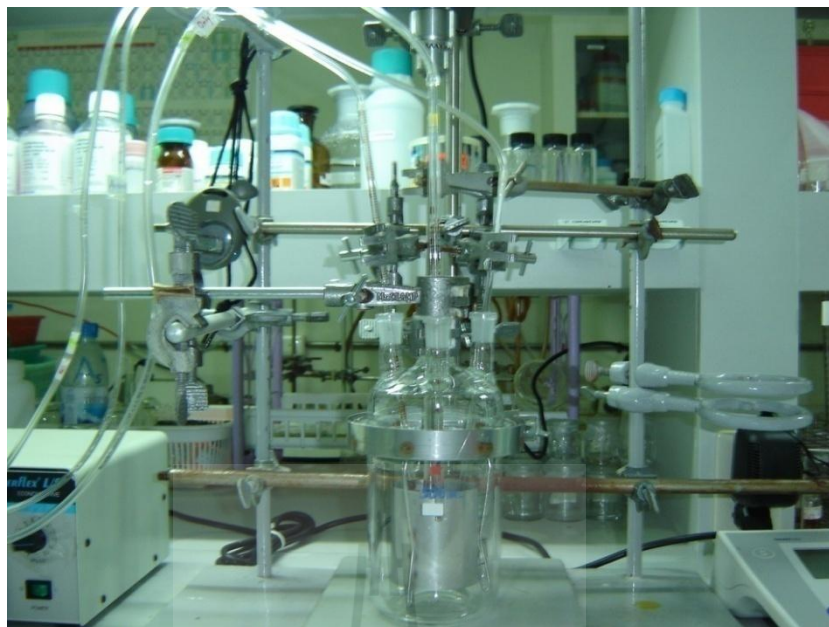
Figure 4.3 Photo (A) and schematic diagram (B) of the continuous crystallization

apparatus.

Characterization of Product

The solid precipitates were characterized by powder X-ray diffraction using a

Bruker Analytical X-ray Systems model D5005 X-ray diffractometer equipped with a

Cu K_α sealed tube X-ray source operating at 40 kV and 35 mA. The data were

collected in the range of 5.0-60.0° two theta in steps of 0.02° and a scan speed of 0.4

sec/step. A transmission electron microscope (TEM) with energy dispersive x-ray fluorescence (TEM/EDX) was used to examine the extremely small size particle morphologies and heavy element in the compounds.

4.3 Results and Discussions

PEUF steady state operation

The spread sheet balance calculation regarding to pilot scale PEUF operation by Gallo and coworker (Figure 4.4) suggests this process is able to reach steady state with about 144 ppb of arsenic concentration in the waste steam (Table 4.1). The calculation result is agree with actual experimental value from Gallo's work which arsenic concentration in waste steam of 160 ppb was achieved after 30-70 min of operation, further supporting that the balance calculation model used in this work is close to results from the experiment. According to pilot scale PEUF process operation using the same parameter with Gallo produce high waste stream of 3.04 Lpm (liter per min) of 13.68 Lpm feed stream. This is create two difficulties; (1) high volume (about 22.22%), and (2) low arsenic concentration (about 144 ppb) in waste stream produced which not good for precipitation process due to too low concentration to precipitate.

Waste
3.04 Lpm

Retentate
4.56 Lpm

Recirculation
1.52 Lpm

40.00
ppb

Inlet
15.20 Lpm

Feed
13.68 Lpm

Permeate
10.64 Lpm
10.00 ppb

Calculation Parameters:
[As] initial: 40 ppb
QUAT/As ratio: 100
Permeate: 60% Inlet
Retentate = Waste +Recirculation

[As] permeate: 10 ppb
Feed: 13.68 Lpm
Inlet: Feed + Recirculation
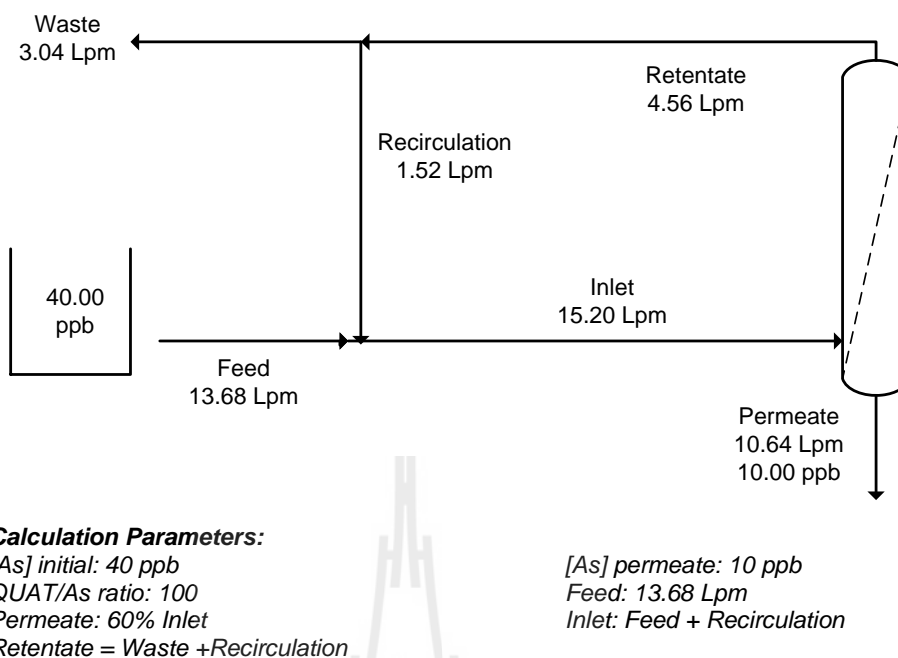
Figure 4.4 Schematic of pilot scale PEUF operational flowrate according to Gallo

and coworker (2006).

By using the same balance calculation model, PEUF steady state operation by

adjusted waste/retentate (Wst/Ret) stream flowrate was performed to studied PEUF

operation condition which provide minimal in volume and high in arsenic

concentration of waste streams. The schematic of PEUF model used for balance

calculation of steady state operation study is shown in Figure 4.5.
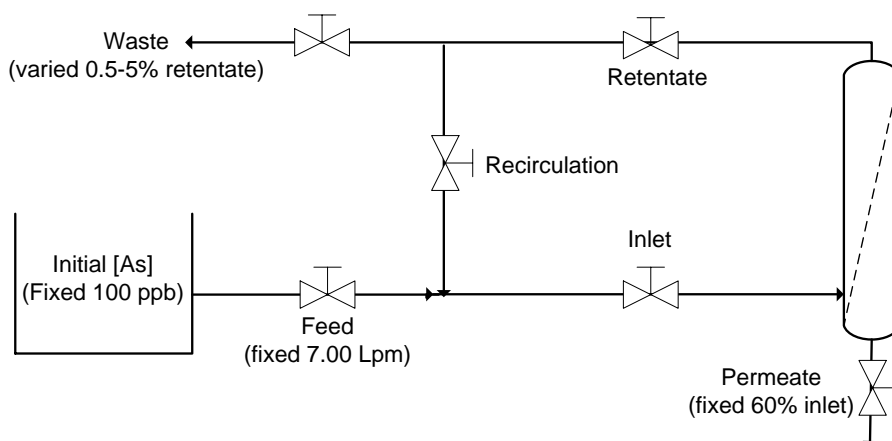
Calculation Parameters:
[As] initial: 100 ppb   *[As] permeate: 10 ppb*
QUAT/As ratio: 100   *Feed: 7.00 Lpm*
Permeate: 60% Inlet   *Inlet: Feed + Recirculation*
Retentate = Waste +Recirculation   *Waste: 1.0-5% Retentate*

Figure 4.5 Schematic of PEUF model used for balance calculation in steady state operation study.

The initial arsenic concentration of the studied solution was fixed at 100 ppb, and QUAT/As molar ratio = 100. Feed stream fixed at 7.00 Lpm, and permeate stream fixed to 60% of inlet stream. The arsenic concentration in the permeate was fixed to the worse case of 10 ppb, the USEPA's MCL for arsenic in drinking water (USEPA, 2001) throughout the operation. Waste stream flowrate is varied from 0.5-5% of retentate stream to minimize volume and also increase arsenic concentration in waste stream.

Table 4.1 Summary of PEUF steady state operation result.

PEUF System	[As] initial ppb	QUAT/As Molar ratio	Wst/Ret %	Flow (LPM) at steady state						Conc in waste at steady state		Wst (%)
				Feed	Inlet	Per	Ret	Waste	Recir	[As], ppb	QUAT, M	
Gallo process	40	100	-	13.68	15.20	10.64	4.56	3.04	1.52	143.79	1.92E-04	22.22
Adapt #1	100	100	0.50	7.00	11.63	6.98	4.65	0.02	4.63	26919.74	3.99E-02	0.33
Adapt #2	100	100	1.00	7.00	11.59	6.95	4.64	0.05	4.59	13599.41	2.02E-02	0.66
Adapt #3	100	100	2.00	7.00	11.51	6.91	4.61	0.09	4.51	6850.00	1.01E-02	1.32
Adapt #4	100	100	3.00	7.00	11.44	6.86	4.58	0.14	4.44	4600.00	6.81E-03	1.96
Adapt #5	100	100	4.00	7.00	11.36	6.82	4.55	0.18	4.36	3475.00	5.14E-03	2.60
Adapt #6	100	100	5.00	7.00	11.29	6.77	4.52	0.23	4.29	2800.00	4.14E-03	3.23

The Summary of PEUF steady state operation result is shown in Table 4.1. The lower waste/retentate percent, the lower volume but higher arsenic concentration of the waste stream. At 0.50% waste/retentate, minimal waste (0.33%) produced with flowrate of 0.02 Lpm. Arsenic concentration in this operating condition can be as high as 27 ppm.

Precipitation of arsenate with calcium phosphate hydroxyapatite by continuous crystallization

The precipitation experiment was set up at initial arsenic concentration fixed to 25 ppm with QUAT/As molar ratio = 100, the precipitation immediately occurs when two feed of mixed anion and calcium cation solutions are mixed, resulting in a turbid solution with particles dispersed in crystallizer. The mixed suspension from absence of QUAT experiment is easily to agglomerate and settle to the bottom of the mixed product tank within 1 hour, clear solution was obtained. In contrast, in the system with QUAT, although most of the mixed product is settled at the bottom of

the mixed product tank after 24, but there are still particles dispersed in the solution, leaving not quite clear solution compared to no QUAT system as shown in Figure 4.6.
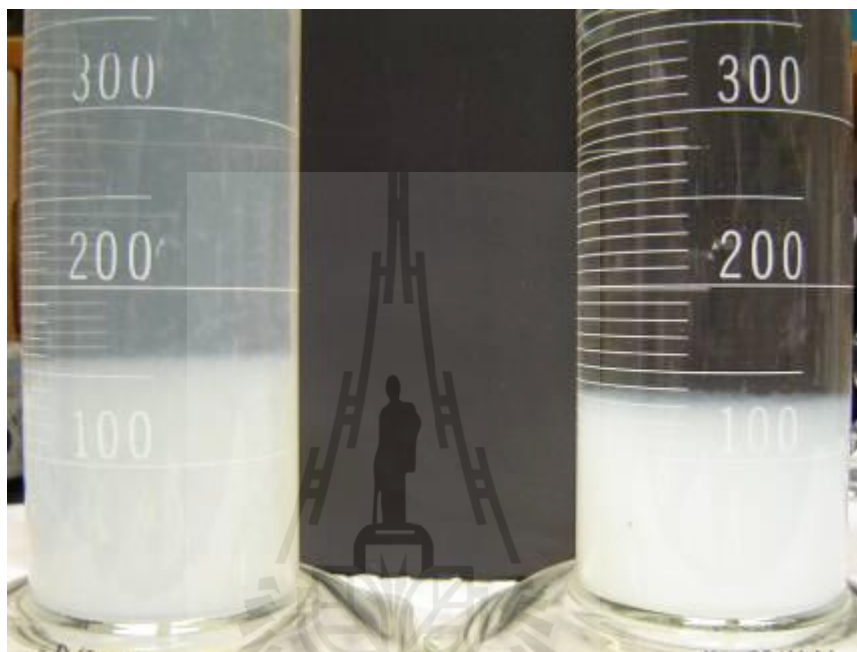
Figure 4.6 Precipitation products in the presence (left) and absence (right) of QUAT after 24 hr of settling

The precipitates were characterized by XRD for phase examination; the similar XRD pattern to calcium phosphate hydroxyapatite in the previous result was obtained (Figure 4.7).
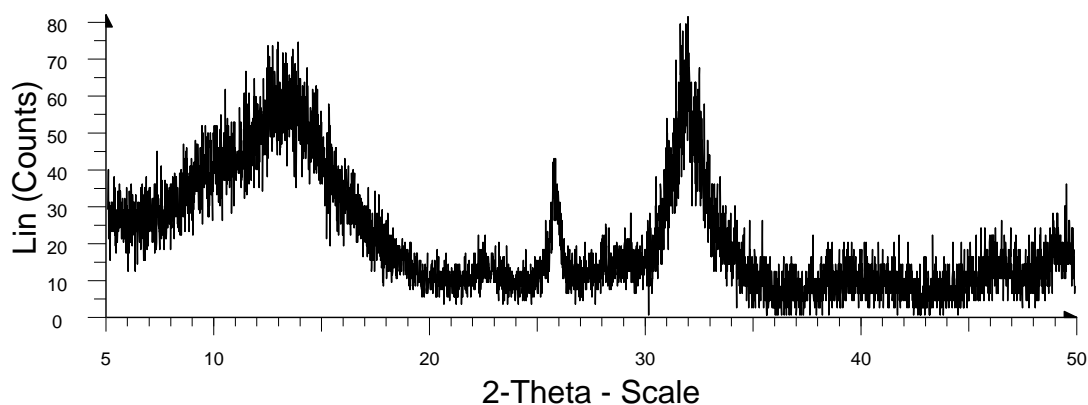
Figure 4.7 XRD pattern of product from continuous crystallization experiment.

The morphological study of arsenate incorporated calcium phosphate hydroxyapatire by TEM technique, which operates at higher energy than SEM providing higher resolution, shows needle-like precipitates with about 100 nm lengths (Figure 4.8A). The very small crystal size leads to poor diffraction in XRD examination. EDX result (coupled with TEM) suggest arsenic constituent in precipitate (Figure 4.8B). Therefore, high arsenic removal is achievable in this study too due to formation of arsenate incorporated calcium phosphate hydroxyapatite.
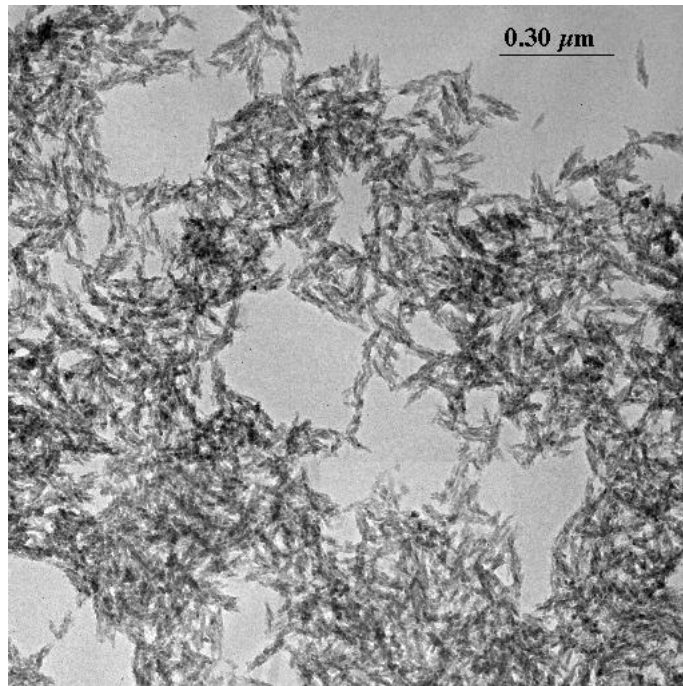
(A)
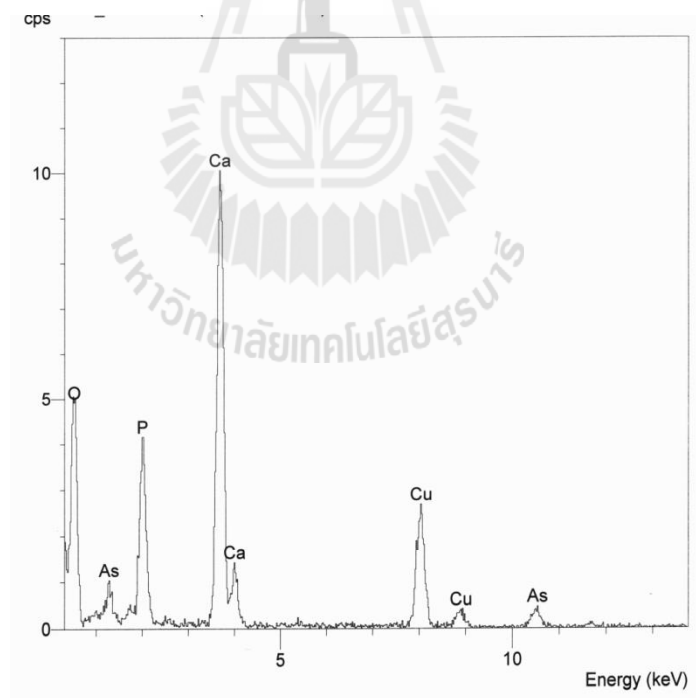
(B)

Figure 4.8 TEM micrograph (A) and EDX result (B) of continuous crystallization

product.

Demonstration of polyelectrolyte recovery

According to PEUF steady state operation by fixed feed stream to 7.0 Lpm and adjust waste/retentate to 0.5%, as low as 0.02 Lpm of waste stream with high arsenic concentration up to 27 ppm was produced. This arsenic concentration is suitable to nearly complete removal by arsenate incorporated calcium phosphate hydroxyapatite precipitation which greater than 99% arsenic removal can be achieved in the previous results. Therefore, the continuous crystallization technique studied in this work can be applied to pilot scale PEUF for polyelectrolyte recovery work as schematic diagram shown in Figure 4.9.
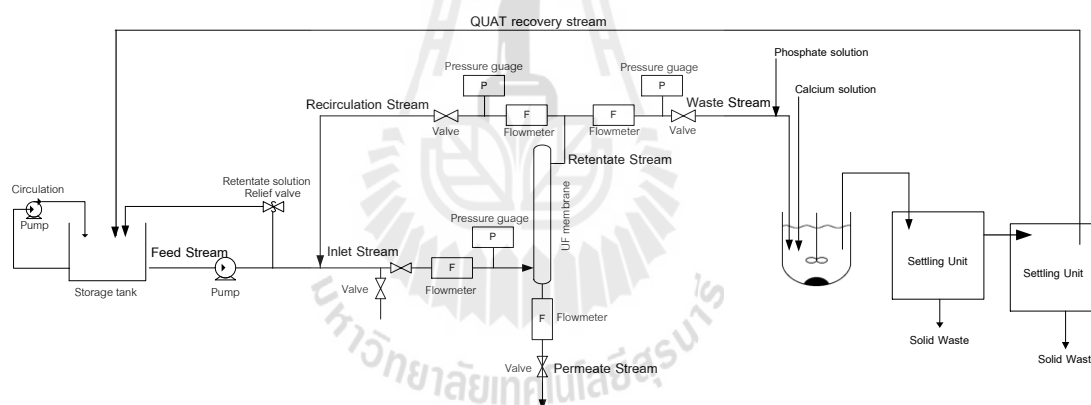
Figure 4.9 Schematic diagram demonstrate continuous crystallization process coupled to pilot scale PEUF for polyelectrolyte recovery.

The waste stream requires to mix with phosphate solution in certain P/As ratio (*i.e.* 5) prior to feed directly into the crystallizer. The P/As ratio should be possible to control accurately due to arsenic concentration in waste stream is stable at steady state operation. The calcium hydroxide solution with certain Ca/(P+As) ratio (*i.e.* 3) is then feed directly to the mixed anion solution creating turbid solution of arsenate

incorporated calcium phosphate hydroxyapatite. The mixed suspension product is removed from the crystallizer when reach certain resident time (*i.e.* 30 min) to the settling unit which should be adequate in size to contains mixed product for two day before require to remove. This is to increase the resident time of the mixed product in settling unit to enhance clarity of the polyelectrolyte solution. The recovering polyelectrolyte solution is then can be reused in the PEUF process

4.4   Conclusions

The continuous crystallization provides similar compound characterized by XRD technique to the arsenate incorporated calcium phosphate hydroxyapatite batch experiment, supporting that high arsenic removal from QUAT-arsenate solution is suspected. The TEM/EDX examination confirmed arsenic constituent in the precipitation product. Therefore, the polyelectrolyte should be free from complexation with arsenate and available in supernatant.

The PEUF process is require to operate at steady state to keep constant volume and arsenic concentration in waste stream prior to transfer to continuous crystallization compartment. Then the certain phosphate stream is require to mixed with PEUF waste stream prior to mixed with certain calcium concentration in the crystallizer to form target compound. The mixed suspension product is then remove to settling unit to separate free polyelectrolyte to be reused. The continuous crystallization is demonstrated in this work to couple with pilot scale PEUF for polyelectrolyte recovery purpose.

4.5 References

Gallo, D., Acosta, E., Scamehorn, J. F., and Sabatini, D. A. (2006). Pilot Scale Study of Polyelectrolyte Enhanced Ultrafiltration for Arsenic Removal. **J. Am. Water Works Assoc.** 98(1): 106-116.

Kim, W. S. and Tarbell, J. M. (1996). Micromixing effects on barium sulfate precipitation in an MSMPR reactor. **Chem. Eng. Comm.** 146: 33-56.

Mandal, B. K. and Suzuki, K. T. (2002). Arsenic Round the World: A Review, **Talanta.** 58: 201-235.

Marchisio, D. L., Barresi, A. A., and Garbero, M. (2002). Nucleation, growth, and agglomeration in barium sulfate turbulent precipitation. **AIChE.** 48(9): 2039-2050.

Pookrod, P., Haller, K. J., and Scamehorn, J. F. (2004). Removal of Arsenic Anions from Water using Polyelectrolyte-Enhanced Ultrafiltration. **Sep. Sci. Technol.** 39(4): 811-831.

Pratora, F., Simons, S. J. R., and Jones, A. G. (2002). A novel experimental device for measurement of agglomerative crystallization forces. **Trans IChemE.** 80: 441-448.

Shan, G. Igarashi, K., Noda, H., and Ooshima, H. (2002). Production of large crystals with a narrow crystal size distribution by a noval WWDJ batch crystallizer, **Chem. Eng. J.** 85: 161-167.

Smedley, P. L. and Kinniburgh, D. G. (2002). A Review of the Source, Behavior and Distribution of Arsenic in Natural Waters, **Appl. Geochem.** 17: 517-568.

Soponvuttikul, C., Scamehorn, J. F., and Saiwan, C. (2003). Aqueous Dispersion Behavior of Barium Chromate Crystals: Effect of Cationic Polyelectrolyte. **Langmuir.** 19: 4402-4410.

Synowiec, P. (2002). How to improve the crystal size distribution (CSD) in crystallizers with the inner suspension circulation, **Chem. Eng. Process.** 41: 585-593.

USEPA (United States Environmental Protection Agency). (1998). **Toxicological Review of Barium and Compounds,** EPA/635/R-05/001.

USEPA (United States Environmental Protection Agency). (2001). **EPA to Implement 10 ppb Standard for Arsenic in Drinking Water,** EPA 815-F-01-010.

Zauner, R. and Jones, A. G. (2000). Mixing effects on product particle characteristics from semi-batch crystal precipitation. **Trans IChemE.** 78A: 894-902.

CHAPTER V

CONCLUSIONS

Arsenate precipitation from aqueous solutions containing polyelectrolyte-arsenate complex was studied. The polyelectrolyte-arsenate solution studied in this work is a synthetic waste stream from polyelectrolyte-enhanced ultrafiltration (PEUF) process using poly(diallyldimethyl ammonium chloride) or QUAT as an active polyelectrolyte. It is proposed that the arsenate anion can be precipitated out from QUAT-arsenate complex solution to free the QUAT for reuse in the PEUF process to enhance the feasibility and make the process more environmentally friendly by minimizing the waste and reusing the polyelectrolyte. Arsenic concentration in the PEUF waste stream is relatively low for precipitation, therefore requiring a metal ion which is able to form a low solubility compound with arsenate at low concentration. Barium is the first metal ion studied in this work for metal-arsenate precipitation due to the low reported solubility product constant (K_{SP}) of $Ba_3(AsO_4)_2$. The precipitation of barium-arsenate compound is affected by pH, Ba/As molar ratio, and the presence of common/diverse ions (sodium and chloride). Three single phases of $BaHAsO_4 \cdot H_2O$, $NaBaAsO_4 \cdot 9H_2O$, and $Ba_5Cl(AsO_4)_3$ and their binary mixtures were formed as the dominant solid phases in different regions of pH, Ba/As molar ratio, and common/diverse ion concentrations. The pH of the solution determines speciation of the arsenate ion in solution and thus has a great effect on the phases formed. The availability of other ions in the system induces formation of certain compounds

containing those ions, thereby inhibiting the formation of $Ba_3(AsO_4)_2$. $NaBaAsO_4 \cdot 9H_2O$ and $Ba_5Cl(AsO_4)_3$ form preferably in such conditions. QUAT in solution affects the morphology and size of barium-arsenate compound, elongation is found in $BaHAsO_4 \cdot H_2O$ and $Ba_5Cl(AsO_4)_3$ crystals, and larger sized crystals are obtained. Values for the $-\log K_{SP}$ value (pK_{SP}) of $BaHAsO_4 \cdot H_2O$, $NaBaAsO_4 \cdot 9H_2O$, and $Ba_5Cl(AsO_4)_3$ determined in this work found values of 5.60(5), 10.8(3), and 35.3(4), respectively. The pK_{SP} value of $BaHAsO_4 \cdot H_2O$ is comparable to the previous literature, while those for $NaBaAsO_4 \cdot 9H_2O$ and $Ba_5Cl(AsO_4)_3$ are the first reported values for these two phases. The incongruent dissolution of barium-arsenate compounds was explored in this study. Incongruent dissolution occurred in $NaBaAsO_4 \cdot 9H_2O$ and $Ba_5Cl(AsO_4)_3$ dissolution systems by formation of a $Ba_3(AsO_4)_2$ phase which is confirmed by saturation index calculations by PhreeqC. This observation further suggests that $Ba_3(AsO_4)_2$ is like to be precipitated but due to the presence of sodium and chloride ions in the system the equilibrium prefer to drive $NaBaAsO_4 \cdot 9H_2O$ and $Ba_5Cl(AsO_4)_3$ to precipitate rather. Based on the precipitation experiment and dissolution study results, barium-arsenate precipitation is not suitable for arsenate precipitation from PEUF waste stream for the polyelectrolyte recovery purpose.

Arsenic in QUAT-arsenate complex solution success to be removed by co-precipitation with low solubility calcium phosphate hydroxyapatite forming arsenate incorporated calcium phosphate hydroxyapatite compounds. Up to 99% arsenic removal was achieved from 25 ppm initial arsenic concentration (the arsenic concentration in waste stream from PEUF steady state calculation) in both the absence and presence of QUAT systems. The Ca/(P+As) and P/As mole ratios play

an important role in arsenic removal efficiency. The higher Ca/(P+As) and P/As mole ratio, the higher arsenic removal efficiency with highest arsenic removal efficiency obtained at Ca/(P+As) = 3 and P/As mol ratio = 5. The pH of the initial anionic solution does not significantly affect the arsenic removal by this process. The advantage of this system is that precipitation can occur at low arsenic concentration implying that a simple and inexpensive process for arsenic removal could be obtained based on this approach. However, the presence of QUAT in the system is able to disperse small particles in the solution resulting in retardation of settling of the precipitates.

The crystallization of arsenate incorporated calcium phosphate hydroxyapatite is demonstrated in this work laying the basis for a coupling with pilot scale PEUF for the purpose of recycling the polyelectrolyte. The semi-batch crystallization provides a similar material to that characterized by the XRD technique for the batch precipitation experiment. The TEM/EDX examination confirms an arsenic constituent in the precipitation product. Extrapolating the batch experiment results supports that high arsenic removal from QUAT-arsenate solution can be expected, yielding polyelectrolyte free from arsenate and available to reintroduce to the PEUF process. This study assumes that the PEUF operation can be adjusted to achieve a stable retentate stream with a significantly reduced volume relative to the processed volume with a significantly higher arsenic concentration than previously demonstrated. Assuming a steady state of 0.5% waste/retentate for the PEUF operation, 0.02 liter per minute of high arsenic concentration up to 27 ppm can be achieved. The PEUF process is required to operate at this steady state to keep constant volume and arsenic concentration in the retentate stream. Phosphate ion at an appropriate concentration

would be mixed with the PEUF retentate stream prior to introducing it into the crystallization compartment where a calcium hydroxide stream of appropriate concentration would be added. The semi-batch product is then removed to a settling unit to separate free polyelectrolyte to be reused. This work provides a basis for further study of a calcium hydroxyapatite precipitation process to sweep the arsenate ions from the arsenate-polyelectrolyte complex in the retentate stream issuing from a PEUF process to remove low-level arsenic from water.

APPENDICES
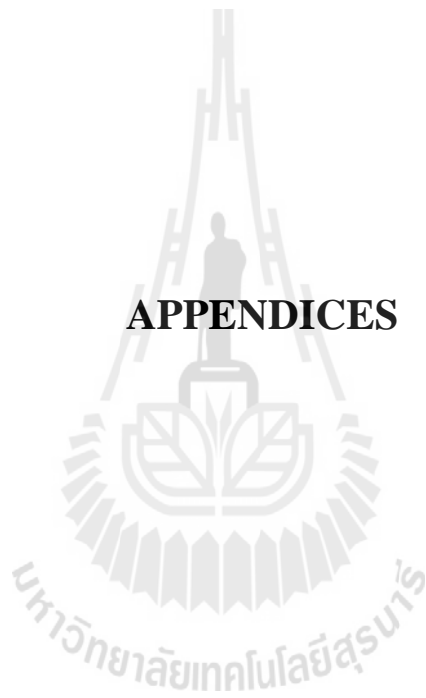
APPENDIX A

SUPPORTING INFORMATION ON

BARIUM-ARSENATE CHARACTERIZATION

1. TGA analysis of Barium-arsenate compounds

BaHAsO$_4$·H$_2$O
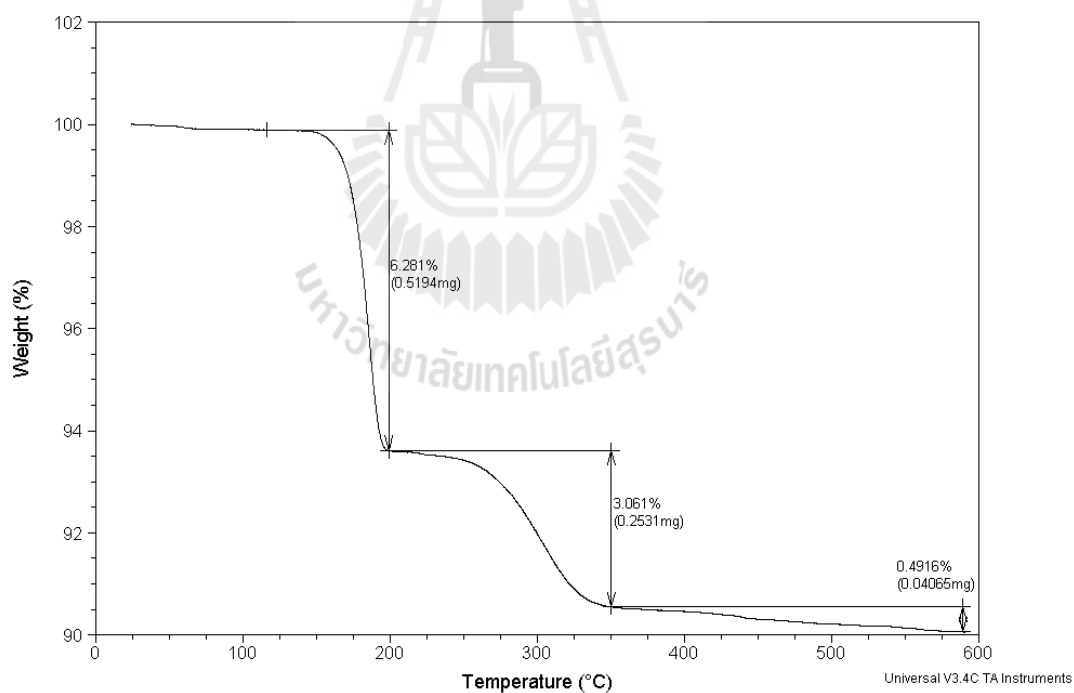
NaBaAsO₄·9H₂O
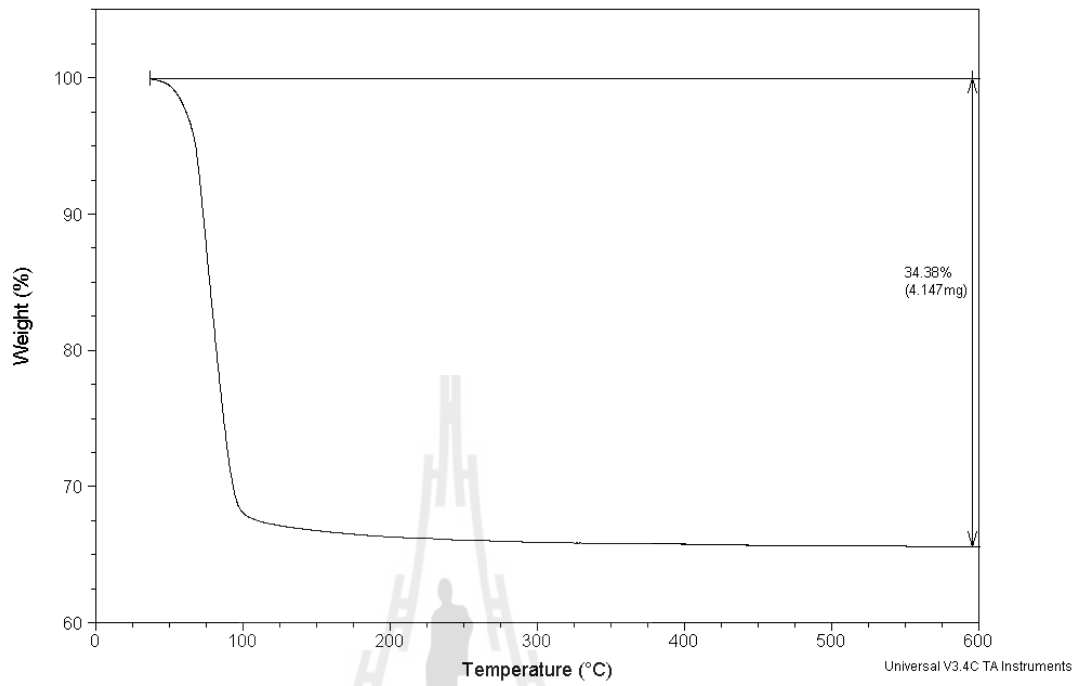
Ba₅Cl(AsO₄)₃
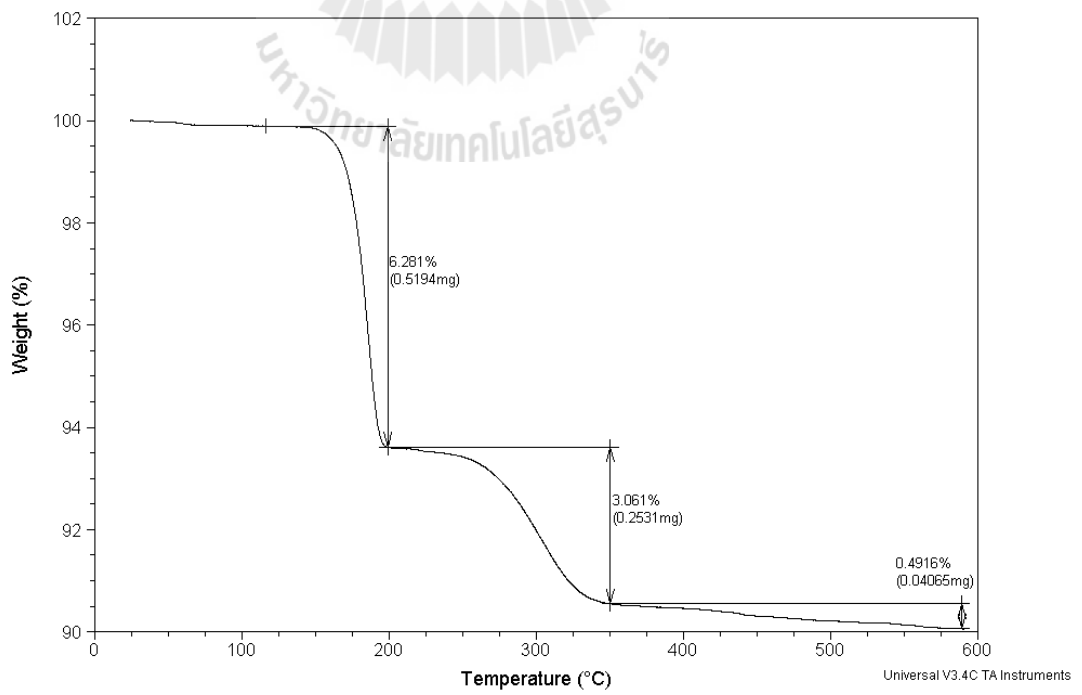
FTIR spectra of barium-arsenate compounds
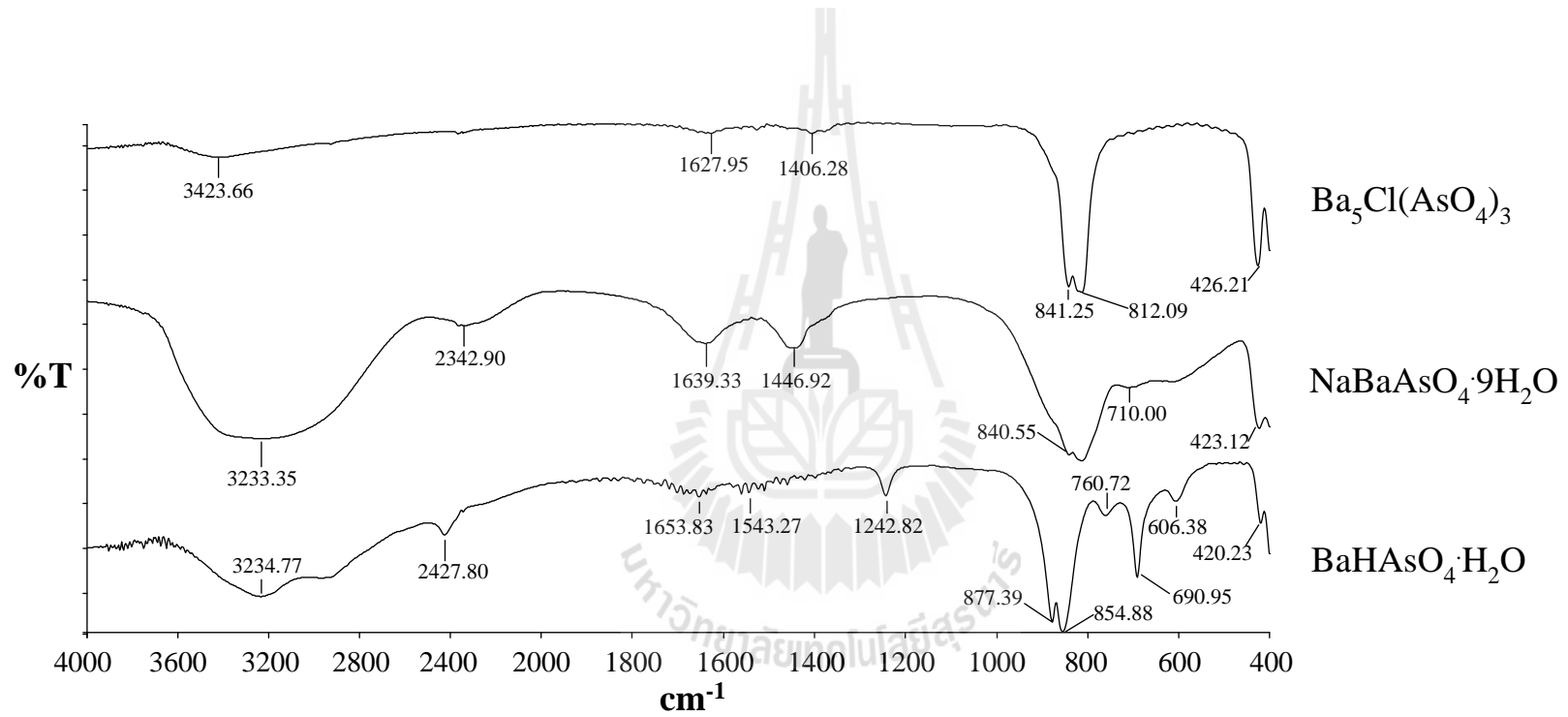
APPENDIX B

THESIS RELEVANT PRESENTATIONS,

PROCEEDINGS, AND PUBLICATIONS

Conferences presentations:

Winya Dungkaew, Preeyaporn Pookrod, Kenneth J. Haller. Phase Precipitation and Characterization of Barium Arsenate. 28th Congress on Science and Technology of Thailand, 24-26 October 2002, Bangkok, Thailand. (Poster presentation)

Winya Dungkaew, Kenneth J. Haller. Phase Diagram of Barium Arsenate. 29th Congress on Science and Technology of Thailand, 20-22 October 2003, Khon Kaen, Thailand. (Poster presentation)

Winya Dungkaew, Kenneth J. Haller, Adrian E. Flood, John F. Scamehorn. Phase Diagram from Barium-Arsenate Precipitation in the Absence and Presence of Polyelectrolyte. 227th ACS National Meeting, 28 March-1 April 2004, Anaheim, CA, USA. (Poster presentation)

Winya Dungkaew, Kenneth J. Haller, Adrian E. Flood, John F. Scamehorn. Effect of Poly(diallyldimethyl ammonium chloride) Polyelectrolyte Solution on Barium-Arsenate Precipitation. The 4th National Symposium on Graduate Research, 10-12 August 2004, Chiang Mai, Thailand. (Poster presentation)

Winya Dungkaew, Kenneth J. Haller, Adrian E. Flood, John F. Scamehorn. Recovery of Poly(diallyldimethyl ammonium chloride) Polyelectrolyte from PEUF Retentate Stream by Precipitation of Arsenate Anion by Barium Cation. Proceeding of the Regional Symposium on Chemical Engineering, December 1-3, 2004, Bangkok, Thailand. (Poster presentation and Proceedings paper JM−210)

Winya Dungkaew, Kenneth J. Haller, Adrian E. Flood, John F. Scamehorn. Effect of pH, Ionic Strength, and Poly(diallyldimethyl ammonium chloride) on Solubility of Barium-Arsenic Compounds. RGJ-Ph.D. Congress VI, 28-30 April 2005, Pattaya, Thailand. (Oral presentation)

Winya Dungkaew, Kenneth J. Haller, Adrian E. Flood, John F. Scamehorn. Phase Precipitation and Solubilization Study of Barium-Arsenate Compounds. 31th Congress on Science and Technology of Thailand, 18-20 October 2005, Nakhon Ratchasima, Thailand. (Oral presentation)

Winya Dungkaew, Kenneth J. Haller, Adrian E. Flood, John F. Scamehorn. Barium-Arsenate Phase Precipitation and Solubilization Study. The International Conference on Hazardous Waste Management for a Sustainable Future, 10-12 January 2006, Bangkok, Thailand. (Poster presentation and Proceedings paper)

Panida Un-arn, Winya Dungkaew, Kenneth J. Haller. Effect of Supersatulation and Polyelectrolyte on Sodium Barium Arsenate Nonahydrate. 32nd Congress on Science and Technology of Thailand, 10-12 October 2006, Bangkok, Thailand.

Winya Dungkaew, Kenneth J. Haller, Adrian E. Flood, John F. Scamehorn. Crystallization of Low Solubility Calcium-Arsenate Compounds for arsenic

removal from Poly(Diallyldimethyl Ammonium Chloride)-arsenate solution. AIChE Annual Meeting, 12-17 November 2006, San Francisco, CA. (Poster presentation)

Winya Dungkaew, Kenneth J. Haller, Adrian E. Flood, John F. Scamehorn. Arsenate Immobilization by Calcium Phosphate Hydroxyapatite: Batch Precipitation Study. The 8th National Symposium on Graduate Research, 10-12 September 2007, Nakhon Pathom, Thailand. (Oral presentation)

Winya Dungkaew, Kenneth J. Haller, Adrian E. Flood, John F. Scamehorn. Effect of Polyelectrolyte on Arsenate Removal by Co-Precipitation with Calcium Phosphate Hydroxyapatite. 33rd Congress on Science and Technology of Thailand, 18-20 October 2007, Nakhon Sri Thammarat, Thailand. (Poster presentation)

Winya Dungkaew, Kenneth J. Haller, Adrian E. Flood, John F. Scamehorn. Arsenate Removal from Polyelectrolyte-Arsenate Complex Solution: the Recovery of Polyelectrolyte from PEUF Retentate Stream. 1st SUT Graduate Conference, 1-2 November 2007, Nakhon Ratchasima, Thailand. (Oral presentation)

Winya Dungkaew, Weenawan Somphon, Kenneth J. Haller. Structural Study of Arsenate Incorporation into Calcium Phosphate Hydroxyapatite. The 8th Conference of the Asian Crystallographic Association, 4-7 November 2007, Taipei, Taiwan. (Poster presentation)

Oratai Saisa-ard, Winya Dungkaew, Weenawan Somphon, Kenneth J. Haller. Structural Study of Copper Incorporation into Calcium Phosphate

Hydroxyapatite. The 8th Conference of the Asian Crystallographic Association, 4-7 November 2007, Taipei, Taiwan. (Poster presentation)

Winya Dungkaew, Oratai Saisa-ard, Kenneth J. Haller. Phase Characterization and Saturation Modeling of the Calcium Phosphate-Arsenate Apatite System. The 14th International Annual Symposium on Computational Science and Engineering, 23-26 March 2010, Chiang Rai, Thailand. (Oral presentation)

Winya Dungkaew, Kenneth J. Haller, Adrian E. Flood, John F. Scamehorn. Arsenic Removal by Precipitation with Calcium Phosphate Hydroxyapatite. Chiang Mai International Conference on Biomaterials & Applications 2011, 9-10 August 2011, Chiang Mai, Thailand. (Oral Presentation)

Conference Proceedings:

Winya Dungkaew, Kenneth J. Haller, Adrian E. Flood, John F. Scamehorn. Recovery of Poly(diallyldimethyl ammonium chloride) Polyelectrolyte from PEUF Retentate Stream by Precipitation of Arsenate Anion by Barium Cation. *Proceeding of the Regional Symposium on Chemical Engineering 2004*, 1-3 December 2004, Bangkok, Thailand.

Winya Dungkaew, Kenneth J. Haller, Adrian E. Flood, John F. Scamehorn. Barium-Arsenate Phase Precipitation and Solubilization Study: Effect of pH, Ionic Strength, and PDADMAC. *Proceeding of the International Conference on Hazardous Waste Management for a Sustainable Future*, 10-12 January 2006, Bangkok, Thailand.

Winya Dungkaew, Kenneth J. Haller, Adrian E. Flood, John F. Scamehorn.

Crystallization of Low Solubility Calcium-Arsenate Compounds for Arsenate Removal from Poly(diallyldimethyl Ammonium Chloride)-Arsenate Solution. *Proceeding of the 2006 AIChE Annual Meeting*, 12-17 November 2006, San Francisco, CA.

Publication:

Winya Dungkaew, Kenneth J. Haller, Adrian E. Flood, John F. Scamehorn. Arsenic Removal by Precipitation with Calcium Phosphate Hydroxyapatite. Manuscript submitted to Advanced Material Research.

Winya Dungkaew, Kenneth J. Haller, Adrian E. Flood, John F. Scamehorn. Phase Precipitation and Solubility Constants: A Cautionary Tale from the Barium-Arsenate System. Manuscript to be submitted to Journal of Physical Chemistry B, in preparation.

CURRICULUM VITAE

WINYA DUNGKAEW

Personal Information:

Born September 06, 1980 at Udonthani, Thailand

Educations:

2002-Present: Ph.D. Candidate in Chemistry, Suranaree University of Technology

Nakhon Ratchasima, Thailand

1999-2002: B.Sc. (2nd Honour), Chemistry, Mahasarakham University,

Maha Sarakham, Thailand

Research Experiences:

Jan' 04-May' 04 and Nov' 06-Apr' 07: Visiting researcher to Prof. John F.

Scamehorn laboratory at The Institute for Applied Surfactant Research

(IASR), the University of Oklahoma, Oklahoma, USA

Aug' 07-Sep' 10: Advisor of engineering department, Alphana Technology

(Thailand) Co., Ltd. on cleanliness improvement research

Scholarships:

2002-2007: The Royal Golden Jubilee Scholarship (The Thailand Research Fund)

Thesis: "Arsenate Precipitation from Polyelectrolyte-Arsenate Complex Solutions"